SHEAR BEHAVIOR OF LARGE-SCALE CONCRETE BEAMS STRENGTHENED WITH FIBRE REINFORCED POLYMER (FRP) SHEETS

BY

David Alan Schnerch

A Thesis Submitted to the Faculty of Graduate Studies
In Partial Fulfillment of the
Requirements for the Degree of

MASTER OF SCIENCE

Department of Civil Engineering
Faculty of Engineering
University of Manitoba

THE UNIVERSITY OF MANITOBA

FACULTY OF GRADUATE STUDIES

*****

COPYRIGHT PERMISSION

SHEAR BEHAVIOR OF LARGE-SCALE CONCRETE BEAMS STRENGTHENED WITH FIBRE REINFORCED POLYMER (FRP) SHEETS

BY

DAVID ALAN SCHNERCH

A Thesis/Practicum submitted to the Faculty of Graduate Studies of The University of Manitoba in partial fulfillment of the requirement of the degree

Of

MASTER OF SCIENCE

ABSTRACT

Shear deficiencies in many bridges are a result of increases in allowable truck weights, deterioration due to age and exposure to deicing salts, and more stringent design provisions in shear. Some buildings also require shear strengthening due to changes in use or occupancy. Many studies conducted on the use of Fibre Reinforced Polymer (FRP) sheets for shear strengthening have been completed on beams that are small in relation to the effective bond length of the FRP. This study focuses on the use of FRP sheets for large-scale concrete members

Two series of large scale concrete beams were strengthened in shear to develop a better understanding of the behaviour of FRP shear strengthening on large specimens and to develop a means of predicting the shear capacity for all sizes of members. The first series of three specimens were obtained from a full sized I-section prestressed concrete bridge girder. One of these specimens was tested as a control, with the remaining two strengthened for shear with different configurations of Carbon Fibre Reinforced Polymer (CFRP) sheets. To develop a better understanding of bond behaviour of large-scale specimens, three reinforced concrete T-section beams were fabricated with a web height that was larger than those found in the literature. One of these beams was strengthened in shear using Glass Fibre Reinforced Polymer (GFRP) sheets and two others were strengthened using CFRP sheets. These beams were tested under static loading conditions.

It was found that FRP effectiveness for shear strengthening is improved when considering large-scale members. Strains in the FRP sheets were higher than in previous tests on smaller beams with progressive debonding occurring some time before failure. Cracks in the concrete were found to be more distributed and smaller in width in areas strengthened with FRP sheets, improving aggregate interlock shear transfer. A model was developed to predict the effective FRP strain in the sheets and the FRP contribution to shear capacity. This model was compared with fifty-three beams found in the literature besides the beams tested in this study. The model could more accurately predict the ultimate capacity of beams of widely different sizes when compared to other models.

TABLE OF CONTENTS

LIST OF FIGURES

2. BACKGROUND

3. EXPERIMENTAL PROGRAM

4. EXPERIMENTAL RESULTS AND ANALYSIS

5. EFFECTIVE STRAIN MODEL

LIST OF TABLES

2. BACKGROUND

3. EXPERIMENTAL PROGRAM

4. EXPERIMENTAL RESULTS AND ANALYSIS

5. EFFECTIVE STRAIN MODEL

LIST OF SYMBOLS

a length of the shear span

A_c effective concrete area

A_{frp} area of FRP shear reinforcement

A_v area of shear reinforcement perpendicular to the axis of a member within a distance s

$A_{v,min}$ minimum allowable area of shear reinforcement

b_w minimum effective web width within depth d

d distance from the extreme compression fibre to the centroid of the longitudinal reinforcement

d_{frp} effective depth of FRP shear reinforcement usually equal to d for rectangular sections and $d - h_f$ for T-sections

d_v distance measured perpendicular to the neutral axis between the resultants of the tensile and compressive forces due to flexure, but need not be taken less than $0.9\,d$

E_{frp} modulus of elasticity of FRP

E_{resin} modulus of elasticity of epoxy resin

f_{ce} compressive stress in concrete due to effective prestress only (after allowance for all prestress losses) at extreme fibre of section where tensile stress is caused by externally applied loads

f_c' specified compressive strength of concrete

f_{cp} compressive stress in concrete (after allowance for all prestress losses) at the centroid of the cross section resisting externally applied loads or at the junction of the web and the flange when the centroid lies within the flange

$f_{frp,e}$ effective tensile stress in the FRP sheet in the direction of principal fibres

f_{fu} tensile strength of FRP

f_y specified yield strength of reinforcement

h overall height of member

h_f slab or top flange thickness

h_{frp} height of FRP reinforcement along the side of a rectangular beam or web of a T-section beam

I_g moment of inertia of gross concrete section about centroidal axis, neglecting reinforcement

k experimentally determined factor

k_a factor to describe the anchorage conditions of the free ends of an FRP sheet (non-integer)

k_e factor to describe the number of free ends of an FRP sheet on one side of the beam (integer)

k_L factor to describe the effect of pseudo-isotropic laminates, equal to 1.0 for unidirectional sheets and 1.4 for sheets containing at least two fibre directions of near equal fibre content

L_e effective bond length for FRP reinforcement

M_{cr} cracking moment

M_f factored moment at section

n_s number of stirrups crossing the potential failure plane

R ratio of the effective FRP strain to the ultimate FRP strain

R_L remaining bonded width over the initial bonded width ratio

s spacing of steel shear reinforcement measured parallel to longitudinal axis of the member

s_{frp} spacing of FRP shear reinforcement measured parallel to longitudinal axis of member

t_{frp} total thickness of FRP sheet(s) on one side of the beam

T_{frp} tension force in the FRP sheet between two consecutive stirrups

V_c nominal shear resistance attributed to the concrete

V_{cg} nominal shear resistance attributed to the concrete using the general method of the Canadian code

V_{cw} shear force causing web-shear cracking

V_{exp} experimentally determined shear capacity of a member

V_f factored shear force at section

$V_{f\,bond}$ shear resistance attributed to the FRP reinforcement based on bond strength

$V_{f,\,govern}$ shear resistance attributed to the FRP reinforcement based on lowest of $V_{f,\,bond}$ and $V_{f,\,stress}$

$V_{f,\,stress}$ shear resistance attributed to the FRP reinforcement based on effective stress

V_{frp} shear resistance attributed to the FRP reinforcement

$V_{frp,\,exp}$ experimentally determined shear capacity of FRP reinforcement usually taken as V_{exp} for a strengthened beam minus V_{exp} for a corresponding unstrengthened beam

$V_{frp,\,pred}$ predicted shear capacity of FRP reinforcement

V_p component in the direction of the applied shear of the effective prestressing force or for variable depth members, the sum of the component of the effective prestressing force and the components of flexural compression and tension in the direction of the applied shear, positive if resisting the applied shear

V_{pred} predicted shear capacity of a member

V_r nominal shear resistance of a member

V_{rg} nominal shear resistance of a member using the general method of the Canadian code

V_s nominal shear resistance attributed to the steel shear reinforcement

V_{sg} nominal shear resistance attributed to the steel reinforcement using the general method of the Canadian code

$V_{s,\,max}$ maximum nominal shear resistance attributed to the steel shear reinforcement

$(w/s)_{frp}$ ratio of width to spacing of FRP shear reinforcement

w_{fe} effective width of FRP strip

w_{frp} width of one FRP sheet

y_t distance from centroidal axis of gross section, neglecting reinforcement, to extreme fibre in tension

β angle between FRP sheets and the longitudinal axis of member, or in the Modified Compression Field Theory, a factor accounting for the shear resistance of cracked concrete

β_1 angle between primary fibre direction of FRP shear reinforcement and longitudinal axis of member

β_2 angle between secondary fibre direction of FRP shear reinforcement and longitudinal axis of member for pseudo-isotropic FRP sheets

ε_{frp} effective strain of FRP reinforcement

$\varepsilon_{frp,o}$ observed strain of FRP reinforcement

$\varepsilon_{frp,p}$ predicted effective strain of FRP reinforcement

ε_{fu} ultimate strain of FRP reinforcement

ε_{max} maximum FRP strain over the remaining bonded width

$\varepsilon_{resin,\ ult}$ ultimate strain of epoxy resin

θ angle of inclination of diagonal compressive stress to the longitudinal axis of the member

λ factor to account for low density concrete

ρ_{frp} FRP reinforcement ratio

ρ_v transverse steel reinforcement ratio

1. INTRODUCTION

1.1 General

With the significant number of structurally deficient bridges in North America, innovative techniques of strengthening and rehabilitating are required to address these problems. Whether the deficiencies are caused by increased truck weights, errors in design or deterioration resulting from environmental exposure, any potential solution must also fit within tight fiscal constraints. Many researchers have found fibre-reinforced polymer (FRP) sheets suitable for shear strengthening of concrete structures. Advantages of this technique include corrosion resistance, ease of application and significant cost savings. Many buildings also require strengthening due to changes in use or occupancy. This technique is also suited for these applications because the size of the strengthened members is not increased and construction disruption is minimal. However, most of the research to date has been completed on much smaller beams than those used in buildings or bridges. This is particularly significant since the effectiveness of shear strengthening with FRP sheets is related to the bond strength and the amount of area available for bonding.

1.2 Objectives

Since full-scale girders and beams are already being strengthened in shear using FRP sheets, there is an urgent need for information relating to the behaviour and performance of these systems when they are applied to larger members. The objective of this experimental program was to examine the behaviour of large-scale concrete beams strengthened in shear with FRP sheets. This includes the cracking behaviour, the strain in the FRP, debonding of the FRP, and the modes of failure.

In addition to understanding the shear behaviour of beams strengthened with FRP sheets, a means of accurately predicting the shear capacity of the

strengthened beam is required. The objective of the analytical phase was to propose a model that could accurately predict the increased capacity provided by a shear-strengthening scheme using FRP sheets for any size of beam. This model must also quantify the effect of different factors affecting the performance of FRP shear strengthening schemes.

1.3 Scope and Contents

An experimental study of FRP strengthening for large-scale members was conducted. This work consisted of two series of beams. The first series utilized three specimens that were cut from a full-scale prestressed concrete I-section girder. One of the specimens was utilized as a control beam, while two others were strengthened in shear using carbon fibre-reinforced polymer (CFRP) sheets. Two different configurations of strengthening were examined in this series. The second series of tests were conducted on reinforced concrete beams with a T-section geometry. These three beams were identical except for their FRP shear-strengthening scheme. One beam in this series was strengthened with unidirectional glass-fibre reinforced polymer (GFRP) sheets, while the two other specimens were strengthened with unidirectional CFRP sheets. The two beams using CFRP used different strengthening schemes to explore methods of improving the bond performance.

A model for predicting the shear capacity of different sized members is proposed. This model includes factors effecting shear-strengthening effectiveness that to this point had not been quantified, including the shear reinforcement ratio and effect of pseudo-isotropic FRP sheets, in addition to the influence of size. The validity of the model is examined using test data for beams found in the literature and strengthened for shear using FRP, as well as the beams examined in this study.

The contents of this thesis are as follows:

Chapter 2 begins with a review of the behaviour of concrete beams subjected to shear. Various models to predict shear capacity of unstrengthened beams are discussed along with code provisions. The properties of FRP sheets bonded to concrete are examined, along with previous research on bond behaviour. The work that has been completed to date on FRP strengthened beams is presented, followed by some models for predicting shear capacity of FRP strengthened beams found in the literature.

Chapter 3 presents details of the experimental program including the geometric and material properties of the test specimens, the test set-up and the instrumentation attached to the beams

Chapter 4 presents the results of both series of beam tests in addition to describing the behaviour of the shear strengthening schemes, the strain behaviour of the concrete and FRP sheets, and the bond performance of full-scale members.

Chapter 5 discusses the development of a model based on beams found in the literature in addition to the tests completed in this study. Factors that have been found to effect shear performance of FRP strengthened beams were quantified using this model. The model is compared to previously developed models in predicting the shear capacity of different sized beams.

Chapter 6 summarizes the research conducted, presents conclusions and suggests direction for future research.

1.3 Acknowledgements

The author would like to thank Dr. Robin Hutchinson, for her encouragement, guidance and advice during the course of the research program. Technical assistance in the laboratory provided by Mr. Moray McVey, Mr. Scott Sparrow and Mr. Grant Whiteside is also greatly appreciated.

The donation of the bridge girder, used in the Series A tests, by Lafarge Canada Inc. is greatly appreciated. In addition, the work of Vector Construction Ltd. is acknowledged in performing the strengthening work for this series of beams.

2. BACKGROUND

2.1 Overview

Increased traffic loads, in conjunction with many bridges coming to the end of their design life, are responsible for many bridges being under capacity. In particular, deficiencies in shear are of significant concern since this type of failure is sudden with little or no sign of distress, occurring below the flexural capacity of the member (Nilson and Winter, 1991). It is also likely that for many structures there will be no load capacity after shear failure occurs. Shear deficiency may be the result of insufficient shear reinforcement, in some cases due to corrosion. Revisions to design codes over the life of a bridge can also result in reductions in allowable capacities. It is estimated that 40% of the bridges in North America are deficient to such a degree, that they require some form of rehabilitation or replacement (McKenna and Erki, 1994).

Typical solutions to this type of inadequacy have been limiting the traffic loads crossing the bridge, replacement of all or part of the bridge structure, or strengthening of bridge girders. Limiting of traffic loads is usually a temporary measure, since infrastructure must respond to the needs of society. Furthermore, policing of vehicle weights is costly and compliance can never be complete, leading to situations where potential overloading is inevitable. Replacement of a bridge structure is generally the most costly of the alternatives. This solution may be unavoidable in cases where limiting traffic loads is not practical and the bridge structure has reached a level of deterioration where repair is not possible. Usually the most appropriate way to address a shear deficiency is by strengthening.

2.1.1 Traditional Methods of Shear Strengthening

Traditionally, deficiencies would be addressed by adding external steel stirrups. These external stirrups may be left exposed, in which case they may be quickly corroded due to their exposure. In addition, the deck must be removed and holes

must be drilled at the location of each external stirrup (Deniaud and Cheng, 2000). Corrosion is accelerated if the bridge is found in a region that uses de-icing salts to melt snow and ice from roadway surfaces. Traffic moving near the bridge lifts the solution of water and chlorides from the roadway in a spray that eventually condenses on the bridge members. Conversely, if the external stirrups are jacketed with concrete for protection and to increase the shear contribution of the concrete, significant additional dead load is imposed on the structure. This results in an inefficient design that must provide capacity to support the strengthening scheme while adding still more capacity to address the overall deficiency. Significant labour and disruption to traffic is still required since the stirrups must be anchored above the top surface of the deck.

A shear strengthening technique that is common in Europe is the bonding of steel plates to the web of a deficient girder. Strengthening by bonding of steel plates has been used since the mid-1970s (Täljsten and Elfgren, 2000). This method may be chosen for its cost savings, as it is less invasive than methods requiring external stirrups. It is not without corrosion problems, however. An even greater area of exposed steel may exacerbate these problems. In addition, the potential exists for corrosion to develop between the steel and concrete surfaces, impeding necessary bond strength (Karbhari, 1995). Corrosion problems can be somewhat abated through the use of protective coatings, but this results in increased maintenance costs. The significant weight of the plates adds significant shoring requirements during construction and considerable dead load during the remaining service life of the structure. Shear strengthening with steel plates also has the problem of properly anchoring the ends of the plates (Täljsten and Elfgren, 2000).

More recent research has dealt with the anchorage problem by bonding plates that are approximately half the height of the web, but continuous over its length (Adhikary *et al.*, 2000). Using this method, the steel plates are mechanically

anchored to the web of the beam, with a gap between the concrete and steel surfaces. Epoxy is poured into this gap and allowed to cure. The problems of corrosion, significant dead weight and the need for heavy lifting requirements were not addressed by this method.

2.1.2 FRP Sheets for Shear Strengthening

The use of Fibre Reinforced Polymer (FRP) sheets for shear strengthening has many advantages over more traditional strengthening schemes. FRP materials are highly resistant to corrosive environments (Volnyy and Pantelides, 1999). Furthermore, they do not degrade at the bond line, suggesting that their service life expectancy may be similar to that of internal reinforcement (Dolan *et al.*, 1998).

Traditional strengthening techniques are more invasive, requiring access to the bridge deck. This means that at least one lane must be closed while the strengthening is progressing. Often, traffic volumes are so high that any closure would result in unacceptable delays. In strengthening with FRP sheets, all lanes on the bridge can remain open since the FRP sheets are applied from the underside of the bridge, without the need for extensive shoring. Labour costs can also be greatly reduced due to the ease of handling of the epoxy and FRP sheets.

The long-term durability of these methods still needs to be addressed. However, several bridges have been strengthened in Canada using this technique. Observations of how these systems perform over the long term will be required to confirm the results of short term testing. Also, the behaviour of these systems in fire needs to be addressed.

2.1.3 FRP Near-Surface Mounted Reinforcement

A relatively new technique is strengthening with near-surface mounted rods (Khalifa *et al.*, 2000c). Using this technique, grooves are cut into the area to be strengthened. These grooves may be inclined or vertical as the designer chooses. After the grooves are cut, epoxy paste is used to embed an FRP rod into the groove. The reported advantage of this technique is that no surface preparation, other than the grooving is required. Tests done by Khalifa *et al.* (2000c) utilized commercially available deformed CFRP rods showed various increases in shear capacity over control specimens. The failure mode of these beams involved progressive cracking of the epoxy used to embed the rods, eventually resulting in splitting of the epoxy cover in one of the rods intersected by a major shear crack. As this is a completely new technique, much additional research is required before significant recommendations for design can be made.

2.2 Shear Behaviour of Concrete Beams

2.2.1 Factors Affecting Shear Behaviour and Capacity

Shear forces in a beam are generated wherever the applied moment changes along its length. Unlike flexural failure, that is designed to be ductile, shear failure may be sudden and brittle. Due to the catastrophic nature of shear failure, the shear strength is designed to be greater than the flexural strength at all points along the beam. Shear behaviour of a beam without shear reinforcement is largely determined by four factors: the ratio of shear span to effective depth, the tensile strength of the concrete, the longitudinal reinforcement ratio and the presence of axial forces (MacGregor, 1988). The influence of increasing size on shear stress at failure is discussed later.

Shear may be transferred by any of the following mechanisms: shear stress in the uncracked concrete, interface shear transfer, dowel action and arch action. Stresses in excess of the tensile shear stress in the concrete result in cracking,

whereas stresses in excess of the compressive shear stress of the concrete result in its crushing. Tensile and compressive strengths may not be equivalent to concrete cylinder rupture strengths and cylinder compressive strengths since the web of the beam is in a biaxial stress state. Combined tension and compression loading significantly reduces both the tensile and compressive stresses at failure (ASCE-ACI Task Committee 426, 1973).

Shear may continue to be transferred across a crack in the concrete by interface shear transfer, also known as aggregate interlock. Interlock forces have been measured to contribute about one-third of the total shear force (Nilson and Winter, 1991). Failure of this mechanism will typically result in slippage along this plane.

If longitudinal reinforcing bars cross a crack, dowel forces in the bars may resist shear displacement. The dowel force induces tensions in the surrounding concrete that may produce splitting cracks along the longitudinal reinforcement. Relative to other mechanisms, the dowel force is generally not dominant (ASCE-ACI Task Committee 426, 1973).

Arch action occurs where shear flow cannot be transmitted. Arch action is dominant in deep beams, where an inclined crack extends from the load point to the reaction. It can also occur in cases where the longitudinal reinforcement is unbonded from the concrete. In this case the compression flexural resultant is equal to the tensile flexural resultant over the length of the shear span, but the distance between the two varies with distance away from the support. For this mechanism to be developed, a tie is required to restrain the thrust developed as a result of the arch. For deep beams, failure is often due to anchorage failure of the bars restraining this thrust (ASCE-ACI Task Committee 426, 1973).

Shear can be carried through beam action, arch action or any combination of the two. Shear is carried through beam action where the distance between the compressive and tensile flexural resultants remains constant and the tensile force in the reinforcement varies through bond stresses. This is the normal assumption of elastic beam theory.

It was found that the dominant factor affecting shear behaviour was the shear span, a, to effective depth, d, ratio (ASCE-ACI Task Committee 426, 1973). MacGregor (1988) divides shear spans into four types according to the a/d ratio: very short, short, slender and very slender. Very short spans ($a/d < 1.0$) develop inclined cracks joining the load and support. Short shear spans ($1.0 < a/d < 2.5$) develop inclined cracks and after internal redistribution of the internal forces are able to carry additional load by arch action. Failure of these types of beams will be by one of two modes. Shear tension failure occurs as a result of loss of bond due to a horizontal crack at the level of the flexural steel that extends to the end of the beam. The alternate failure mode is by crushing of the concrete above an inclined crack near the load point. This is known a shear compression failure. In slender spans ($2.5 < a/d < 6.0$), failure is the result of disruption of equilibrium due to inclined cracking. For very slender beams ($a/d > 6.0$), the failure mode will be in flexure before the formation of inclined cracks.

The shear stress at cracking is determined by the tensile strength of the concrete. For beams without shear reinforcement, it is the load at cracking that determines the capacity of the member. Whereas in beams with shear reinforcement, Collins *et al.* (1996) found that even after cracking, tensile stresses exist in the concrete, contributing to the ability to resist shear stresses. However, it is the load at cracking that is used for the design capacity of the member.

Beams with very low longitudinal reinforcement ratios generally fail in flexure before the shear capacity can be reached. However, for beams without stirrups, with a longitudinal reinforcement ratio of between 0.75 to 2.5% shear failure is typical. In this range, beams with lower reinforcement ratios tend to fail at lower shear stresses. This is attributed to inclined cracking occurring at a lower load due to the presence of wide flexural cracks that are longer in length (MacGregor, 1988).

Axial force also affects the shear behaviour of the beam. Axial forces in beams may be present due to restraint of strains developed through temperature changes or intentionally through the application of prestressing forces. Tensile forces in the member decrease the cracking load, while compressive forces increase it.

2.2.2 Shear Cracking

Shear cracking occurs when a beam is subjected to load that causes the principal tensile stresses to exceed the tensile strength of the concrete. Shear cracks, or diagonal tension cracks, are inclined cracks that occur in a region of combined shear and flexure. These cracks usually begin as flexural cracks perpendicular to the longitudinal axis of the beam since the tensile stress at the bottom of the beam is usually the first to reach the tensile rupture strain of the concrete. With increasing applied load, these cracks propagate at an angle toward the load points. At locations of high shear to moment ratio there will be little flexural cracking before the development of inclined cracks.

Inclined cracks must exist before shear failure can occur. In some pretensioned beams, or less frequently in reinforced concrete I-section beams with a narrow web, the principal tension stresses in the web may exceed those at the bottom flange. In this case, web-shear cracking occurs, wherein inclined cracks are generated starting in the web. Secondary cracks may occur along the

longitudinal reinforcement from splitting forces due to loss of bond or from dowel action forces in the longitudinal bars.

2.2.3 Internal Steel Shear Reinforcement

The basic philosophy of the ACI Code in providing shear reinforcement is to restrain the growth of inclined cracking and to increase ductility (ASCE-ACI Task Committee 426, 1973). Beams are provided with stirrups to ensure that failure is in flexure, which is typically a ductile failure mode, preceded with large deformations and cracking before loss of load carrying capacity. The increase in ductility is especially important in situations where the members are subjected to unexpected shear forces due to settlements, catastrophic loadings or earthquake. Because of these reasons, shear reinforcement is required in most members.

Internal steel shear reinforcement is generally conceived of as the tension members of a truss. These members are assumed to carry tension equal to the yield stress of the stirrups multiplied by their cross-sectional area. Besides the tension carried by the shear reinforcement, this reinforcement may also contribute to the concrete shear capacity by maintaining interface shear transfer, dowel action and arch action by preventing the widening of cracks.

Belarbi and Hsu (1994) conducted tests to determine average stress-strain relationships for steel reinforcement in reinforced concrete panels. The stress-strain behaviour of steel reinforcement is usually assumed to be elastic-perfectly plastic with a distinct yield stress. This is typically true for bars tested alone, however when concrete surrounds the bars their behaviour is different due to tension stiffening. The most significant difference is to lower the yield stress due to strain being localized to the crack location. After yielding, the steel does not behave perfectly plastic but its stiffness is reduced from 1.8 to 2.5% of the elastic modulus (Belarbi and Hsu, 1994). Although most shear models do not

account for these effects, the force carried by the stirrups at ultimate is similar to that described by elastic-perfectly plastic behaviour.

2.2.4 Models for Concrete and Steel Shear Contribution

2.2.4.1 Fixed Angle Truss Model

The truss model for shear was first proposed in 1899 for the design of reinforced concrete beams in shear (MacGregor, 1988). Compression and tension forces are developed in the top and bottom flanges of the truss. Tensile chords in the truss represent the tension in the stirrups. Inclined compression struts in the truss represent compression in the concrete. The compression struts are assumed to be inclined at 45 degrees, although in reality the slope of shear cracks may differ from this angle.

A simplifying assumption is to group the stirrups crossing a single failure plane together. An example of this model is shown in Figure 2.2.4.1a. The truss model is then statically determinate if it is assumed that the stirrups yield before the concrete crushes. Results from the 45-degree truss analogy are typically conservative (Collins and Mitchell, 1980).

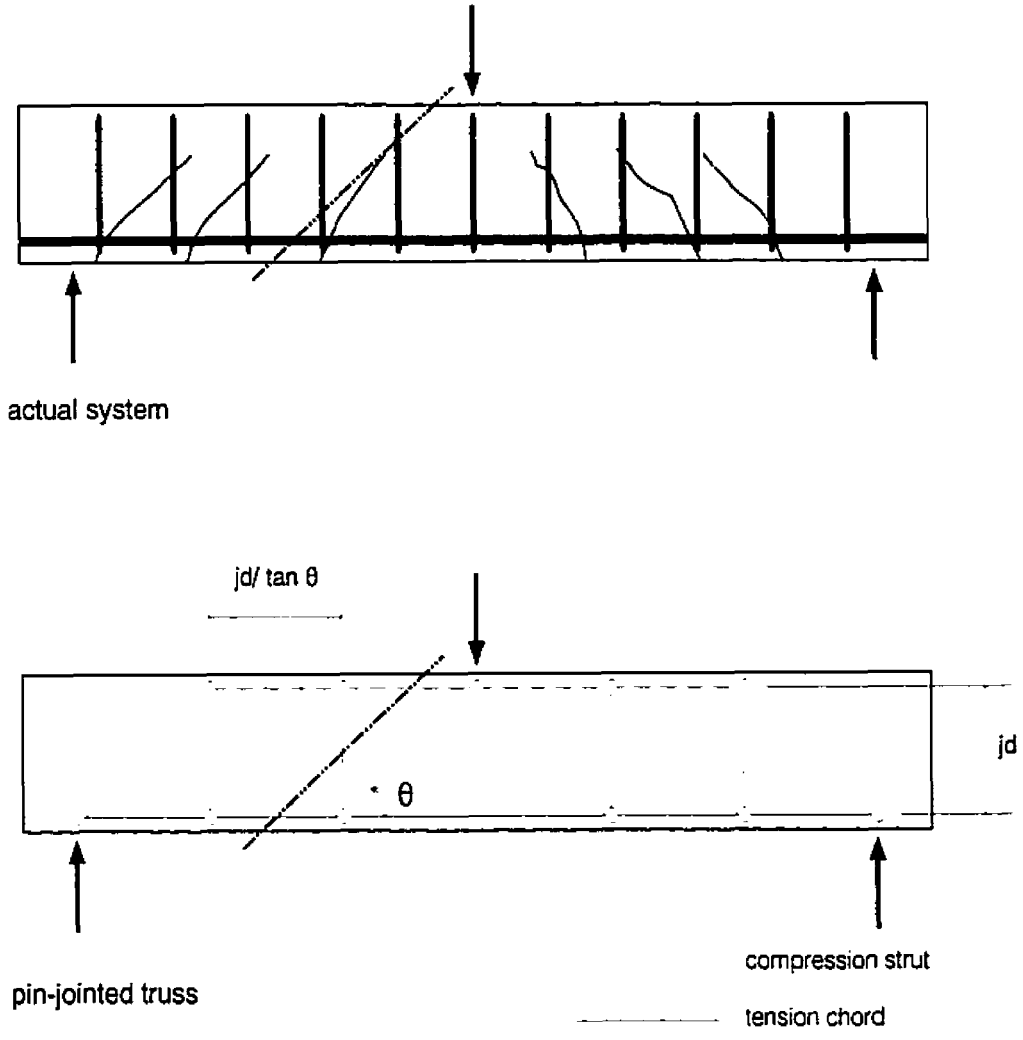

Figure 2.2.4.1a Truss analogy (adapted from MacGregor, 1988)

2.2.4.2 Variable-Angle Truss Model

In variable-angle truss models, the designer is allowed to choose the angle of the angle of inclination of the compression struts. Lower angles will typically result in less transverse reinforcement and additional longitudinal reinforcement, while larger angles will result in additional transverse reinforcement. This gives the engineer flexibility in design (Ramirez and Breen, 1991). The designer may choose lower angles to minimize congestion of reinforcement. For beams were the shear varies along the length, changes in strut inclination can result in almost constant stirrup spacing, simplifying construction.

The variable angle truss model forms the basis for the Modified Compression Field Theory that is used in the Canadian code. For design, a range of possible values for the angle of principal stresses, θ, is allowed (Rahal and Collins, 1999). The minimum value of θ coincides with the diagonal compressive stress being greater then the strength of the cracked concrete, whereas the maximum value of θ results in the stirrups not yielding. The variable angle truss model is also the basis for the European CEB-FIP code. In this code, the angle of the compression strut can be varied between 18.4 and 45 degrees (Polak and Dubas, 1996).

2.2.4.3 Shear Friction Model

The shear friction model is based on the amount of stress generated along the rough surface of a potential failure plane. Since the surface of a potential failure plane is quite rough, the coefficient of friction may be quite high (Nilson and Winter, 1991). The force that holds the two surfaces together is equal to the yield stress multiplied by the cross-sectional area of any steel crossing the crack for bars perpendicular to the failure plane. In addition to the friction of the failure plane surface, the model accounts for shearing of the reinforcement and the dowel action they generate. The main drawback to the use of shear friction models for beam shear is that the critical failure plane is typically unknown, so an interactive approach must be conducted to find the weakest or most critical failure plane.

2.2.5 Code Provisions for Concrete and Steel Shear Contribution

2.2.5.1 ACI Code Shear Provisions

The ACI Code shear provisions are based on the 45-degree truss model with an additional empirical concrete contribution to offset the typically conservative predictions of the truss model (Collins and Mitchell, 1980). According to the ACI Code, the shear capacity of a beam multiplied by a strength reduction factor must be greater than the shear force due to factored loads. The nominal

shear resistance of a section is to be taken as the sum of the shear contribution of the concrete and the shear contribution of any steel stirrups used.

For beams without web reinforcement, failure will occur shortly after longitudinal cracking, therefore the shear capacity is taken as the capacity at cracking. MacGregor (1988) indicates five variables that influence the inclined cracking load: the tensile strength of the concrete, the longitudinal reinforcement ratio, the shear span to depth ratio, the beam size and the presence of axial load. The ACI Code permits the neglect of most of these factors allowing the concrete contribution to be taken as,

$$V_c = \frac{\sqrt{f'_c}\, b_w\, d}{6} \qquad (2.1)$$

This equation is typically very conservative in regions where the shear to moment ratio is high (Nilson and Winter, 1991) and unconservative for beams with little longitudinal reinforcement (MacGregor, 1988). An increase in the concrete shear contribution is permitted for members subjected to axial compression.

ACI requires a minimum amount of web reinforcement if the applied shear force exceeds half the inclined cracking shear. A limited number of exceptions are permitted for slabs, footings, concrete joist construction and small beams.

The shear contribution of vertically oriented stirrups is calculated assuming all the stirrups yield at failure,

$$V_s = \frac{A_v\, f_y\, d}{s} \qquad (2.2)$$

Since the stirrups are unable to resist shear unless they are crossed by a crack, the maximum spacing of the stirrups is limited to half the effective depth or 610 mm whichever is smaller. If the required stirrup contribution is high, then the maximum allowable stirrup spacing is half of those listed above.

2.2.5.2 Canadian Code (CAN3-A23.3-M94) Simplified Method

The simplified method is based on the 45-degree truss model. Similar to the ACI approach upon which it is based, the simplified method sums contributions to shear strength based on the concrete strength and the steel strength separately. The concrete shear strength is presumed to equal the strength corresponding to diagonal cracking. The size of the beam is considered in calculating the concrete contribution.

In calculating the concrete contribution to shear capacity, the simplified method uses different material factors than the ACI approach. Lower material factors allowed in the Canadian code were not intended to make the concrete shear contribution more conservative, so the coefficient used in calculating the nominal concrete contribution was increased from 0.167 to 0.2. This is equation is given as,

$$V_c = 0.2\,\lambda\,\sqrt{f'_c}\,b_w\,d \qquad (2.3)$$

The use of this equation is limited to beams having at least the minimum amount of transverse reinforcement or an effective depth less than 300 mm. For beams not meeting this requirement the shear contribution is calculated,

$$V_c = \left(\frac{260}{1000 + d}\right)\lambda\,\sqrt{f'_c}\,b_w\,d \;>\; 0.1\,\lambda\,\sqrt{f'_c}\,b_w\,d \qquad (2.4)$$

For prestressed concrete members,

$$V_c = 0.06\,\sqrt{f'_c}\,b_w\,d + \frac{V_f}{M_f}M_{cr} \qquad (2.5)$$

with the cracking moment given by,

$$M_{cr} = \frac{I_g}{y_t}(0.6\,\sqrt{f'_c} + f_{ce}) \qquad (2.6)$$

For prestressed concrete members,

$$V_c \geq 0.17\,\sqrt{f'_c}\,b_w\,d \qquad (2.7)$$

and the concrete shear contribution should not exceed the web shear-cracking load,

$$V_c \le V_{cw} = 0.4\sqrt{f'_c}\left(\sqrt{1+\frac{f_{cp}}{0.4\sqrt{f'_c}}}\right) b_w\, d \;+\; V_p \qquad (2.8)$$

When vertical steel stirrups are provided, their nominal capacity may be taken as,

$$V_s = \frac{A_v\, f_y\, d}{s} \qquad (2.9)$$

This assumes that the stirrups will yield, which is the case if adequate detailing of the stirrups ends is followed. To provides safety against web crushing, or failure of the concrete compression struts in the web, the maximum nominal shear contribution is given as,

$$V_{s,max} = 0.8\,\lambda\sqrt{f'_c}\, b_w\, d \qquad (2.10)$$

The maximum allowable stirrup spacing is dependent on the applied shear stress and the effective depth of the beam.

Just as with the ACI code, the Canadian code requires a minimum amount of web reinforcement if the applied shear force exceeds half the inclined cracking shear, except in certain cases. However, compared with the ACI code, the Canadian Code recognizes that as the compressive strength of the concrete increases, the tensile strength also increases resulting in the need for a greater amount of web reinforcement (MacGregor and Bartlett, 2000). The minimum area of transverse reinforcement is given as,

$$A_{v,min} = \frac{0.06\sqrt{f'_c}\, b_w\, s}{f_y} \qquad (2.11)$$

The nominal shear capacity of a concrete beam with stirrups is calculated,

$$V_r = V_c + V_s + V_p \qquad (2.12)$$

2.2.5.3 Canadian Code (CAN3-A23.3-M94) General Method

The general method is allowed for the design of reinforced and prestressed concrete members, and is considered equivalent to the simplified method for design use. It is based on the variable angle truss model. In this method, the concrete contribution is modified by a factor, β, that indicates the ability of cracked concrete to transmit shear (Collins *et al.*., 1996). This factor is a function of the angle of inclination of the principal compressive stress in the cracked concrete, spacing of the cracks and the amount of strain in the effective shear area. This strain is conservatively taken to equal the strain in the flexural reinforcement up to a maximum of 2.0 millistrain. It also includes the effect of any axial force or prestressing. The other modification to previous expressions is that the distance between the compressive and tensile flexural resultants, d_v, replaces the effective depth. This equation is given as,

$$V_{cg} = 1.3\beta\sqrt{f'_c}\, b_w\, d_v \qquad (2.13)$$

The contribution of the steel shear reinforcement is given by,

$$V_{sg} = \frac{A_v\, f_y\, d_v \cot\theta}{s} \qquad (2.14)$$

The nominal shear capacity of a concrete beam with stirrups is calculated,

$$V_{rg} = V_{cg} + V_{sg} + V_p \qquad (2.15)$$

2.2.6 Size Effect

Initially it was thought that a change in depth beyond some critical value would not result in a change in concrete shear stress at failure. A comprehensive study was done by Kani (1967) on beams without transverse reinforcement. In this study it was determined that while crack spacing was almost independent of the effective depth, the crack length is greatly influenced by the effective depth. Furthermore, the safety factor was found to decrease with increasing depth. There was no indication that this reduction in safety factor associated with size effect approached a limiting value. Unlike effective depth, no influence of beam width on shear strength was found.

2.2.6.1 Beams without transverse reinforcement

Bažant *et al.* (1984) studied the effect of size on reinforced concrete beams without transverse reinforcement. Using non-linear fracture mechanics, a statistical analysis was completed to achieve the best fit of 296 tests by seven different researchers. It was found that both size-independent strength criterion and linear fracture mechanics contradict experimental evidence. Furthermore, designing against crack initiation rather than ultimate failure does not ensure a uniform safety margin for larger beams. For shear crack initiation it was found that size effect was almost undetectable, agreeing with theory that it should be nonexistent. The slight difference was attributed to the fact that crack initiation is more easily observed on large specimens, reflecting the lower recorded cracking stress.

The proposed shear strength formula of Bažant *et al.* (1984) was based on ultimate shear strength rather than crack initiation. This formula includes the effect of the longitudinal reinforcement ratio, the concrete strength, the beam depth, concrete aggregate size and the shear to moment ratio. Since the effect of shear reinforcement is to mitigate size effect, finding the total shear capacity as the sum of the individual concrete and steel contributions was questioned. It was later found by Bažant *et al.* (1986) that the effect of size was the same for prestressed concrete beams without transverse reinforcement as for longitudinally reinforced concrete beams.

Size effect of beams tested in shear was also studied by Kim and Park (1994). In this study it was found that crack spacing increased proportionally to the effective depth regardless of the longitudinal steel content. They also found that since the behaviour of high strength concrete is more brittle than normal strength concrete, size effect was more important for beams using high-strength concrete.

Collins and Kuchma (1999) discussed the findings of Kani (1967) in addition to conducting additional tests to confirm hypotheses based on the Modified Compression Field Theory. They indicate that tests conducted by Kani (1967) were flawed in that the beams were tested with a concrete age of only seven days. At this stage the ratio of tensile strength to compressive strength is 25% greater, influencing the shear behaviour of the concrete. This allowed the beams to meet ACI Code predictions for shear strength even though the factor of safety decreased with increasing size.

For concrete members without transverse reinforcement, shear stress at failure decreases as the member becomes larger and as the percentage of longitudinal reinforcement becomes lower (Collins and Kuchma, 1999). Results from experimental work showed that as members without stirrups become deeper, the shear stress at failure decreases, with thirteen of twenty beams failing at stress below that predicted by ACI Code equations. It was also found that members with distributed longitudinal reinforcement fail at higher shear stresses than members with concentrated longitudinal reinforcement of the same reinforcement ratio. This is due to the difference in crack spacing in the two beams, with distributed reinforcement allowing a greater number of cracks of smaller crack width. This has a positive influence in shear strength since the ability for aggregate interlock forces to be generated is enhanced. Collins and Kuchma (1999) found that the influence of the reinforcement ratio and the bond characteristics of the longitudinal reinforcement to be less significant than the distribution of the longitudinal reinforcement. Kim and Park (1994) also found that there was little difference in the spacing and development of cracks with differences in the longitudinal reinforcement ratio.

In the Modified Compression Field Theory, the shear strength of members without stirrups is a function of crack width that is related to crack spacing and straining of the longitudinal reinforcement. Since the crack spacing is greater

for larger members, the shear stress at failure is lower. The size effect in shear depends on the distance between the layers of reinforcement rather than on the overall depth of the beam. The Modified Compression Field Theory predicts that if a member contains at least the minimum amount of transverse reinforcement, the reduction in failure stress as a result of size effect will become insignificant.

2.2.6.2 Beams With Transverse Reinforcement

The earlier formula to describe size effect of unreinforced beams was extended to include the influence of aggregate size and the effect of stirrups Bažant *et al.* (1987). Code provisions neglect the beneficial effect of stirrups on the concrete shear contribution. This benefit is due to the closer spacing of cracks with a corresponding reduction in crack width. The stirrups also prevent splitting along the longitudinal reinforcement. The effect of size for beams with transverse reinforcement was found to be "small but nevertheless appreciable" (Bažant and Sun, 1987).

2.2.7 Effect of High Strength Concrete

Concrete considered high strength in the past is quickly becoming normal strength with increased understanding of concrete chemistry and quality control. Ahmad *et al.* (1986) and Elzanaty *et al.* (1986) found that some beams using high-strength concrete might be unconservatively designed using ACI Building Code design provisions for shear. The compression response of a cracked element is different from ordinary concrete in uniaxial compression (Vecchio *et al.*, 1994). Large transverse strains, generated by shear stress, decrease the strength of concrete in the direction of principal compression. This degradation is related to the amount of transverse strain and transverse cracking. However, in high-strength concrete the crack pattern is substantially different from normal strength concrete. High-strength concrete is more brittle, generating cracks that pass through the aggregate. This results in a smoother

fracture plane with less possibility for generation of aggregate interlock forces. Also, since the cracks pass through the aggregate, they are unaffected by differences in aggregate size (Collins and Kuchma, 1999)

Vecchio *et al.* (1994) considered the effect of high-strength concrete by testing shear panels constructed with concrete of compressive strengths ranging from 43 to 73 MPa. It was found from these tests that the constitutive models used in the Modified Compression Field Theory were found to simulate the responses observed in the test panels accurately. This was true even though a slightly increased degree of softening was found to develop in the panels constructed with high-strength concrete. The conclusion of this research was that compressive-softening formulas and analysis procedures previously developed for normal-strength concrete elements were found to apply equally well to high-strength concrete elements.

Polak and Dubas (1996) examined the two shear design provisions of the most recent Canadian code (CAN3-A23.3-M94) analysing tests of forty-nine beams by other researchers. These beams varied in concrete compressive strength from 21 to 94 MPa, with the majority of the tests above 60 MPa. It was found that for reinforced concrete beams with transverse reinforcement the factor of safety decreases with increasing strength using either the simplified or general methods such that for the four tests with concrete strengths in the range of 120 and 125 MPa, three predictions were unconservative. For prestressed members with transverse reinforcement, the simplified and general methods produce results that are conservative and have uniform safety factors over the range of concrete strengths studied. However, the general method produces results that are more conservative than the simplified method. Table 2.2.7a summarizes the findings of Polak and Dubas (1996).

Table 2.2.7a Ratio of experimental to predicted shear capacity using Canadian code (CAN3-A23.3-M94) provisions, (Polak and Dubas, 1996)

Beam Type	Number of Beams	Simplified Method		General Method	
		Mean	Std. Dev	Mean	Std. Dev
Reinforced concrete with transverse reinforcement	33	1.12	0.19	1.10	0.31
Prestressed concrete with transverse reinforcement	16	1.17	0.07	1.56	0.08

MacGregor and Bartlett (2000) report work by Mphonde and Frantz in addition to Elzanaty *et al.* (1986) that finds that the decrease in concrete contribution for large beams composed of high-strength concrete is offset by greater effectiveness of the stirrups in these beams. For beams without stirrups, Collins and Kuchma (1999) found that size effect is more pronounced in beams made from high strength concrete.

2.3 Properties of FRP Sheets

2.3.1 General Characteristics

Fibre Reinforced Polymer (FRP) materials consist of two parts, fibres and resin. The load-carrying component is the fibres. These fibres may be aramid, carbon, glass or Kevlar but natural fibres have also been used. Generally, the type of fibre used dictates the strength and stiffness properties of the FRP. The polymer component of FRP consists of a resin into which the fibres are embedded. The primary function of the resin is to allow stresses to be transferred between individual fibres. Epoxy, vinylester and polyester are the most common resins used.

FRP materials can be found in the form of bars, plates, and sheets. The application dictates which form of FRP material is the most practical to be used in a structure. Bars are generally used in new construction where they may be a suitable substitute for the steel in a reinforced or prestressed concrete member. Plates and sheets are more commonly used for strengthening or rehabilitation, where the application requires that they be bonded to the surface of a structure.

Plates, sometimes also referred to as strips, are often used for flexural reinforcement since they have a relatively high thickness to width ratio and there is generally limited surface area on the soffit of a beam for bonding to take place. Sheets are most commonly used for shear reinforcement, confinement of concrete columns or flexural strengthening of thin slabs or decks. Sheets have a low thickness to width ratio, so there is a large bonded area over which to transmit bond stresses. The flexibility of the sheets, when applied in a wet lay-up process, also allows them to follow irregular surface geometry, such as curved surfaces or rounded corners.

The primary advantages of FRP materials are their high strength to weight ratio, typically good fatigue behaviour and corrosion resistance to aggressive chemicals. High strength to weight is important for two reasons in the strengthening and rehabilitation of structures. The materials are light enough that strengthening can be accomplished without adding dead weight to the structure, which would otherwise negate the strengthening added. Furthermore, the lightweight eases handling by construction workers and reduces the need for staging and schemes for temporary support of the strengthening material. Both of these factors significantly reduce the labour cost compared with other types of strengthening schemes. High fatigue resistance is particularly important for bridge structures. Carbon fibres offer very good fatigue resistance. Much of the infrastructure problems in concrete structures are directly attributable to corrosion of the steel reinforcement. Corrosion causing cracking and spalling of concrete, leading to further ingress of water and chlorides, which exacerbate the corrosion problem. Ultimately corrosion, if left unabated, leads to significant loss in cross-sectional area of the steel reinforcement, potentially leading to an unsafe condition. FRP materials do not suffer this problem, since they cannot corrode with exposure to chlorides.

2.3.2 Material Properties

The behaviour of FRP materials is linear elastic to failure. Ultimate elongation strains are considerably higher than steel yielding strains. This results in ultimate tensile strengths that are typically between four and nine times the yield stress of steel. Failure is sudden and brittle with no load carrying capacity after failure. Unlike steel or concrete, the properties of FRP materials may differ from one manufacturer to another, since the materials may be unique to that manufacturer. For this reason, the necessary material properties are obtained from the manufacturer.

Mechanical properties of composites vary to a high degree depending on the orientation of load with respect to the fibre orientation and the fibre to resin volume ratio (Volnyy and Pantelides, 1999). FRP materials exhibit the highest strength when loaded in the direction of the fibres, and have only the strength of the resin when loaded perpendicular to the fibres. Using FRP sheets with the fibres woven orthogonally to produce a fabric that has the same properties in two directions can offset this effect. Sheets with three fibre directions are also available.

2.3.3 Bond Behaviour Between FRP and Concrete

2.3.3.1 Bond Behaviour and Failure Modes

In regions where FRP sheets cross a crack, tensile stresses resulting from shear cracking must be transferred to the concrete. The means by which this is achieved is by interfacial bond. Strength capacity is generally limited more by the bond between the FRP and the concrete than by the tensile capacity of the laminate. Bond may be developed by any of four mechanisms of adhesion: mechanical interlocking, diffusion, electronic, and absorption, with mechanical interlocking by far the most prevalent mechanism of adhesion (Karbhari, 1995). Mechanical interlocking occurs because of the linking of uneven surfaces of concrete and epoxy wherein epoxy occupies voids in the concrete surface. A

roughened concrete surface, free from loose material is essential in providing good mechanical interlocking.

Karbhari (1995) gives five possible modes of failure between the FRP and concrete substrate: peeling within the concrete substrate, interfacial failure between the concrete and adhesive surfaces, cohesive failure within the adhesive, failure between the adhesive and concrete surfaces and finally failure that alternates between the two surfaces. Most common failure modes in the literature for bonded specimens include shearing of concrete beneath the glue line and FRP failure after development of its full tensile capacity.

The typical assumption of perfect bond between the FRP and concrete surface was found to be initially justified in the linear elastic range of the concrete (Lee *et al.*, 1999). After the concrete cracks, there is a load level at which the strain at the crack reaches a peak and begins to decrease abruptly (Bizindavyi and Neale, 1999). At the same time the shear stress in the region adjacent to the crack begins to increase. The decrease in shear stress near the crack is attributed to distributed cracking in that region, resulting in shear stresses being transferred to the adjacent region. This finding was similar to that of Maeda *et al.* (1997) who found that, in the initial stages of loading, strain is limited to a region within the effective bond length. Once delamination progresses in this area, the area of active bonding is shifted further away from the crack. This phenomenon progresses until the entire sheet is debonded, often rapidly. This failure mechanism is reported by Täljsten (1997) to be governed by tensile strain in the concrete, in tests of bonded steel and CFRP plates. The concrete begins to fracture of about 0.8 to 1.0 millistrain as measured on the plate above the area of debonding.

2.3.3.2 Bond Strength

Use of average bond strength is limited to shorter length samples, since bond stress is developed over a relatively short distance (Dolan *et al.*, 1998). This implies that average bond strength decreases as the bond length becomes longer since at a certain bond length the ultimate strength cannot be increased any further. Samples with a longer bonded length will exhibit progressive debonding where bond stresses are shifted further away from the crack as debonding progresses.

The bond strength of FRP to concrete has been found to be limited by the strength of the adhesive bond to concrete, the concrete substrate shear strength, and the amount of bond area available (Dolan *et al.*, 1998). The adhesive must have sufficient toughness to dissipate energy from cracking as well as sufficient strength and stiffness to transfer stress between the concrete and the composite (Xie and Karbhari, 1998).

Bond strength increases with increasing concrete strength (Horiguchi and Saeki, 1997, Izumo *et al.*, 1998, and Khalifa, 1998). If shearing of the concrete beneath the bonded area governs failure, the value of bond strength will be proportional to the square root of the concrete strength (Chajes *et al.*, 1996). However, the properties of the bulk concrete within the member may be different from the surface properties of the concrete since the surface is more prone to bleeding, segregation and improper curing. Some researchers propose bond strength can be estimated by the concrete strength alone, since the dominant mode of failure, shear within the concrete substrate, is independent of the fibre type (Horiguchi and Saeki, 1997 and Izumo *et al.*, 1998). In the work of these researchers, the bond strength was found to be proportional to the 2/3 power of the concrete compressive strength.

Concrete surface properties affect the bond strength that can be developed. Surfaces should be mechanically abraded, sandblasted or hydro-blasted and a primer should be applied to achieve the best bond. Chajes *et al.* (1996) compared different concrete surface preparations. Grinding improved bond strength by a small amount as compared to using the surface as formed, but mechanical abrasion (with a wire wheel) gave a 10% increase in bond strength. This finish was claimed to be similar to what could be achieved with sand blasting. Yoshizawa *et al.* (1996) found that surface treatment with hydro-blasting, with a high-pressure water jet, increases bond strength as compared to grinding the surface of the concrete. Above this level of roughness, Khalifa *et al.* (2000c) found that there was no further improvement in strengthening beams in shear using additional hydro-blasting or in drilling holes in the surface of the concrete at a grid spacing of about 25 mm to produce rougher surfaces. Bond tests completed by Sato *et al.* (1997a) suggested that by using mechanical anchorage, the bond strength could be more than doubled. Full bond strength could not be determined since the failure mode of the specimens was by splitting of the concrete. This anchorage consisted of bolts passing through the bond specimen, applying a clamping force to the bonded region.

Bond strength has also been found to vary according to the test set-up (Horiguchi and Saeki, 1997). Tensile tests result in the highest estimate of bond strength followed by bending tests and shear tests. The peel tests used by Karbhari (1995) are a mixture of a direct tension test and a shear test, but are not intended as a structural efficacy test, but a means to evaluate the effects of environmental exposure on various materials.

2.3.3.3 Strain Distribution

Profiles of strain distribution were found to change depending on the level of loading (Bizindavyi and Neale, 1999). As the load is initially applied, strain exhibits an exponentially decreasing trend, from the maximum strain at the

crack to no strain some distance away from the crack. The length over which the strain goes to zero is defined as the initial transfer length. The initial transfer length was found to be constant for all loads lower than those causing cracking (Bizindavyi and Neale, 1999). The second stage results in a bilinear decreasing strain profile with the change in slope occurring at the initial transfer length. The third stage was found to differ depending on the type of fibre. For GFRP the third stage exhibited a linear decreasing trend, while for stiffer CFRP the trend was non-linear decreasing.

These findings were somewhat different from what had previously been found. Strain data from Izumo *et al.* (1998) shows an exponentially decreasing trend for all load stages with the maximum strain found to occur just away from the crack and a bond length of approximately 100 mm for all types and configurations of fibres studied. Maeda *et al.* (1997) found two stages in the strain distribution, a parabolic distribution at early stages of loading followed by a bilinear decreasing trend for the strain distribution at ultimate. Chajes *et al.* (1996) found the strain distribution would decrease at a nearly constant rate, indicating uniform bond stress.

Bizindavyi and Neale (1999) found that the width of the bonded laminate had little influence on its strain distribution. However, the only widths considered were 25.4 mm and 50.8 mm, considerably smaller than what would be necessary for shear strengthening of civil engineering structures. Furthermore, the strain distribution was only considered with the crack running perpendicular to the fibre direction.

2.3.3.4 Effective Bond Length

There is no increase in bond strength when the bond length exceeds the effective bond length (Izumo *et al.*, 1998). A number of researchers have reported the bond length to be approximately 100 mm (Izumo *et al.*, 1998,

Volnyy and Pantelides, 1999, and Yoshizawa *et al.*, 1996). However, this is dependent on the thickness of the sheets or plates being used since Bizindavyi and Neale (1999) reported effective bond lengths as low as 55 mm for CFRP sheets with a thickness of 0.111 mm, while Täljsten (1997) reported an effective bond length of approximately 300 mm for a thickness of CFRP plate of 1.2 mm.

The effective bond length was also found to decrease as the stiffness of the fibres increases (Bizindavyi and Neale, 1999). Furthermore effective bond length was found to be affected by geometry, test method, and plate width (Volnyy and Pantelides, 1999). Volnyy and Pantelides (1999) also predicted the effective bond length based on fracture mechanics theory. Stiffness of the FRP was used to predict the effective bond length in the following equation by Maeda *et al.* (1997),

$$L_e = e^{\left[6.134 - 0.580 \ln\left(t_{frp} E_{frp}\right)\right]} \qquad (2.16)$$

This equation was determined from the least squares method using test results. The average bond stress could also be calculated based on observation that the strain gradient, or the slope of the strain distribution curve, was approximately constant at 110 $(10)^{-6}$ /mm. This was less than the average strain gradient found by Sato *et al.* (1997) of 168 $(10)^{-6}$ /mm.

2.4 Shear Strengthening with FRP Sheets

2.4.1 Shear Strengthening Configurations and Previous Experimental Work

One of the advantages of strengthening with FRP sheets is the number of options available to the designer in determining the strengthening scheme. Sheets may be applied to each side of the web, or wrapped around the soffit of the beam forming a U-shaped jacket. The free edges of the sheet may be left bonded or mechanically anchored. Sheets may in some cases be fully wrapped around the beam, largely eliminating the possibility of debonding and resulting in different behaviour and failure modes. Gaps may be left between the sheets to allow the pore structure of the concrete to breathe, or the sheets may be

applied continuously without any gap between them. The angle of the fibres with respect to the longitudinal axis of the beam may be chosen just as with steel stirrups. Finally, unidirectional laminates or multidirectional laminates may be chosen for the strengthening.

Considering beams strengthened with FRP applied to each side of the web or wrapped around the soffit of the beam, the bond strength of the FRP to concrete is essential for strengthening. Yet, much of the research has been done where the height of the beam was small with respect to the typical effective bond lengths of 50-100 mm reported by various researchers. Rectangular beams were tested by Uji (1992) using FRP sheets applied to the sides of the beams that were 200 mm in height. Pre-cracked beams, 150 mm in height, were repaired and strengthened by Al-Sulaimani *et al.* (1994). Repair was completed by bonding GFRP plates to the sides of the beam or wrapping the plates around the bottom of the beam. These plates were either applied continuously or with a gap left between them. Beams tested by Triantafillou (1998a) were the smallest tested with a height of only 110 mm. Rectangular beams with a height of 305 mm used by Khalifa *et al.* (2000a) were tested either as simply supported or as continuous beams. The maximum recorded FRP strain in these beams was reported to be between 1.9 and 6.2 millistrain.

Beams with a T-section geometry strengthened in shear have typically been larger than rectangular beams. However, the overall height is not as important as the height available for FRP bonding. Chajes *et al.* (1995) tested T-section beams 191 mm in height with a web height of 127 mm and no internal shear reinforcement. Horizontal and vertical strains in the FRP at failure were between 4 and 6 millistrain. Since the principal strains at the locations of the gauges were at approximately 45 and 135 degrees, the horizontal and vertical strains were expected to be approximately equal. In predicting the shear capacity of the beams, a value of 5 millistrain was used. Beams with a T-section

geometry were also tested by Sato *et al.* (1997a). These beams were 300 mm in height with a web height of 200 mm.

Tests were done by Khalifa *et al.* (2000b) on T-section beams with a height of 405 mm and a web height of 305 mm. Vertical strain in the FRP at failure for a beam strengthened with unidirectional CFRP sheets ranged from less than 1 millistrain to 10 millistrain, when using five gauges in the shear span. For a similar beam using continuous unidirectional CFRP sheets the strains in the FRP were between 2 and 4 millistrain. Khalifa *et al.* (2000b) recognized that the strain measurements were not absolute since the values depend on the location of a gauge with respect to a crack. It should be noted that in each case lower strains were observed near the top of the sheet than at the bottom of the sheets wrapped around the soffit.

Deniaud and Cheng (2000) performed tests on T-section beams with heights of 400 and 600 mm. The height of the webs was 250 and 450 mm respectively, making the second series of beams in particular, larger in depth than those previously studied. These beams were reinforced in the longitudinal direction with 26 mm diameter high strength Dywidag bars. Anchorage was provided at the ends of the bars to prevent bond slip. Web shear cracking developed first in these beams with the lower end of the crack following the longitudinal reinforcement. This reinforcement did not yield in the tests. Measured FRP strains at ultimate were between 4 and 6 millistrain, with the fibres crossing a concrete crack exhibiting the same strain along the length of the crack. Debonding of the sheets above the crack was the primary mode of failure. The tests also showed that the effectiveness of FRP strengthening was dependent on the amount of internal shear reinforcement provided.

Large-scale tests are few in number. Deniaud and Cheng (2000) report tests on type E girders that are commonly used in concrete bridges in Alberta. Figure

2.4.1a gives the dimensions of this type of girder. With all of the girders tested failing in shear, the shear capacity was increased by 21 to 55% with different strengthening configurations. In a subsequent study, Deniaud and Cheng (2000) performed tests on smaller type G girders shown in Figure 2.4.1b. These girders were found to be deficient in shear based on current code requirements and increases in allowable truck weights. The objective of testing was to compare the use of glass and carbon FRP sheets in different repair configurations. In total eight tests were performed, one on each shear span of four girders obtained from bridge structures. Failure was typically due to shear cracks in the end diaphragm resulting from the loading that induced a combination of shear and torsion in this region. The strengthening techniques were effective in strengthening the girders between 5 and 17% in shear. Very small strains of 1.8 millistrain were recorded in the sheets.

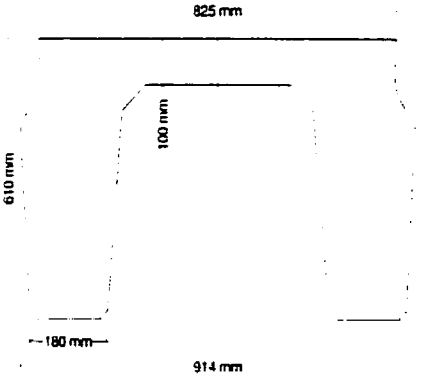

Figure 2.4.1a Dimensions of type E girder

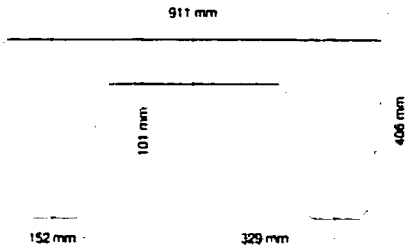

Figure 2.4.1b Dimensions of type G girder

In Germany, tests were completed on large-scale T-section beams (Limberger and Vielhaber, 1996). Inadequate internal steel reinforcement had been used in beams constructed in the period from 1950 to the 1960s. While simply supported beams of this type are typically adequate in shear, in cases where the beams are continuous, with a small cantilever past the support, large cracks have been observed. Tests were conducted in order to examine methods of addressing this inadequacy. In this case the shear capacity may be reduced to one-half of the original capacity due to the effect of the negative moment over the support. Cracking in the negative moment region of the beam, was typically at 60 degrees, originating from the deck slab and ending near the support. The

beams tested were 10 m in length with a height of 950 mm. Strengthening with three plies (vertical, horizontal and 45 degree) of CFRP was successful in strengthening the continuous beams. In total, 1200 grams of CFRP material was able to prevent shear failure at 600 kN and change the mode of failure to a flexural one at a load of 1200 kN.

While no tests using large I-section beams have been found in the literature, an experimental program on scaled I-section beams, 475 mm in height has been conducted by Hutchinson (1999). These girders were scaled at 1:3.5 from a bridge in Winnipeg, Manitoba that was constructed with bent-leg stirrups. Two series of tests were conducted, one utilized the detailing of the bent-leg stirrup of the actual girders in use and the other series used straight-leg stirrups that current codes require. Unidirectional CFRP sheets were applied either vertically or at a 45-degree inclination to improve the shear capacity of the beams.

A consequence of the geometry of this type of section is that strain in the sheets results in peeling stresses at the interior corners of the section. As peeling occurs, strain in the sheets is lost as the sheets effectively become longer as they straighten. This peeling was observed to be most critical at the bottom of the section. Despite the peeling, shear capacity of the beam was increased as compared to control beams. Two methods were used to restrain peeling, horizontally bonded sheets and mechanical clamping with bolts passing through the web attached to tubular steel sections. Bonding a horizontal sheet over the primary shear resisting sheets was somewhat effective in resisting peeling and improved the shear capacity over similar beams without the horizontal ply. The mechanical clamping scheme was most effective in resisting peeling and increasing the shear contribution of the CFRP. Observation of strain in the CFRP sheets at ultimate was between 4 and 6 millistrain for beams with straight leg stirrups. A rational model was proposed to predict the increase in shear

capacity using a maximum strain in the sheets at failure of 4 millistrain regardless of whether restraint against peeling was provided.

2.4.2 Shear Behaviour of Concrete Beams Reinforced With FRP

It has been found that FRP sheets do not delay the onset of initial cracking (Uji, 1992 and Limberger and Vielhaber, 1996). This observation was explained rationally by Uji (1992) by comparing a section strengthened with FRP sheets to a transformed concrete section with an increased apparent width. Sheet thickness is typically on the order of tenths of a millimetre. Although the stiffness of the FRP sheet may be about ten times the stiffness of concrete in tension, the apparent width of the section is only marginally increased. Limberger and Vielhaber (1996) found crack widths to be smaller in the concrete strengthened with FRP sheets. Even if cracks cannot be prevented, it was found the restraint of their growth allows greater aggregate interlock forces to be activated. Khalifa and Nanni (1999) reported that the addition of FRP strengthening results in greater shear capacity and ductility than a beam under reinforced in shear.

Chajes *et al.* (1995) found that for beams strengthened with FRP sheets, strains in the FRP increased slowly until the beam reached the load of the corresponding unstrengthened beam. After this point, the strains in the FRP increase significantly until sudden failure of the FRP fibres. Failure was marked by vertical strains of about 6 millistrain. This type of failure was unique among beams strengthened on the sides of the web or wrapped under the soffit with FRP sheets.

Excluding beams that were fully wrapped with FRP sheets, Khalifa *et al.* (2000a) noted two types of shear failures for beams strengthened with CFRP sheets, debonding or concrete splitting on a vertical plane. Debonding is also the predominate mode of failure reported by other researchers as can be seen in

Table 5.2c. For sheets bonded separately to each side of the web, debonding may occur either from the top or the bottom of the web. This strengthening configuration was found to be less effective than wrapping the sheets around the soffit of the beam. The debonded sheets typically have concrete still attached to their bonded surface. For beams with the sheets wrapped around the soffit, debonding may only occur from the top of the web.

By comparison, for beams that are fully wrapped, failure of the beam typically occurs simultaneously with sheet rupture (Araki *et al.*, 1997, Funakawa *et al.*, 1997, and Umezu *et al.*, 1997). Sheet rupture typically occurs at a strain lower than the tensile ultimate strain reported by the manufacturer, due to stress concentrations at rounded corners or at debonded areas (Triantafillou, 1998b). Unlike in beams where the bond strength governs failure, the increase in shear capacity of the beam is directly proportional to the reinforcement ratio of the FRP (Araki *et al.*, 1997). Although the capacity of fully wrapped beams is typically greater than for other application methods, their use is not practical for rehabilitation work since the top surface of the beam will typically be cast with the deck. To wrap the beam in this case, large slots must be cut in the deck, adding considerable labour costs and eliminating many advantages of using FRP sheets.

2.4.3 Factors Affecting Shear Behaviour of Concrete Beams Reinforced With FRP

For T-section beams in particular, bond failure starting from the top of the web is typically critical in failure. Mechanical anchorage may to be used to attempt to limit this failure mode. One means of mechanically anchoring the sheet at the underside of the flange was examined by Sato *et al.* (1997a). Mechanical anchorage by means of bolts passing through the top of the web were able to delay, but not completely prevent debonding, increasing the capacity of the beam compared with a corresponding beam with no anchorage. A subsequent series of tests by Sato *et al.* (1997b) examined additional means of anchoring the

sheets including nails driven through thin plates. Even with these methods, debonding was still the dominant failure mode. Bond failure was prevented in a test using an anchorage system in which the end of the sheet is wrapped around an FRP rod embedded in the top flange of the beam (Khalifa *et al.*, 2000a). However, the mode of failure of this specimen was in flexure so the shear capacity of this system could not be evaluated.

Khalifa and Nanni (1999) reported that the shear capacity appeared to increase with an increasing shear span to effective depth ratio. However, as the beams had either a shear span to effective depth ratio of either three or four, further research is clearly required. It was recommended to include the effect of this variable as the database of strengthened beams increases. Khalifa *et al.* (2000a) found that externally applied FRP sheets could be used for shear strengthening of both the positive and negative bending moment regions.

Täljsten and Elfgren (2000) examined different techniques of applying the FRP to the surface of the beam. In particular, hand lay-up, vacuum injection and heat-activated pre-pregs were examined. Although the material properties were better using the vacuum injection and pre-preg methods, the hand lay-up system was easier to apply and was as effective in strengthening.

It was found by Uji (1992) that strengthened beams with an equal fibre content showed different increases in strength depending on fibre orientation. The beam strengthened with a fibre orientation of 45 degrees had a 27% greater capacity than the beam with vertically oriented fibres. Chajes *et al.* (1995) also found that the orientation of the fibres influences the shear strength contribution. Triantafillou (1998a) found that the effectiveness of the FRP strengthening scheme increases as the fibre direction becomes closer to perpendicular to the diagonal crack.

Khalifa *et al.* (1998) commented that the use of pseudo-isotropic reinforcement was recommended, although not quantifiable at the time. The beneficial effect of using sheets with at least two orthogonal fibre directions was examined. Although generation of a shear crack involves displacement, there is also rotation about the crack tip. In beams with steel stirrups, this rotation is resisted by dowel action of the stirrup, but with FRP the only method of resisting this rotation is by an additional fibre direction. Later research found that using a horizontal layer of sheets over the continuous vertical sheets resulted in an increase in capacity of 17% compared with using the vertical sheets alone (Khalifa and Nanni, 1999). It also resulted in a change of failure mode to concrete splitting from debonding. For beams strengthened with triaxial GFRP by Deniaud and Cheng (2000), the failure was reported to be more ductile than tests using either unidirectional GFRP or CFRP sheets. This was reported to be the result of restraint, provided by the other fibre directions, of the nearly vertical cracks that developed near the supports.

The contribution of FRP was found more significant for beams without steel shear reinforcement than for beams with steel shear reinforcement (Khalifa and Nanni, 1999). Furthermore, increasing the FRP reinforcement ratio may not result in a proportional increase in the shear strength, particularly if the failure mode of the specimen is governed by debonding. This is contrary to tests involving fully wrapped beams.

Size may also affect behaviour of beams strengthened with FRP sheets. Chajes *et al.* (1995) recommended that before shear strengthening was carried out using web bonded sheets, full scale tests should be conducted in addition to studies on durability and cyclic loading. Triantafillou (1998a) noted that most of the tests completed at that time, including tests by the author were of beams that were small compared with members in use in bridges and buildings. As such, the available bond transfer length would be larger than for those beams tested

experimentally. This implied that experimental results to this point might be conservative.

2.4.4 Design Approaches for Predicting the Capacity of FRP Strengthened Beams

2.4.4.1 Design Approach proposed by Triantafillou

Triantafillou (1998a) proposed an analytical model for the design of beams strengthened in shear using CFRP laminates. Realizing that the ultimate strain cannot be reached in the sheets due to debonding, tensile fracture below the ultimate capacity of the sheets and stress concentrations at corners, an effective FRP strain was proposed in determining the nominal FRP contribution to shear capacity. This equation is given as,

$$V_{frp} = 0.9\,\rho_{frp}\,E_{frp}\,\varepsilon_{frp}\,b_w\,d\,(1+\cot\beta_1)\sin\beta_1 \qquad (2.17)$$

Unknown in the equation is the effective FRP strain. This strain was argued to be largely dependent on the FRP development length, which in turn was almost proportional to the FRP axial rigidity, or the area of FRP multiplied by its elastic modulus. Triantafillou (1998a) suggests that as the amount of FRP is increased, or its stiffness is increased, the effective strain is reduced since debonding dominates over tensile fracture.

In determining a best-fit equation for the effective strain, the work of eight different researchers was included in addition to nine tests completed by Triantafillou (1998a). Although it was recognized that beams that are fully wrapped with FRP fail by a different mechanism than those that are not fully wrapped, a different equation for the two cases was deemed unnecessary since all the data was seen to follow the same trend. The relationship between the effective FRP strain and the FRP area fraction multiplied by the elastic modulus, $\rho_{frp}\,E_{frp}$, was given by the following two equations,

$0 \le \rho_{frp}\,E_{frp} \le 1$:

$$\varepsilon_{frp} = 0.0119 - 0.0205\,(\rho_{frp}\,E_{frp}) + 0.0104\,(\rho_{frp}\,E_{frp})^2 \qquad (2.18)$$

$\rho_{frp} E_{frp} > 1$:

$$\varepsilon_{frp} = -0.00065 (\rho_{frp} E_{frp}) + 0.00245 \qquad (2.19)$$

It was also predicted that the FRP contribution increases almost linearly for values of $\rho_{frp} E_{frp}$ up to 0.4 GPa. Beyond this point, there was seen to be no increase in the effectiveness of the FRP strengthening.

2.4.4.2 Design Approach proposed by Khalifa *et al.*

Khalifa *et al.* (1998) modified the equation presented by Triantafillou (1998a), rewriting it in ACI code format as,

$$V_{frp} = \frac{A_{frp} f_{frp,e} (\sin \beta_t + \cos \beta_t) d_{frp}}{s_{frp}} \qquad (2.20)$$

Here the effective strain was replaced with an effective stress, and the definition of the effective depth of FRP reinforcement was used rather than the effective depth of the section. This definition is an improvement in describing the effectiveness of the FRP strengthening. For T-section beams, where the laminates are applied to the underside of the flange rather than to the top of the beam, the effective depth of the FRP may be considerably smaller than the effective depth and is more clearly related to the FRP capacity.

In determining the effective strain, the same approach as that used by Triantafillou (1998a) was utilized, but additional experimental data that had since become available was included. Furthermore, to limit the effect of different types of sheets, with different ultimate elongations, the ratio of effective FRP strain to ultimate FRP strain, R, was used. Again a polynomial was used as a best fit to the data for all cases where $\rho_{frp} E_{frp}$ was less than 1.1 GPa,

$$R = 0.5622 (\rho_{frp} E_{frp})^2 - 1.2188 (\rho_{frp} E_{frp}) + 0.778 \leq 0.50 \qquad (2.21)$$

The limit on R of half the ultimate effective strain was proposed to maintain the shear integrity of the concrete by effectively limiting the concrete crack widths.

Introduction of additional equations based on the bond strength were included to describe the potential failure mode of debonding. If the sheets are not fully wrapped around the beam, stresses generated by concrete cracking must be transmitted by bond from the concrete to the sheet on either side of the crack. The proposed bond-based design approach determined the bond that could be developed between the FRP sheet and the concrete surface based on the work of Maeda *et al.* (1997). It was also modified to include the effect of different strength concretes, which was not studied by Maeda *et al.* (1997). The effect of concrete strength was included by introducing a term proposed by Horiguchi and Saeki (1997).

The area that is effective for bond was limited to the effective depth of the FRP sheets multiplied by their effective width. The effective width was proposed as the following, utilizing the effective bond length, L_e developed by Maeda *et al.* (1997),

$$w_{fe} = d_{frp} - L_e \qquad (2.22)$$

for FRP laminates wrapped around the soffit of the beam, or

$$w_{fe} = d_{frp} - 2\,L_e \qquad (2.23)$$

for FRP laminates bonded separately on two sides of the beam. The effective bond length used was proposed by Maeda *et al.* (1997) as follows,

$$L_e = e^{6.134 - 0.58 \ln(t_{frp} E_{frp})} \qquad (2.24)$$

The final expression developed for the ratio of effective FRP strain to ultimate FRP strain base on bond failure was given as,

$$R = \frac{0.0042\,(f'_c)^{2/3}\,w_{fe}}{(E_{frp}\,t_{frp})^{0.58}\,\varepsilon_{frp,u}\,d_{frp}} \qquad (2.25)$$

The overall effective stress was limited to the lowest of the three R values, based on effective stress, bond length, and maintaining shear integrity of the concrete. A detailing requirement was made in order to prevent failure from occurring in any gap between the sheets,

$$s_{frp} = w_{frp} + \frac{d}{4} \qquad (2.26)$$

These equations were found to provide "acceptable and conservative" results for the beams tested by Khalifa and Nanni (1999).

2.4.4.3 Design Approach proposed by Deniaud and Cheng

Deniaud and Cheng (2000) used a significantly different approach in predicting the capacity of beams strengthened in shear using FRP. This model is based on the shear friction theory with the lowest shear strength among all potential failure planes governing the shear strength of the beam. The shear strength of a beam reinforced with steel stirrups is,

$$V_r = 0.25\, k^2\, f'_c\, b_w\, h \tan\theta \;+\; A_v\, f_y\, n_s \qquad (2.27)$$

where k is an experimentally determined factor and n_s is the number of stirrups crossing the potential failure plane, if any. Normally the factor k is taken as 0.5 for normal concrete strengths, but Deniaud and Cheng (2000) reported and used the modification proposed by Loov and Peng to account for the use of high strength concrete where,

$$k = 2.1\left(f'_c\right)^{-0.4} \qquad (2.28)$$

In addition, the additional friction contributed by the concrete flange was included as an effective area, A_s, replacing the rectangular area implied by the $b_w h$ term in equation 2.27. A continuous equation utilizing these modifications was developed to eliminate the need to determine the critical shear path,

$$V_r = 2.1\left(f'_c\right)^{-0.4}\sqrt{f'_c\, A_c\left(A_v\, f_y + T_{frp}\right)\frac{d}{s}} \;-\; A_v\, f_y \qquad (2.29)$$

In this equation T_{frp} is calculated using equations developed in a parametric study using the strip method. The shear contribution of the FRP sheets is given as,

$$T_{frp} = \frac{s}{d}\, h_{frp}\, t_{frp}\, E_{frp}\, \varepsilon_{\max}\, R_L \qquad (2.30)$$

The maximum strain in the FRP sheets in millistrain is determined as,

$$\varepsilon_{max} = 30.3318 - f'_c{}^{0.51503}\, h_{frp}{}^{0.160524} \left(t_{frp}\, E_{frp}\right)^{-1.53175} \left(\sin\beta_1\right)^{-0.09557} \left(k_a\right)^{-0.111054} \qquad (2.31)$$

In this equation, k_a represents the number of free edges for debonding. For sheets applied to each side of the web separately this value is two and for sheets wrapped around the soffit this value is one. In addition, Deniaud and Cheng (2000) allow non-integer values to account for varying degrees of anchorage. However, at the present these values must be determined experimentally. The value resulting from this equation must be checked to ensure that it is below the ultimate tensile strain reported by the manufacturer. The ratio of bonded to total length of the FRP, R_L, is calculated in dimensionless form,

$$R_L = 1 - 1.196 \exp\left[-\left(\frac{h_{frp}}{k_e\, L_e \sin\beta_1}\right)^{0.4008}\right] \qquad (2.32)$$

In this equation, k_e represents the number of free edges for debonding and is equal to two in the case of sheets wrapped around the soffit. No allowance for anchorage condition is made in this case. The effective length of the FRP sheets, L_e, is calculated using equation 2.24 given by Maeda *et al.* (1997). The same maximum sheet spacing of Khalifa *et al.* (1998) is used. The application of this method to beams found in the literature is given in Chapter 5.

3. EXPERIMENTAL PROGRAM

3.1 Introduction

The objective of the experimental program was to determine the shear behaviour of Fibre-Reinforced Polymer (FRP) sheets when applied to full-scale specimens. Two series of specimens were used in the testing program. The first tests completed utilized a full-size girder intended for use in a bridge crossing the Assiniboine River in Winnipeg. This girder was cut into three segments, two end segments and a symmetric middle segment. One segment was tested without strengthening in shear while the remaining two segments were strengthened with Carbon Fibre Reinforced Polymer (CFRP) sheets. The second series of three tests used beams fabricated in the laboratory. These reinforced concrete beams used either Glass Fibre Reinforced Polymer (GFRP) or CFRP sheets for shear strengthening and were considerably larger than those found in the literature.

3.2 Series A: Prestressed Girder Tests

3.2.1 Introduction

A prestressed concrete girder intended for use in the Moray Street Bridge in Winnipeg, Manitoba was used in the first series of tests. The structure, built in 1995, consists of two skew bridges each with four spans five girders across. In the course of shipping the girder to the construction site some superficial damage was done to the girder. This damage consisted mainly of bending of a portion of the exposed transverse reinforcement for composite action with the cast-in-place deck slab and some minor transverse cracking on the top flange. Although the damage was minor, the small chance that the girder would have to be repaired or replaced after the bridge was completed, at considerable expense, made the choice of fabricating a replacement girder more reasonable. Thus, the girder used for this series of tests was stored in the yard of the fabricator for a number of years, being unused in the bridge. Wardrop Engineering was in charge of design of the bridge and Lafarge Canada Inc. was the fabricator of the

40 girders used in the bridge, both of Winnipeg, Manitoba. Drawings were issued for construction on the 19th of December 1994, implying that the age of the girder was approximately five years before testing.

3.2.2 Test Specimens

The original bridge girder was 39 250 mm in length (out-to-out) with fifty-eight prestressing strands 13 mm in diameter. Sixteen of these strands were draped with the tie-downs located 4000 mm on either side of the centreline of the girder. Of the forty-two straight strands, twenty were debonded over lengths of 2, 4 or 6 metres from the end of the beam. The girder consisted of three cross-section geometries: the rectangular end block, an intermediate section and an I-shaped midspan section. Dimensions for each of the cross-sections are given in Figure 3.2.2a along with the locations of the prestressing strands. Figure 3.2.2b shows the variation of the cross-section along the length of the girder. The transverse reinforcement consisted of 16.0 mm diameter deformed, epoxy-coated steel stirrups. Spacing of the stirrups varied from a minimum of 75 mm at the ends of the girder to a maximum of 400 mm near the centre of the section. Figure 3.2.2c shows the variation of the stirrup spacing along the length of the girder.

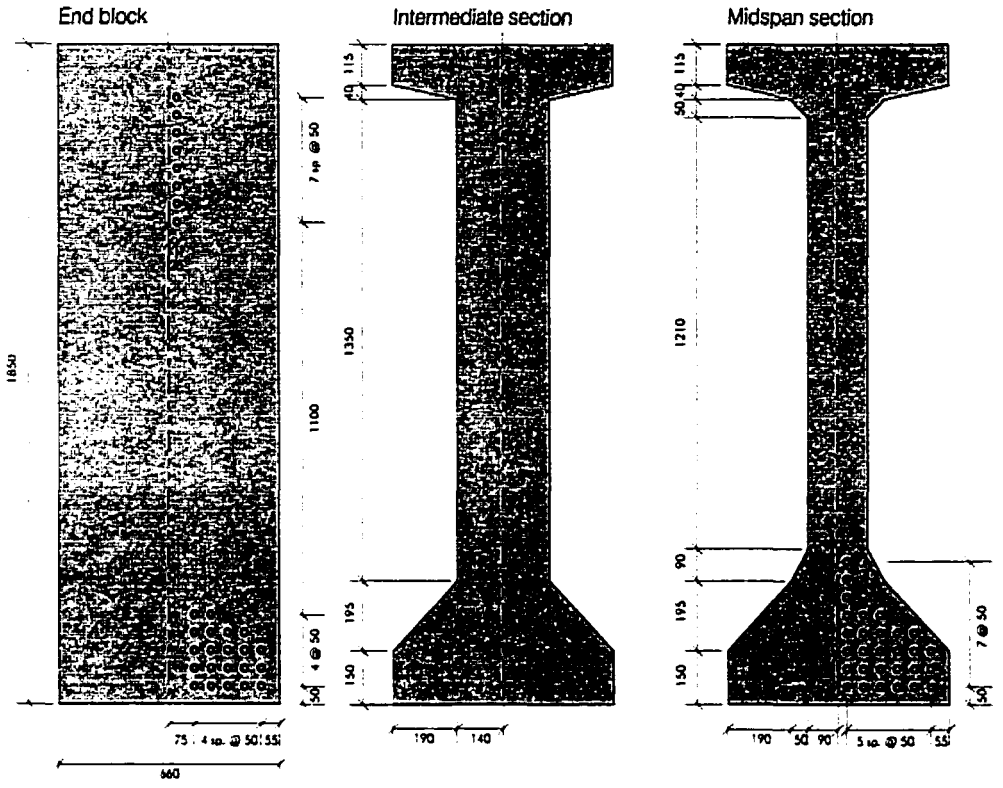

Figure 3.2.2a Concrete cross-section dimensions and prestressing strand locations

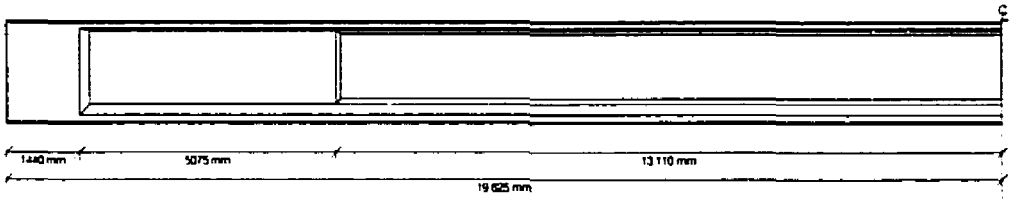

Figure 3.2.2b Variation of cross-section along girder length

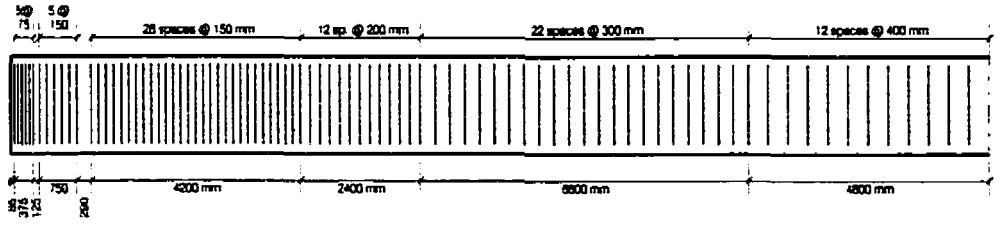

Figure 3.2.2c Variation of stirrup spacing along girder length

The 39 250 mm bridge girder was cut into three beam specimens. This was necessitated by size limitations of the structural floor in the W. R. McQuade Laboratory in addition to weight constraints for shipping. Making the beam specimens shorter, by cutting the girder into more specimens, was avoided to ensure the specimens had an adequate shear span to depth ratio. Each of the beam specimens was approximately 13 000 mm in length. The exact cutting location was halfway between two stirrups, leaving two unsymmetrical beam specimens with an end block at one end, an intermediate section and an I-shaped section at the other end. The draped prestressing strands were at a constant slope from the end block down to the cut end for these two beam specimens. The remaining specimen, from the middle of the girder, was symmetric and consisted of only one I-shaped cross-section geometry. Prestressing strands in this case were draped down to the tie-downs that are located at 4000 mm on either side of the girder centre line. Table 3.2.2a lists the designation for each of the beam segments based on their geometry and strengthening regime.

Table 3.2.2a Beam designations for Series A prestressed girder tests

Beam Designation	Segment Type	Shear strengthening
END-U	End	None
END-S	End	Vertically oriented CFRP sheets
MID-S	Middle	Vertically and horizontally oriented CFRP sheets

Analysis of the three beam specimens indicated that the existing shear capacity was high and that if strengthened with FRP, the beams would not fail in shear. To better study the shear behaviour to the ultimate capacity of the beam specimens, the shear capacity of the specimens was reduced, favouring a shear over a flexural failure mode. To reduce the shear capacity prior to strengthening a portion of the existing transverse reinforcement was cut, reducing the stirrup contribution while maintaining the overall integrity of the beam.

The existing stirrup spacing in the critical shear span was 300 mm in each of the end beam specimens and 400 mm in the middle beam specimen. In order to reduce the capacity sufficiently, every other stirrup was cut over a length of 1800 mm in the critical shear span for the end beams and over a length of 1600 mm for the middle beam specimen. This left a stirrup spacing of 0.39 times the depth and 0.47 times the depth for the two types of beam specimens.

Since the stirrups were deformed, the bond between the stirrups and the concrete would allow even the cut stirrups to be stressed during the initial stages of loading. The stirrups were limited to half their capacity by cutting each stirrup in two places along their length and choosing the distance between cuttings to be one development length. Calculation of the stirrup development length was based on the procedure developed by Orangun *et al.* shown in MacGregor and Bartlett (2000). The cuts were located an equal distance above and below the neutral axis depth at flexural concrete cracking.

A core drill with a diameter 64 mm was used to drill through the concrete and cut the internal stirrups. Figure 3.2.2d shows the chosen arrangement of cutting for each type of beam specimen. For the end segments of the beam, the cores in the top row were drilled the entire way through the web, cutting both legs of the stirrup in one core. For the bottom row , cores were drilled from each side of the web due to avoid cutting through the draped prestressing tendons in the centre of the web. For beams END-S and MID-S the holes remaining after the stirrups were cut were filled with concrete of a stiff consistency and allowed to cure at least seven days before testing.

Beams END-U and END-S

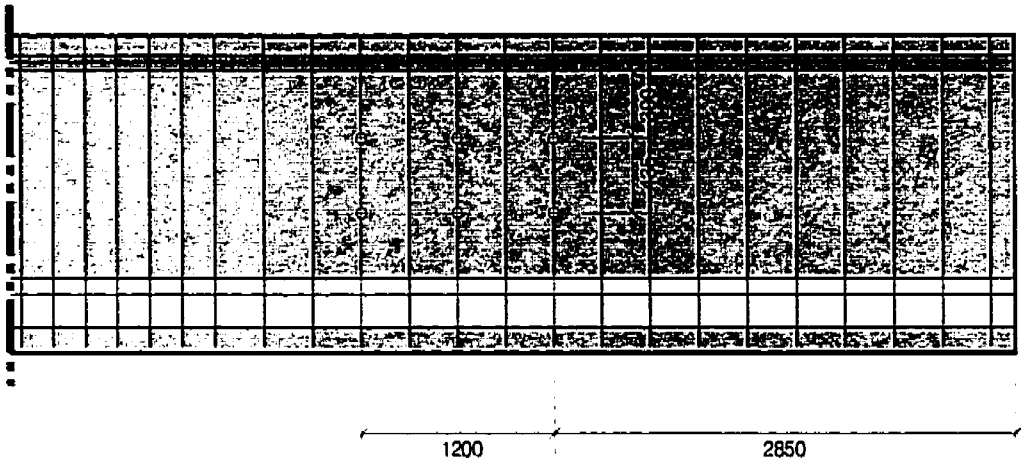

Beam MID-S

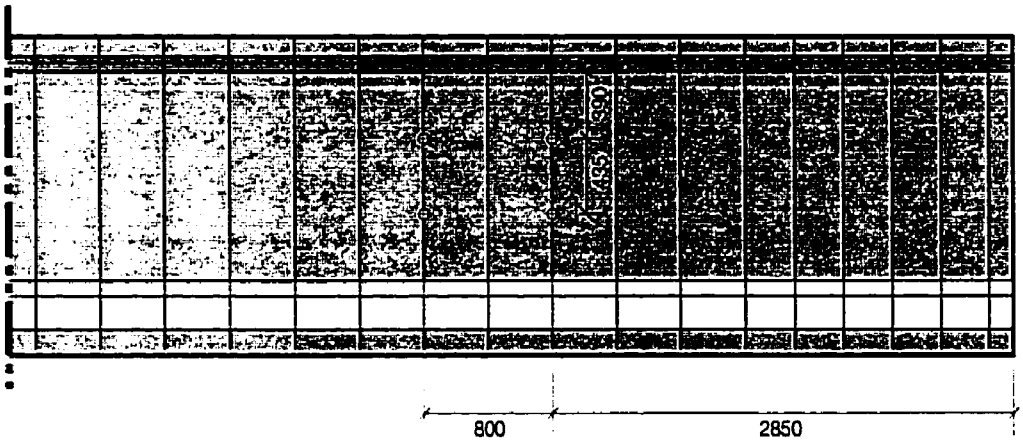

Figure 3.2.2d Location of cores to cut stirrups for each beam specimen

Vector Construction Ltd. completed the strengthening of two of the beam specimens, beam END-S and beam MID-S. Preparation of the concrete before sheet application was performed using grit blasting, to achieve a roughened surface free of laitance. The strengthening procedure was the same as that used in the following series of testing and is discussed in greater detail in that section. The width of the CFRP sheets used was 610 mm. Spacing of the sheets varied according to the degree of strengthening required and to conform to the geometrical changes of the beam.

For Beam END-S a sheet spacing of 900 mm on centre in the critical shear span was used with a closer spacing over a portion of the longer shear span to avoid shear failure in this zone. Beam MID-S had a sheet spacing of 1000 mm on centre in the critical shear span with a spacing of 700 mm in the longer span. In addition, for beam MID-S, two half-width sheets were placed longitudinally beneath the vertical sheets at the top and bottom of the web. Figure 3.2.2e shows the geometry of the sheets for both of the beams tested.

Since strengthening of the beam occurred before cutting of the stirrups, several CFRP patches were required on the beam where the core had cut through an already bonded CFRP sheet. In this case, after refilling the cores with concrete, a strip of CFRP sheet the same width as the core diameter was bonded to the existing sheet, extending from 200 mm above the top hole to 200 mm below the bottom hole. This procedure was only necessary for beam END-S.

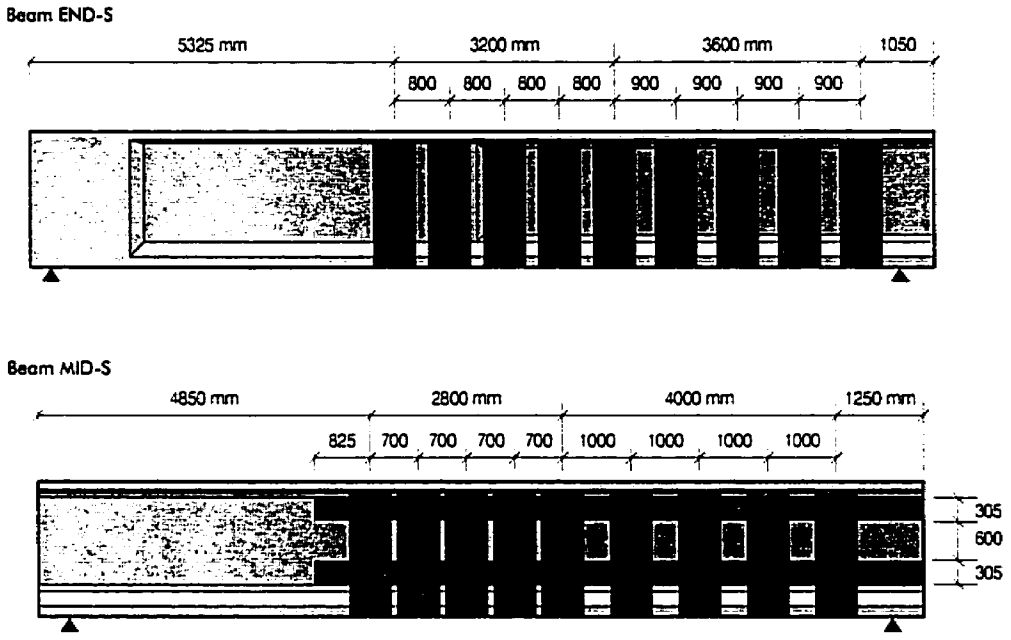

Figure 3.2.2e FRP shear strengthening configuration for beams END-S and MID-S

3.2.3 Material Properties

The concrete strength of the girder was determined after testing, by taking a series of core samples from both ends of the girder. Cores that were 100 mm in diameter were taken from a region of the girder that was largely undisturbed by testing. The end block of the girder satisfied this requirement while providing a region with a large volume of concrete in which to drill. As is typical, the end block reinforcing consisted of closely spaced mild steel reinforcement on the outside of the section with the interior of the end block free of steel other than the prestressing tendons. The cores were drilled through the outer cage of reinforcement and later any steel passing through the end of the core was removed as the core was cut to a length of twice its diameter for testing.

Provisions of ASTM C 42-90 were followed in obtaining and testing the 100 mm diameter drilled cores. The cores were tested in a dry state, after allowing the surface water resulting from drilling to dry completely. Sulphur capping

compound was used to ensure both ends of the core were flat and parallel. Three cores were taken from both of the end blocks resulting in a total of six cores being taken from the girder.

Steel properties were not measured directly, but were expected to conform to Canadian Standards Association standard G30.18 for the reinforcing steel and CSA G279 for the prestressing tendons. All transverse reinforcement in the girder consisted of epoxy-coated deformed bars 16.0 mm in diameter. Temperature reinforcement consisted of uncoated deformed bars that were 11.3 mm in diameter. The prestressing tendons were seven-wire strand with a diameter of 12.7 mm.

Vector Construction Ltd. completed the strengthening of two of the beams, END-S and MID-S, using the MBrace composite strengthening system manufactured by Master Builders Technologies of Cleveland, Ohio. This system consists of an epoxy primer, putty and saturant besides the fibre reinforcement.

The manufacturer has reported the physical properties of the three epoxy resins as listed in Table 3.2.3a (Master Builders Technologies, 2001). The primer is a low viscosity polyamine-cured epoxy compound used to permit high tensile bond strength to the concrete substrate. To fill any irregularities in the surface, putty is used. The putty is a non-sag paste epoxy material that has a high viscosity. The saturant is a low temperature-cure impregnation resin used to bond the sheets to the substrate and the fibres to each other.

Table 3.2.3a Material properties for the various epoxy components

Epoxy type	Tensile Strength (MPa)	E_{resin} (MPa)	$\epsilon_{resin, ult}$ (mS)
Primer	12	717	30
Putty	12	1800	15
Saturant	14	1138	53

Unidirectional carbon fibre sheets (MBrace CF 130) from Master Builders Technologies were used for the shear reinforcement. According to the information provided by the manufacturer these fibres have a tensile strength of 3480 MPa with a tensile modulus of 230 GPa (Master Builders Technologies, 2001). The ultimate tensile elongation is 1.5%. The effective sheet thickness is 0.165 mm and the supplied sheet width was 610 mm.

3.2.4 Test Set-up

Testing was conducted in the W. R. McQuade Structures Laboratory at the University of Manitoba. Due to modifications to the loading arrangement and in the length of the two types of beams, the test set-up varied for each of the three specimens tested. The first test, of beam END-U, utilized two equal concentrated loads that were asymmetrically placed on the simply supported beam. The span for this test was 12 125 mm with the critical shear span 4225 mm in length, giving a shear span to depth ratio of 2.7 if the average depth over the length of the shear span is taken. The constant moment region was 1200 mm in length. Remaining dimensions are as shown in Figure 3.2.4a. Load plates were each sized 175 mm by 300 mm and each plate had a roller. Plaster was used to distribute the load from the steel plate to the concrete. The supports used in this test and all the remaining tests in this series had dimensions of 150 mm by 560 mm and rested on rollers. No plaster was used at the supports for any of the tests in this series.

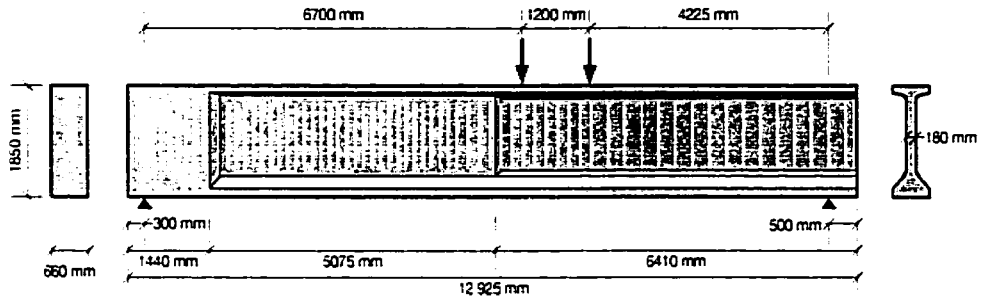

Figure 3.2.4a Test set-up of beam END-U

The test of END-S used a single concentrated load that was asymmetrically placed. Length of the span was 12 370 mm and the length of the critical shear span was 4855 mm, with a shear span to depth ratio of 3.1. Other dimensions are given in Figure 3.2.4b. The dimensions of the load plate were 305 mm by 340 mm with plaster used to distribute the load.

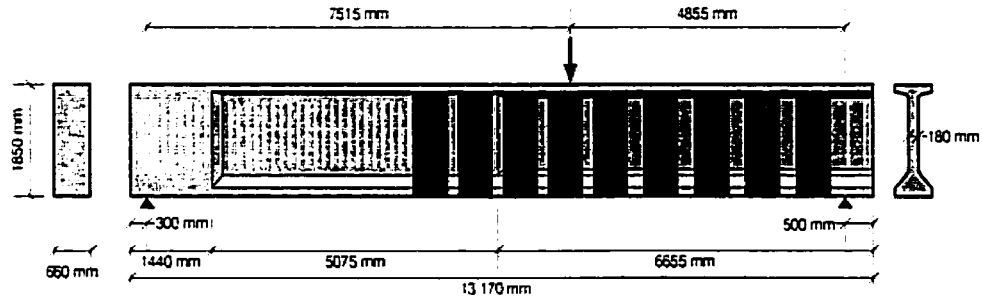

Figure 3.2.4b Test set-up of beam END-S

Like the previous test, the test of MID-S used a single concentrated load asymmetrically placed on the simply supported beam. Because the beam specimen was cut from the centre of the girder, the concrete cross-section was a constant geometry. The span for this specimen was 12 000 mm with a critical shear span of 4825 mm. The shear span to depth ratio was 2.9. The dimensions of the overhangs are given in Figure 3.2.4c. In this test the size of the loading plate was increased to 535 mm by 545 mm with plaster placed between the load plate and the top of the beam.

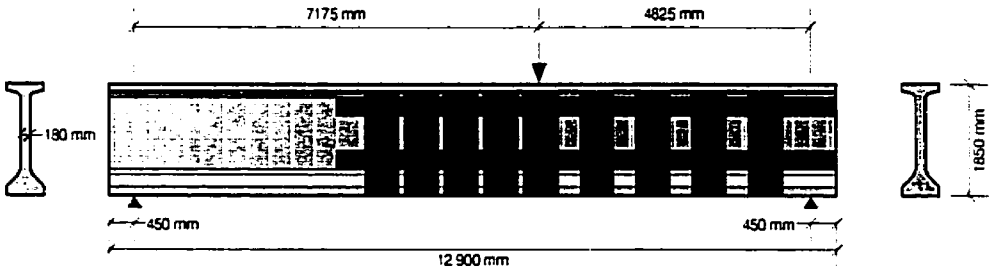

Figure 3.2.4c Test set-up of beam MID-S

Monotonic static load was applied to the beams using a 5000 kN capacity MTS testing machine. The full load range of the machine was used in conjunction with a range for the machine stroke of 200 mm. For beam END-U the load rate was 0.2 mm/minute before flexural cracking, 0.3 mm/minute after flexural cracking and 1.0 mm/minute after 4000 kN. For beam END-S the load rate was 0.2 mm/minute before flexural cracking, 0.3 mm/minute after flexural cracking and 0.5 mm/minute after a load of 4400 kN. The final test of beam MID-S used a load rate of 0.3 mm/minute throughout the test.

3.2.5 Instrumentation

The beams in this series were instrumented with linear voltage displacement transducers (LVDTs) to monitor deflection and strain gauge type displacement transducers to measure strain. The strain gauges used had a gauge length of either 100 mm, 200 mm or 300 mm with 200 mm being the most common gauge length used. For the beams with CFRP sheets electrical foil gauges with a 6 mm gauge length were used. The strain gauges used were type FLA-6-11-5L, manufactured by Sokki Kenkyujo Co., Ltd. of Tokyo, Japan. These gauges had a resistance of 120 ohms. All of the strain gauges were oriented vertically, with the majority of gauges on the web and a few additional gauges located on the bottom flange near the interior corner of the concrete cross-section. A light sanding of the sheet surface down to the level of the fibres preceded application of the gauges, and M-Bond adhesive was used to attach the gauges to the surface. A ninety-six-channel data acquisition system using a Pentium II processor with

Labview software was used to record all the data from the gauges as well as the machine load and stroke at a sample rate of 1.0 Hz.

Displacement of beam END-U was measured as close to the load points as possible, 450 mm on either side of the centreline of the two applied concentrated loads. All of the strain gauges used on beam END-U were applied directly to the concrete surface in the arrangement shown in Figure 3.2.5a. In total, twenty-four strain gauges were used on the web and bottom flange of the beam. An additional gauge was positioned longitudinally on the bottom flange at the level of flexural reinforcement at the centre of the constant moment region. This LVDT had a gauge length of 500 mm, a sufficient length to determine the flexural tensile strain over a distance of several cracks

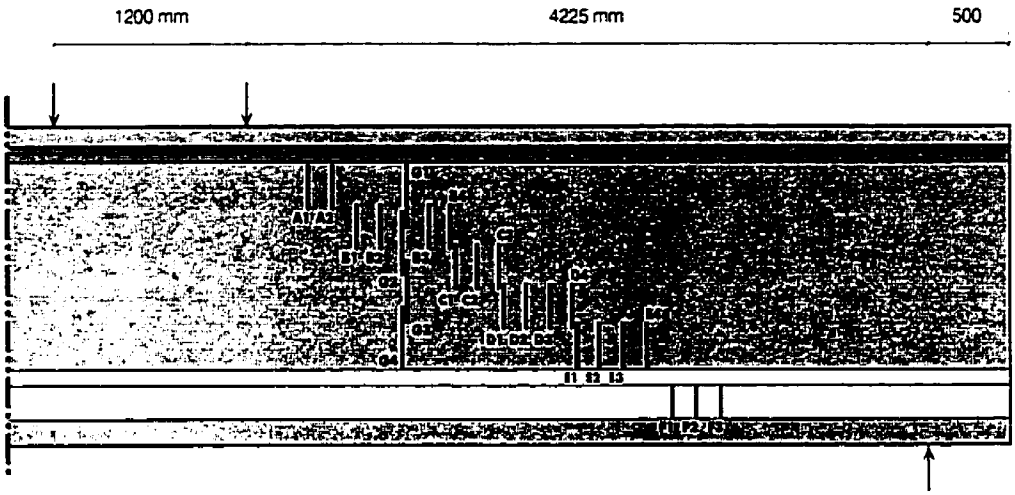

Figure 3.2.5a Instrumentation for beam END-U

For beam END-S, displacement was measured at the centre line of loading on both sides of the top flange. Vertical strain gauges were positioned on the web and flange in the same arrangement used for the previous test of beam END-U. Some of these gauges were attached to the CFRP sheets rather than directly to the concrete. In addition, electrical foil gauges were placed in vertical rows in three locations (gauges H, I and J). These gauges were spaced 25 mm apart

except at the transition from the web to the bottom flange (for gauges in rows I and J). These gauges are shown in Figure 3.2.5b. Like the previous test, an LVDT was used to measure longitudinal strain 100 mm above the soffit of the beam on the side of the flange.

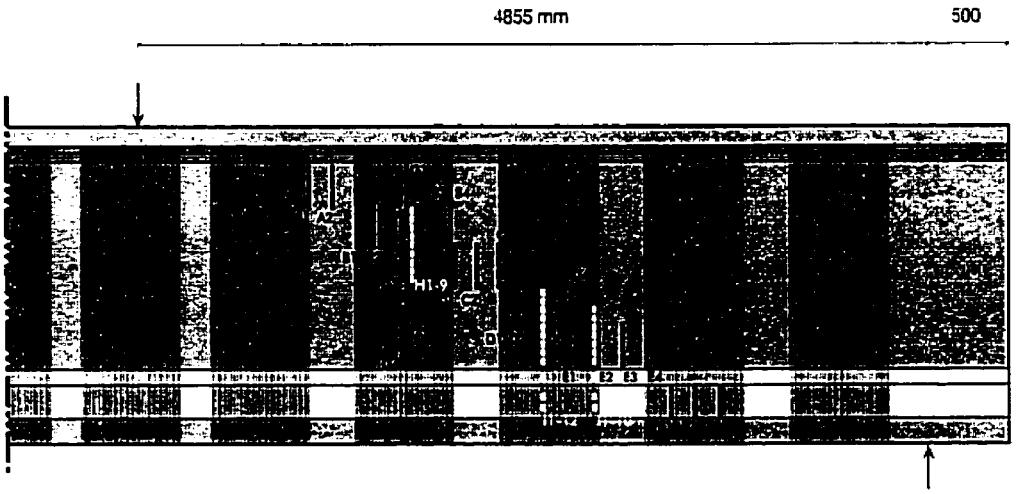

Figure 3.2.5b Instrumentation for beam END-S

Displacement was recorded for beam MID-S on both sides of the top flange at the centreline of loading. Strain gauges were arranged somewhat differently to account for the difference in stirrup spacing, location of cut stirrups and the region of expected cracking in the web. Again, a number of the gauges were attached to the CFRP sheets and others were directly attached to the concrete. Like the test of END-S, three vertical rows of electrical foil gauges were attached to the sheets. Figure 3.2.5c shows the positions of all the gauges on the web of the beam. Two LVDT gauges were positioned longitudinally for this beam based on the experience gained from the test of beam END-S. One was positioned under the concentrated load point on the side of the bottom flange 100 mm up from the bottom of the beam. The other was placed 15 mm above the top surface of the beam, centred 750 mm away from the concentrated load point in the longer shear span. Both gauges were used to measure strain over a 500 mm gauge length.

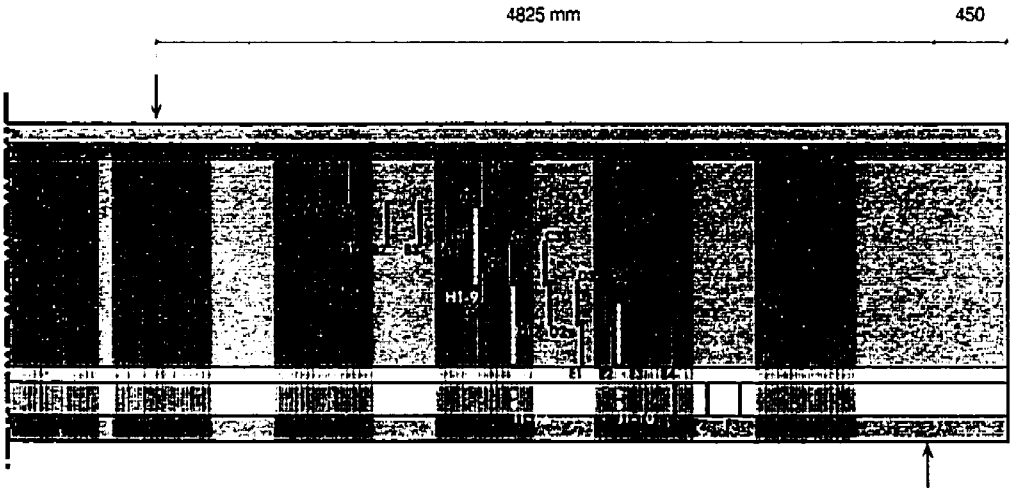

Figure 3.2.5c Instrumentation for beam MID-S

3.3 Series B: T-Section Reinforced Concrete Beam Tests

3.3.1 Introduction

For the second series of tests another set of three beams was fabricated. These reinforced concrete beams were designed to be larger than those commonly found in the literature, providing a depth of external FRP shear reinforcement that is large in comparison to its development length.

3.3.2 Test Specimens

In order to design a beam critical in shear strength, while maintaining reasonable stirrup spacing, a T-section shape was used. The soffit of the beam was cast with rounded corners using a fabric-forming technique in order to reduce the amount of surface preparation required before application of the FRP sheets to the concrete. Dimensions of the concrete section are given in Figure 3.3.2a. Figure 3.3.2b illustrates the formwork used for casting along with the configuration of the woven polypropylene fabric used to generate the rounded corners.

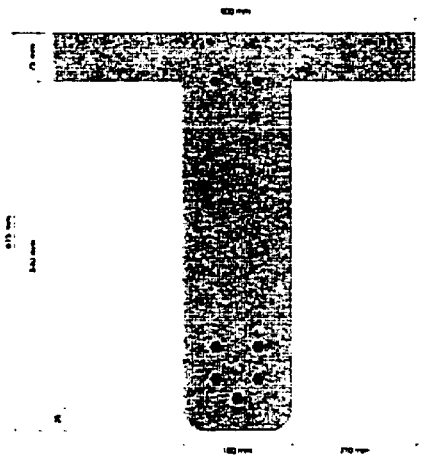

Figure 3.3.2a Concrete section dimensions for Series B beams

Due to their small size, many of the beams found in the literature use small diameter undeformed stirrups. For the beams in Series B, deformed steel reinforcing bars were used as transverse reinforcement since they are more common in actual full-scale structures and their behaviour is different from that of undeformed stirrups. Since anchorage requirements for the transverse reinforcement dictate that the bar be anchored by at least one longitudinal bar, a two-legged u-shaped stirrup was required. To minimize the width of the beam web, this stirrup was bent in the tightest allowable radius for that size of bar. For anchorage at the top, two additional longitudinal steel bars were utilized in the compression zone. The stirrup configuration is shown in Figure 3.3.2c. Stirrup spacing in the critical shear span was designed to allow additional strengthening with the FRP shear reinforcement, while still permitting shear failure to occur in this zone. Additional stirrups at a reduced spacing were provided in the untested shear span to ensure that failure would not occur in this region. Spacing of the internal steel stirrups over the length of the beam is given in Figure 3.3.2d.

Figure 3.3.2b Formwork used to cast Series B beams

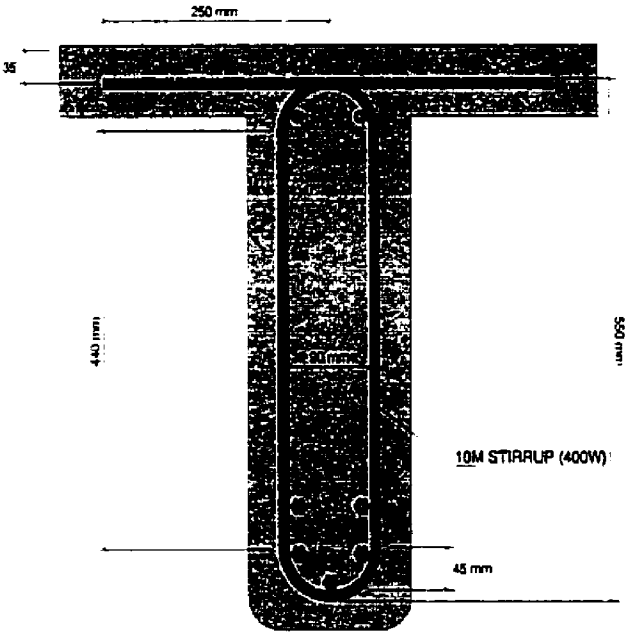

Figure 3.3.2c Stirrup configuration for Series B beams

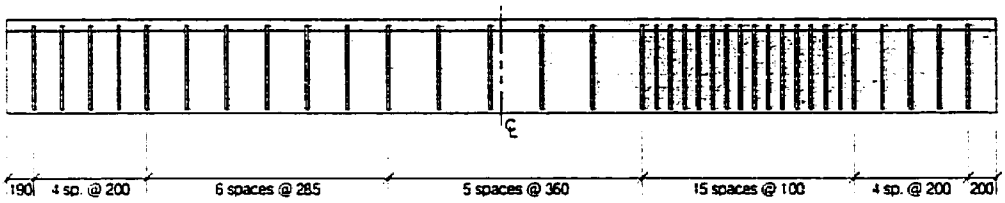

Figure 3.3.2d Stirrup spacing for Series B beams

Longitudinal reinforcement was designed such that the beam would not fail in flexure. If deformed bars were chosen, they would have needed to be quite large in diameter with corresponding large spacing between the bars. This size of bar would have contributed to an unrealistic amount of dowel action for this size of beam. Thus, instead of mild steel deformed bars, the longitudinal reinforcement consisted of prestressing strands. Since the yield stress of the prestressing tendons is considerably greater than for deformed bars, a smaller cross-sectional area of steel could be used and smaller tendons could be used at a relatively close spacing. It should be emphasized that no prestressing was applied to these tendons before casting. To prevent anchorage failure of the tendons, the beam extended well beyond the centre line of the supports, providing a region for development of the required stress in the prestressing tendons beyond the span of the beam. Details of the longitudinal reinforcement are shown in Figure 3.3.2e.

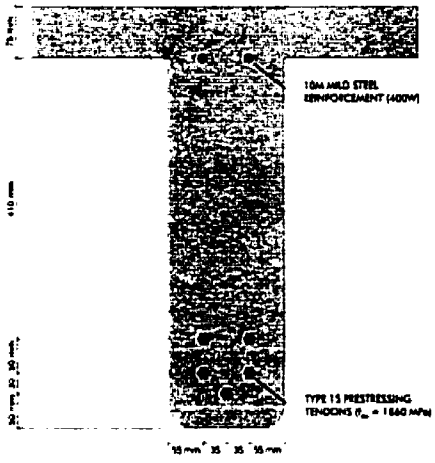

Figure 3.3.2e Configuration of the longitudinal reinforcement for Series B beams

Two types of FRP were used for external reinforcement of the web. Beam A-G used uniaxial glass fibre sheets supplied by Master Builders Technologies, while beams B-C and C-C were strengthened using uniaxial carbon fibre Replark Type 20 sheets from Mitsubishi. Both the glass and carbon fibre sheets were oriented with the fibres perpendicular to the longitudinal axis of the beam. The

width of all sheets used was 250 mm and the spacing used was 375 mm on centre as shown in Figure 3.3.2f. The difference between beam B-C and beam C-C was that beam C-C had an additional sheet placed longitudinally over the vertical sheets to improve anchorage.

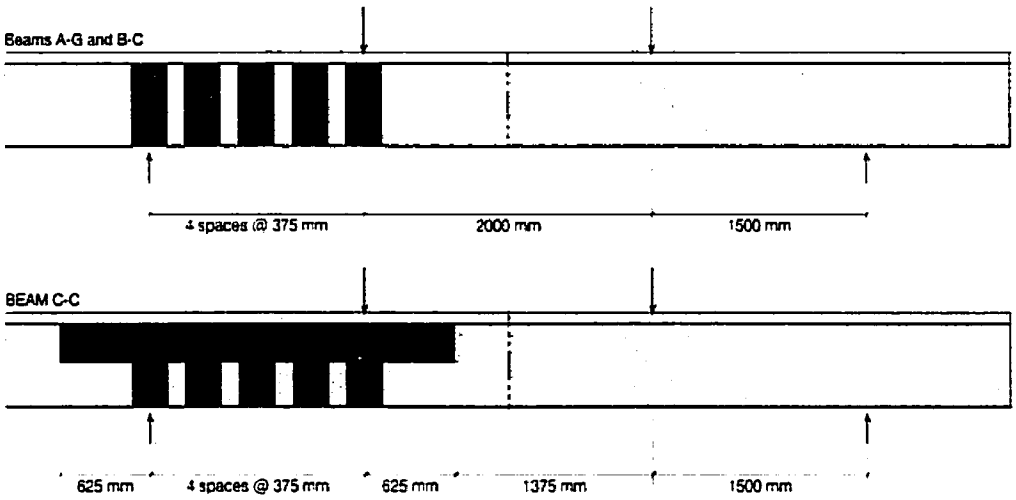

Figure 3.3.2f Configuration of external FRP sheets

3.3.3 Specimen Fabrication

Beams B-C and C-C were cast from the same concrete batch on October 4, 2000, while Beam A-G was cast on October 13, 2000. After casting, the top surface of the beams was covered using polyethylene sheeting. A wet surface was maintained for one week at which time the sheeting was removed and the beams were allowed to air cure at least twenty-eight days from the date of casting. All three beams were then prepared to accept the FRP shear strengthening system by surface grinding.

Grinding of the concrete surface to remove all laitance and expose air voids near the surface was completed using a concrete grinder with a revolving head. Figure 3.3.3a shows the difference between the ground and natural concrete surface. Special care was taken to smooth any areas where joints in the formwork may have resulted in a raised surface. Grinding was completed on all

surfaces where the sheets were to be adhered, both sides of the web, the soffit of the beam as well as the rounded corner. The depth of grinding was controlled visually by ensuring that the finer particles within the cement paste were exposed with an appearance similar to terrazzo. Once grinding was completed, the surface was cleaned using compressed air.

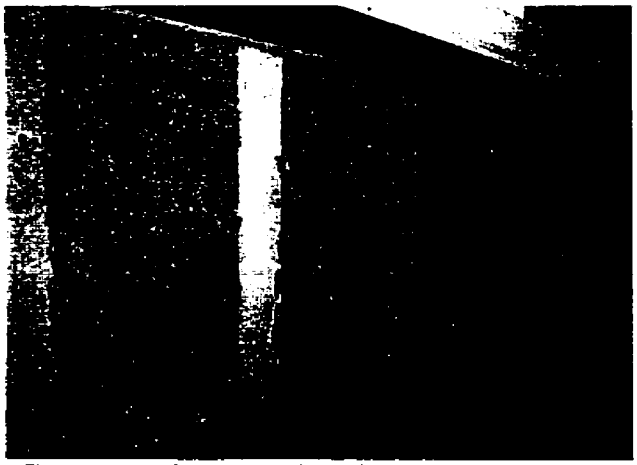

Figure 3.3.3a Concrete surface after grinding in strengthened shear span

Once the concrete surface was thoroughly cleaned, a low viscosity epoxy primer, was applied. By introducing epoxy within the fine pore structure of the concrete, a high bond strength is achieved between the FRP sheet and concrete surface. The epoxy primer was applied at a coverage of 5.5 m^2/L. Although the ground surface of the beam was level and straight, the grinding process exposed many larger pores that were too large to be filled with the low viscosity primer. Non-sag paste epoxy putty with a high viscosity was used to fill these voids, achieving a smooth uniform surface. The application coverage for the epoxy putty was at a rate of 0.3 m^2/L. The putty was applied by trowel to achieve a uniform surface, and was applied within two days of the primer application as recommended by the manufacturer.

Application of the FRP sheets followed hardening of the putty. The FRP sheets were cut in length and then cut in half along the fibre direction to achieve the desired sheet width. The final step was application of the saturant to the beam, using a thick nap roller, into which the dry fibre sheets were pressed into the saturant in the desired location and orientation. After allowing the sheets to set a short time, an overcoat of the same saturant was applied to the sheets

completing the strengthening. The average amount of saturant used for both coats was 1.4 m^2/L.

Testing did not commence for a minimum of seven days after application of the FRP sheets to allow curing of the epoxy to take place. Curing took place at room temperature. The entire strengthening process took place with the beam in its final orientation. That is, the beam was not flipped upside down to make the strengthening work more accessible.

3.3.4 Material Properties

The concrete used for the beams in this series was supplied by Lafarge Canada Inc. and delivered to the laboratory by transit mixer. Casting was done in the lab using plywood forms. The target twenty-eight day compressive strength for the concrete was 40 MPa. The concrete had a slump of approximately 100 mm and a maximum aggregate size of 12 mm. Two different batches of concrete were used. Six cylinders with a diameter of 152 mm were cast for the first batch and three cylinders were cast for the second batch. These cylinders were later tested in compression on the day of testing to determine the concrete strength.

Steel transverse reinforcement as well as the compression longitudinal reinforcement consisted of deformed steel reinforcing bars that were 11.3 mm in diameter. These bars conformed to Canadian Standards Association standard G30.18, allowing a minimum tensile and compressive yield strength of 400 MPa with a stiffness modulus of 200 GPa. The longitudinal tension reinforcement utilized seven-wire prestressing strand conforming to CSA G279. The diameter of this strand was 15.24 mm with an ultimate tensile strength of 1860 MPa and a stiffness modulus of 190 GPa.

Unidirectional glass fibre sheets (MBrace EG 900) from Master Builders Technologies of Cleveland, Ohio were used for shear reinforcement of

beam A-G. According to the information provided by the manufacturer these fibres have a tensile strength of 1730 MPa with a tensile stiffness modulus of 72.4 GPa (Master Builders Technologies, 2001). Ultimate tensile elongation is 2.0%. The effective sheet thickness is 0.353 mm and the supplied sheet width was 500 mm. These sheets were cut to length and cut in half along the direction of the fibres to achieve a sheet width of 250 mm for application to the beam.

Replark type 20 unidirectional carbon fibre sheets from Mitsubishi Chemical of Japan were used for beams B-C and C-C. These sheets use Dialead fibres that are coal tar pitch based. The manufacturer reports a tensile strength for these fibres of 3400 MPa with a tensile stiffness modulus of 230 GPa (Mitsubishi Chemical Corporation, 2001). Ultimate tensile elongation is 1.5%. The effective sheet thickness is 0.111 mm and the sheets used were 250 mm in width.

Regardless of the fibre type, the epoxy resins used were part of the MBrace system. The properties of the resins used are the same as those listed in the material properties for the Series A prestressed girder tests.

3.3.5 Test Set-up

The beams, spanning 5000 mm, were subjected to a four-point flexural bending test with two equal loads applied symmetrically about the centre of the beam. Both shear spans were 1500 mm in length and the constant moment region was 2000 mm in length. This gave a shear span to effective depth ratio of 2.91. Rollers were used at both supports and both load points. Figure 3.3.5a shows the configuration of the test set-up. The load plate was 75 mm by 500 mm across the width of the flange and the support plate was 200 mm long and accommodated the full width of the beam soffit. Plaster was used to distribute the load from the steel to the concrete at both load points and at the supports.

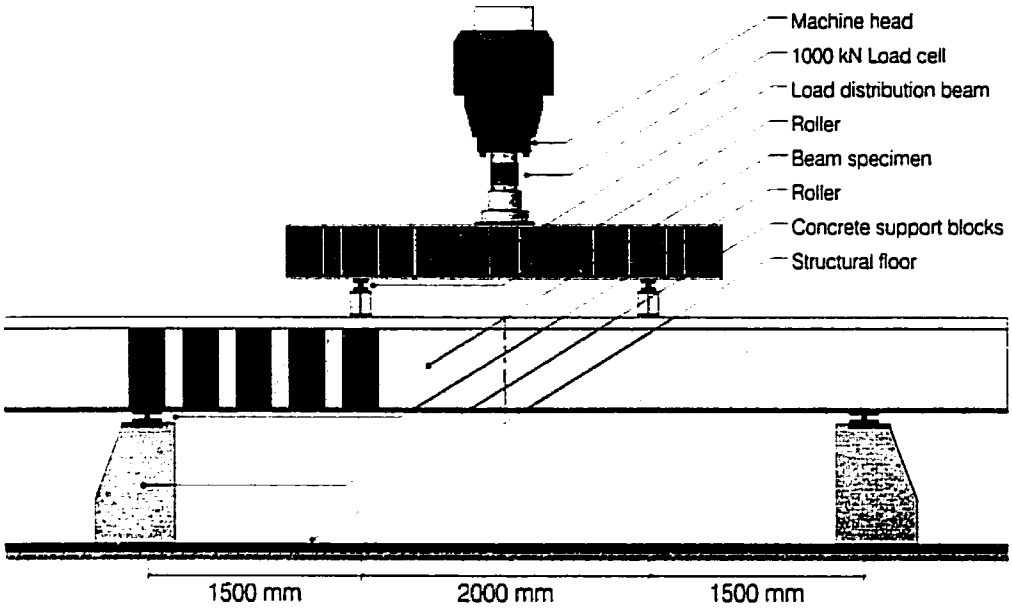

Figure 3.3.5a Test set-up for Series B beams

A 5000 kN capacity testing machine was used to apply the monotonic static load with the load range governed by the 1000 kN capacity of the load cell. The range for the machine stroke was 200 mm. All tests in the series were performed under conditions of stroke control. The stroke rate prior to flexural cracking of the concrete was 0.3 mm/minute. After cracking, the rate was increased to 0.5 mm/minute.

3.3.6 Instrumentation

All the beams in this series were instrumented with three linear voltage displacement transducers (LVDTs) to monitor deflection. One LVDT was placed at each of the load points and another was positioned at midspan. Electrical strain gauges were used at various locations on the FRP sheets to measure localized strain over a small gauge length (6 mm). Twenty-one gauges, 6 mm in length, were oriented in the direction of the fibres and positioned as shown in Figure 3.3.6a. These strain gauges had a resistance of 120 ohms and were of the same type as those used in the Series A tests. Eight electrical strain gauges were also bonded to the transverse steel reinforcement prior to casting,

and were positioned as shown in Figure 3.3.6b. These gauges were protected with waterproofing prior to casting.

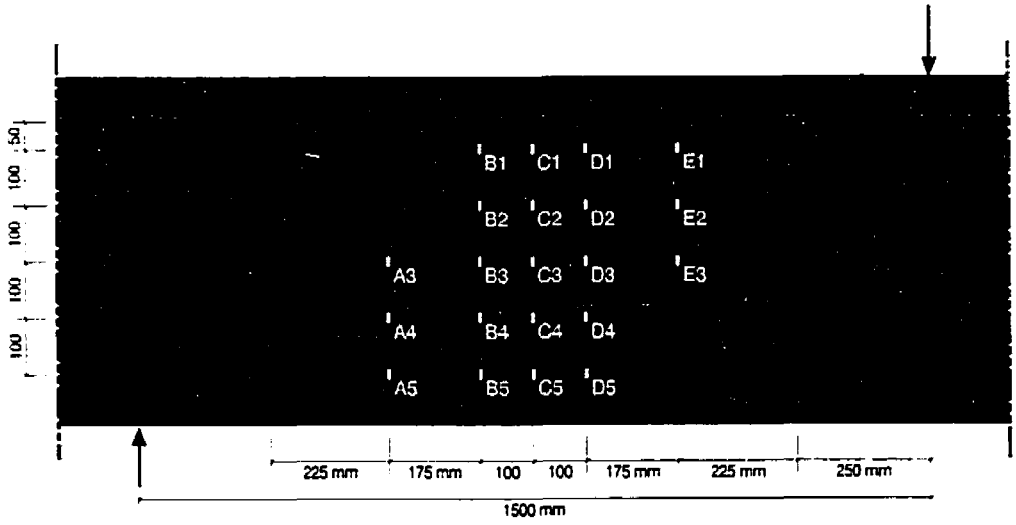

Figure 3.3.6a Locations of vertically-oriented strain gauges on FRP sheets

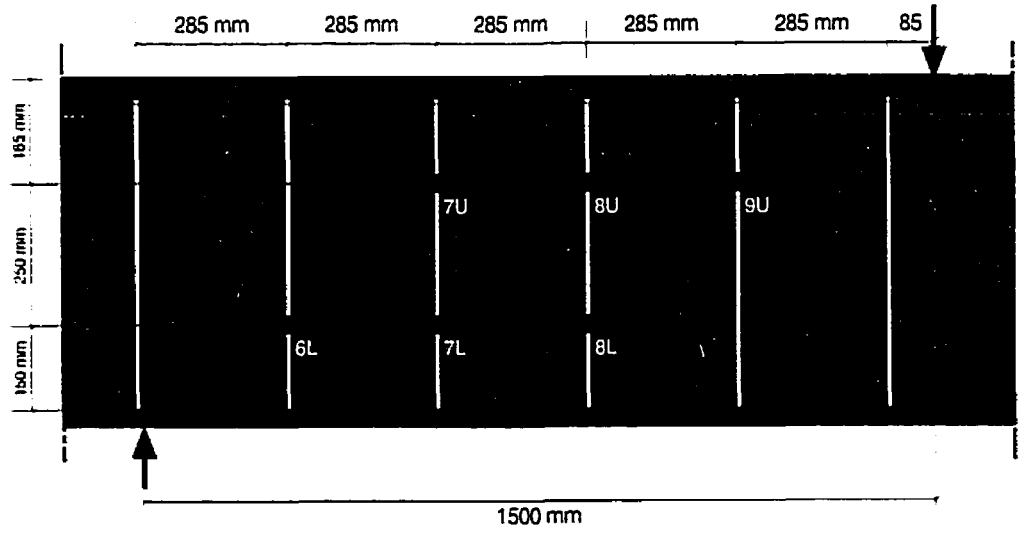

Figure 3.3.6b Locations of internal strain gauges on steel stirrups

Strain gauge type displacement transducers were used to measure vertical strain over a 200 mm gauge length. They were positioned either on the surface of the FRP or directly to the concrete as shown in Figure 3.3.6c. Two additional

displacement transducers with a 300 mm gauge length were used to measure longitudinal strain at the centre of the span within the constant moment region. One gauge was positioned 15 mm above the top surface of the beam and the other positioned horizontally on the web, 450 mm below the bottom of the flange approximately at the level of the longitudinal reinforcement. Data was recorded through a ninety-six-channel data acquisition system using a Pentium II processor and Labview software. All gauges plus the machine load and stroke were recorded at a frequency of 1 Hz for the duration of the test. Loads were monitored with a 1000 kN capacity load cell.

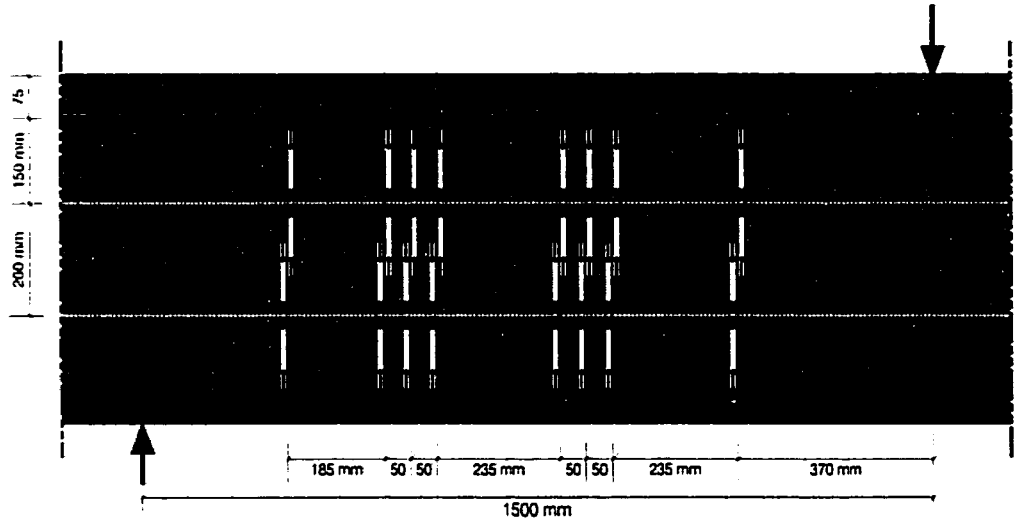

Figure 3.3.6c Locations of strain gauges with a gauge length of 200 mm

4. EXPERIMENTAL RESULTS AND ANALYSIS

4.1 Introduction

The experimental program was carried out in two phases. Both phases were designed to study the size effect of full-scale members strengthened for shear using FRP sheets. In particular, the modes of failure, the bond behaviour of the FRP Sheets and the shear contribution provided by each component were examined in detail.

The first phase, Series A, utilized a prestressed concrete girder with an overall height of 1850 mm that was originally intended for use in a Winnipeg bridge and donated by Lafarge Canada, Inc. Cut into three segments, the girder was utilized in three separate tests using beam specimens designated END-U, END-S and MID-S. The first beam specimen tested, END-U, was not strengthened with FRP and was used as a control specimen for comparison with the results of the next two tests. The second beam, specimen END-S, was strengthened with vertical unidirectional CFRP sheets applied perpendicular to the longitudinal axis of the beam. The final beam specimen tested in Series A, MID-S, was taken from the middle of the original girder and was symmetric about its centre line. This beam specimen was also strengthened with vertically applied uniaxial CFRP sheets, but in addition, horizontal CFRP sheets were applied within the web of the beam.

The second phase, Series B, utilized reinforced concrete beams that were fabricated in the laboratory. In this series, the concrete section properties, the flexural reinforcement, the steel transverse reinforcement and the loading condition were all kept constant. The only difference among the specimens was in the externally applied shear reinforcement. The three beams were fabricated, using either unidirectional glass fibres or unidirectional carbon fibre, as signified by the second letter of their designation. The first beam, A-G, utilized GFRP sheets applied perpendicular to the longitudinal axis of the beam at a spacing of

375 mm on centre. The second beam, B-C, used a sheet spacing identical to that of beam A-G, but with CFRP sheets. Beam C-C was identical to beam B-C except for an additional horizontal sheet that extended the length of the shear span just under the flange of the beam.

4.2 Series A: Prestressed Girder Tests

4.2.1 Material Properties

After testing of the beam specimens, concrete cores were taken from the undamaged end-block of the beam according to ASTM C42-90. These cores were drilled horizontally through the outer layer of mild steel reinforcement over the support of the untested shear span at mid-height of the specimen. The length of the core drilled out of the beam was longer than necessary so that any reinforcement within the core could be removed when cutting the cores to their final length for testing. The final length of the sulphur-capped cores was twice their diameter.

In total, three cores, 100 mm in diameter, were taken from beam END-U. These cores were tested in a cylinder-testing machine in a dry state within two days after the time of the beam test. The average strength for these cores was 97.5 MPa. It has been found that the insitu strength of concrete is larger than the core strength due to damage and microcracking sustained in drilling cores, partially bonded aggregate in concrete cores, and different placing and compaction methods. Factors of between 1.06 and 1.08 have been suggested in determining the equivalent cylinder strength from the core strength (Bartlett and MacGregor, 1994 and McIntyre and Scanlon, 1990). Using a factor of 1.06, this results in an equivalent cylinder strength of 103.3 MPa for this beam specimen. Note that this is double the design twenty-eight day concrete strength of the bridge girder of 50 MPa.

Similar to beam END-U three concrete core samples were taken from the end block of beam END-S. The average strength of the three cores was 99.1 MPa. Since all of the cores in this series of testing were from the same girder and the age of the girder concrete is greater than five years, the concrete strength is not expected to vary appreciably between specimens or over time between tests. Therefore, the overall average of all cores can be taken as the concrete strength for each of the beams in this series. The average of the six cores was found to be 98.3 MPa resulting in an equivalent concrete cylinder strength of 104.2 MPa.

4.2.2 Load-Deflection Behaviour

The first two tests both used the end specimens of the original bridge girder, thus their stiffnesses could be directly compared except for the fact that the loading condition was changed slightly for the second test. As discussed in Chapter 3, the first test utilized four-point loading, with a transfer beam spanning 1200 mm to transfer the point load applied by the testing machine into two equal point loads on beam END-U. Testing of beam END-S utilized three point loading, with the testing machine directly applying the full load to the beam. Deflection was measured for beam END-U at each of the two loading points. For beam END-S deflection was recorded on each side of the single load point. The stiffness of beam END-U was calculated based on the deflection at both of the load points. An average of the two calculated stiffnesses was taken and an equivalent deflection was calculated assuming the case of three-point loading had been used in the test. For beam END-S the deflection is taken as the average of the two deflection measurements that were taken at either side of the load point. These load-deflection relationships are shown in Figure 4.2.2a. It can be seen from this figure that despite the change in loading condition, the response for the two tests were comparable.

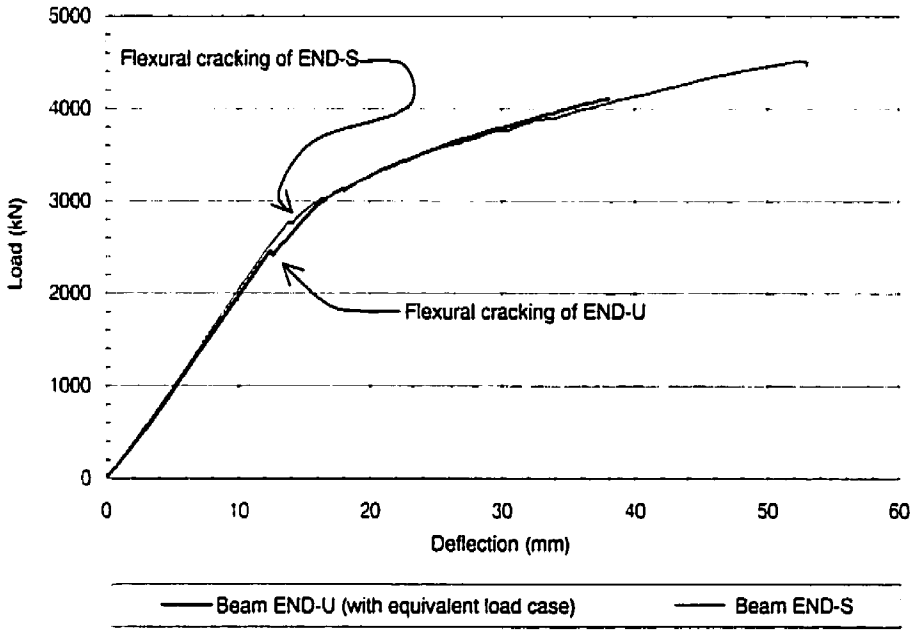

Figure 4.2.2a Load versus deflection at the load point for beam END-U with equivalent load case as strengthened beam END-S

As expected, the stiffness did not vary greatly for the two beams, but it can be seen that flexural cracking did occur at a slightly lower load for beam END-U than for beam END-S.

Results for beam MID-S are not directly comparable since the stiffness of the section was affected by the larger depth of the prestressing strands, the single cross section shape and the change in span for this test. Figure 4.2.2b shows the load-deflection curve for this beam.

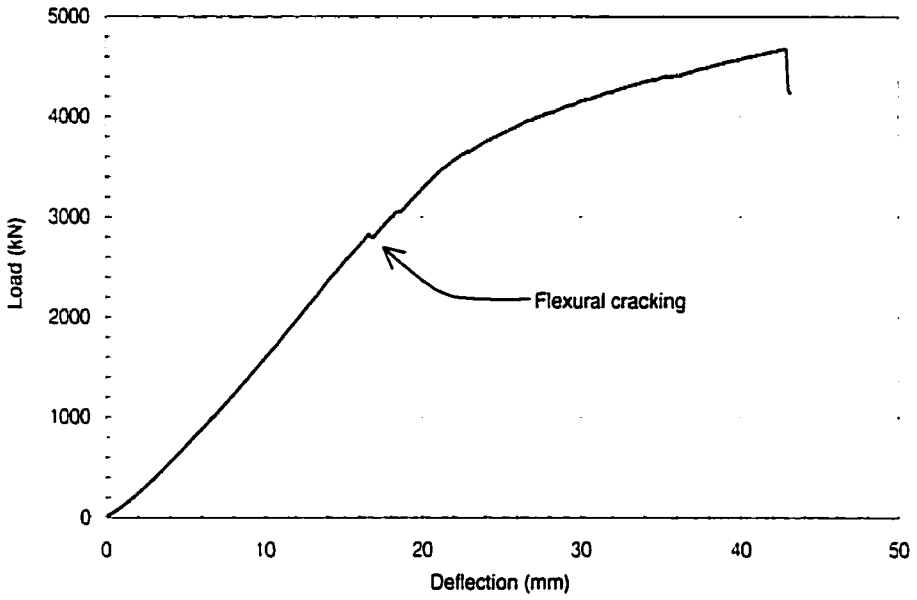

Figure 4.2.2b Load versus deflection at the load point for beam MID-S

4.2.3 General Behaviour and Failure modes

4.2.3.1 Beam END-U

The unstrengthened beam END-U exhibited the first flexural crack at a moment of 6775 kN-m and shear force of 1530 kN. This is compared with the predicted cracking moment of 7900 kN-m calculated using strain compatibility and the concrete compressive strength as determined through core testing.

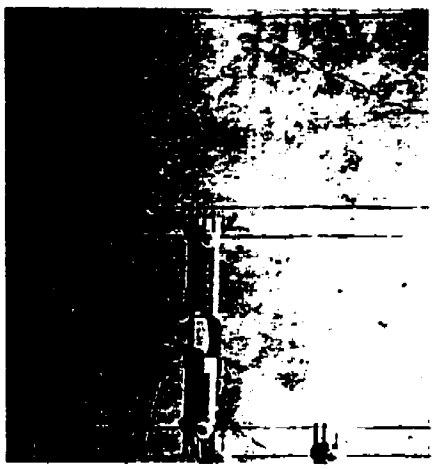

Figure 4.2.3.1a Initial cracking of beam END-U

Small web-shear cracks in the shorter shear span were first visible corresponding to a shear force of 1805 kN. Three cracks initially developed at an angle of 23 degrees, each of which passed through one of the holes drilled to reduce the effectiveness of the transverse reinforcement. These cracks were spaced

approximately 200 mm apart, measured perpendicular to the crack. Figure 4.2.3.1a shows three such typical cracks.

Increasing applied load resulted in increased the crack widths, followed by considerable additional cracking parallel to the cracks formed earlier. The degree of cracking that had developed at a shear force of 2385 kN is shown in Figure 4.2.3.1b.

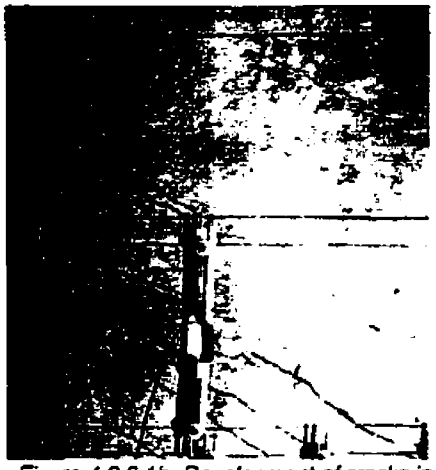

Figure 4.2.3.1b Development of cracks in beam END-U near failure

Shear compression failure occurred at a shear force of 2476 kN, when the failure crack was able to propagate through the compression flange to the load point. Crack angles through both the top and lower flanges remained at the same angle as the cracking that had first developed in the web. Figure 4.2.3.1c shows the crack causing failure in relation to both the support and one of the loading points.

Figure 4.2.3.1c Beam END-U after failure

4.2.3.2 Beam END-S

Beam END-S was strengthened with unidirectional CFRP sheets bonded to the side of the web and wrapped around the bottom flange. These sheets were oriented with the fibre direction perpendicular to the longitudinal axis of the beam. This beam was geometrically similar to beam END-U except that the load was applied at a single point. The same process of cutting stirrups to reduce the shear capacity of the section was undertaken as for beam END-U. Flexural cracking took place at a moment of 8175 kN-m and

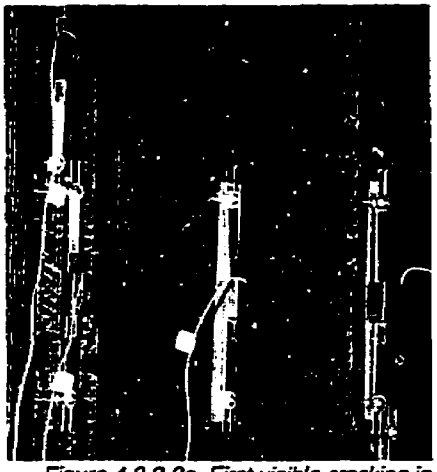

Figure 4.2.3.2a First visible cracking in beam END-S

shear force of 1685 kN, compared with a calculated value of 7900 kN-m.

Web-shear cracking was visible at a shear force of 2035 kN. Two web-shear cracks are visible in Figure 4.2.3.2a occurring at an angle of approximately 25 degrees. Crack width continued to increase with increasing load, but there was no peeling of the CFRP sheets at either the top or bottom interior corners of the I-section. Failure took place at a shear load of 2740 kN. The increase in shear force at failure was 10.7% above that of the unstrengthened section. However, the failure was the result of compression failure of the concrete at and directly below the load point. Figure 4.2.3.2b shows the concrete crushing underneath the sheets below the load point.

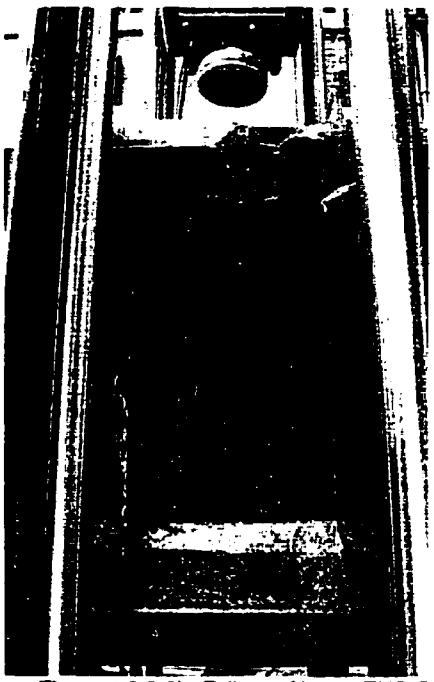

Figure 4.2.3.2b Failure of beam END-S

Figure 4.2.3.2c Cracking in the shear span of beam END-S (after removal of the CFRP sheets)

Although the failure was not in shear, there was considerable shear cracking prior to failure. After failure, the CFRP sheets were removed in order to more clearly observe the cracking. These cracks are visible in Figure 4.2.3.2c in the three light-coloured regions where the CFRP sheets were removed. Compared with the unstrengthened beam END-U, the cracks appeared finer and more closely spaced. Also compared to beam END-U, the cracks are significantly more distributed over the web with some steeper flexural-shear cracks occurring

near to the load point (on the bottom right of Figure 4.2.3.2c). There was no evidence of peeling at the interior corner of the tension flange as a result of the flexural-shear or web-shear cracks.

Figure 4.2.3.3a Beam MID-S after failure

4.2.3.3 Beam MID-S

Beam MID-S had, in addition to vertically oriented CFRP sheets, two horizontally oriented CFRP sheets that were applied underneath the vertical sheets at the top and bottom of the web. These sheets made visual observation of shear cracking difficult. Flexural cracking occurred corresponding to a moment of 7910 kN-m. Cracking was expected at a moment of 9115 kN-m using strain compatibility and the concrete strength determined from core testing. Shear compression failure occurred at a shear force of 2710 kN. The failure crack was 25 degrees in inclination as can be seen in Figure 4.2.3.3a.

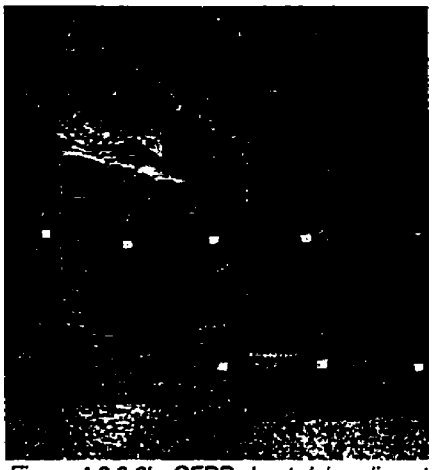

Figure 4.2.3.3b CFRP sheet debonding at the interior corner of beam MID-S

Some evidence of sheet debonding was observed at the interior corner at the bottom flange especially for sheets where the web-shear crack passed just

Figure 4.2.3.3c Cracking of beam MID-S in the shear span (after removal of the CFRP sheets)

above this corner. However, this peeling was largely restrained and did not prevent the FRP sheets from straining significantly This can be seen more closely in Figure 4.2.3.3b. The peeling of the vertical sheets was restrained somewhat by the horizontal sheets since a portion of the horizontal sheet remained bonded to the concrete and the two sheets remained fully bonded to each other. No peeling of the sheets was observed in the region where flexural-shear cracking was observed.

Just as with beam END-S, the sheets of beam MID-S were removed after failure. Figure 4.2.3.3c shows the distributed nature of cracking, with the primary web-shear crack. In addition, flexural-shear cracking is evident through the bottom flange, closer to the load point.

4.2.4 Strain Behaviour

4.2.4.1 Beam END-U

Beam END-U was instrumented with seventeen displacement transducers with a gauge length of 200 mm. Although the strain in the stirrups was not measured directly on the surface of the stirrups, it can be inferred from strains measured by gauges positioned on the concrete surface directly over one leg of the stirrups. Other gauges were located in between stirrups or at the location of a cut stirrup. A comparison of vertical strain measurements recorded at ultimate is provided in Table 4.2.4.1a based on the location of the gauge in relation to the stirrups. Average ultimate strain values are provided for all the 200 mm gauges on the web and for only the gauges precisely crossing the failure crack.

Table 4.2.4.1a Average ultimate strain (mS) at different positions on the web of beam END-U

Location	For all web gauges	For web gauges crossing the failure crack
At a stirrup	4.24	5.76
In between stirrup and a cut stirrup	6.64	8.13
At a cut stirrup	7.95	12.00

All of the strain measurements presented in Table 4.2.4.1a suggest that the stirrups were yielding at ultimate. In addition, it can be seen that the vertical strain increased with greater distance from a stirrup. Even for a beam with closely spaced stirrups, stirrups are discontinuities within the web concrete. As such, the web concrete is subjected to different magnitudes and direction of stresses relative to its proximity to a stirrup. The average vertical strain across the shear crack at failure was 8.20 millistrain, although the vertical strain in the web is sizeably different depending on the proximity to a stirrup.

The displacement transducers were positioned at five different heights along the web at the location of the potential failure crack. The maximum vertical strain for each depth was plotted against the applied shear force to illustrate the distribution of strain within the web along the failure crack in Figure 4.2.4.1a.

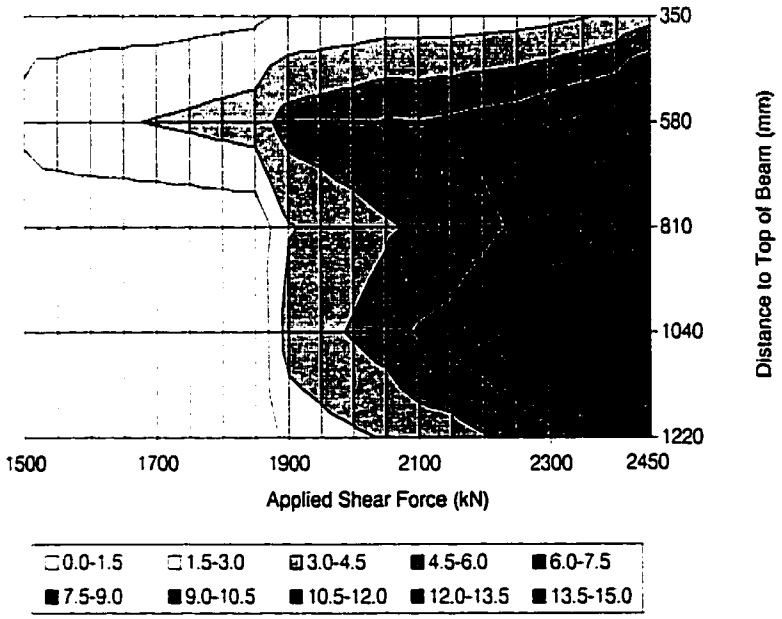

Figure 4.2.4.1a Maximum vertical strain (mS) at five depths on the web of beam END-U

It can be seen that strains approaching yielding were first observed at a height of 580 mm below the top of the beam commencing from an applied shear force of

approximately 1500 kN. The highest strains were recorded at 580 mm and 1040 mm from the top of the beam corresponding to the locations of the cut stirrups, as expected where the vertical strain in the concrete is highest.

4.2.4.2 Beam END-S

Beam END-S did not fail in shear so the magnitude of vertical strain at ultimate cannot be directly compared with that of beam END-U and the strains across the shear crack are expected to be somewhat smaller for beam END-S at ultimate. However, at loads below ultimate the behaviour of both beams may be directly compared. For beam END-S, six displacement transducers were attached directly to the concrete surface, while eleven were attached to the CFRP sheets. Considering the overall shear span, the average vertical strain at the ultimate flexural strength of the beam for gauges attached to the concrete and FRP is presented in Table 4.2.4.2a. It is suspected that the reason for the lower measurement of strain in the concrete is that most of the gauges attached to the concrete were not located at the largest shear crack and also several gauges attached to the concrete were lost during testing. The gauges attached to the fibres were more numerous and some were located directly over the primary shear crack. Strains in the FRP are quite localized, resulting in gauges directly over a shear crack recording large strains with others considerably lower. In particular, the highest three vertical strain measurements for the CFRP were 12.98, 9.75 and 9.08 millistrain over a gauge length of 200 mm. Strains along the potential failure crack were significantly higher than the effective strain proposed for design of 4.0 millistrain.

Table 4.2.4.2a Average ultimate vertical strain (mS) at different positions on the web of Beam END-S

Attached to	For all web gauges	For web gauges crossing the potential failure crack
Concrete	3.03	not available
CFRP sheet	5.87	8.20
Overall Average	5.11	not available

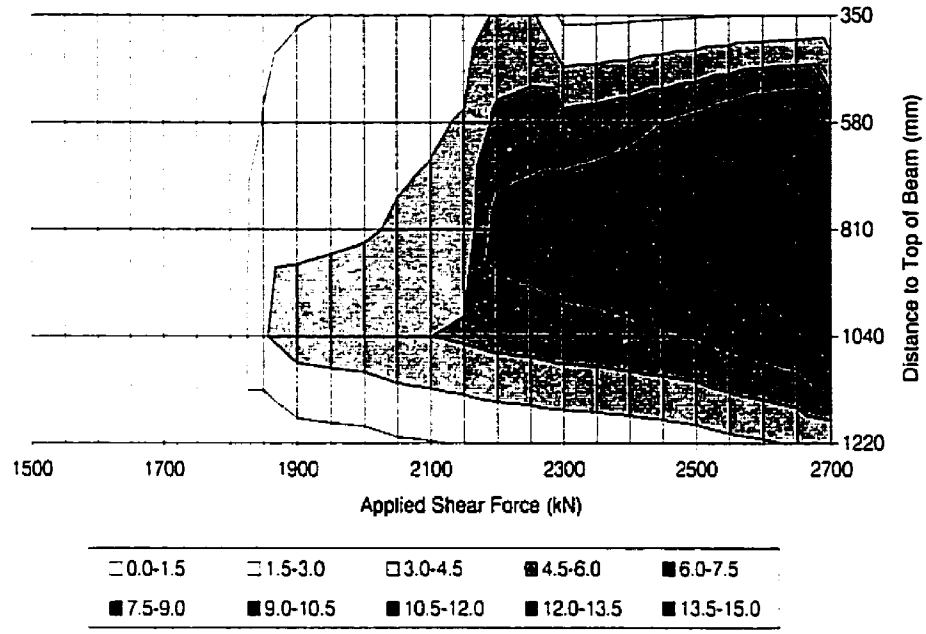

Figure 4.2.4.2a Maximum vertical strain (mS) at five depths on the web of beam END-S

The maximum vertical strain for each depth was plotted against the applied shear force to illustrate the distribution of vertical strain within the web along the failure crack in Figure 4.2.4.2a. For this beam, the yield strain was not reached until about 1850 kN, with the highest strains recorded at mid-depth of the web.

Strain gauges with a 6 mm gauge length were positioned in the direction of the fibres at three locations with 50 mm between the gauges to determine the profile of the vertical strain in the sheets. One location consisted of nine gauges positioned only on the web. The other two locations included gauges on both the web and the sloped portions of the bottom flange in order to determine how much strain could be developed in the CFRP sheet before it debonded and straightened at the interior corner between the web and the flange.

The first location of gauges, bonded only to the web at the location of the failure shear crack, are shown in Figure 4.2.4.2b. This figure shows the increase in

strain for the nine gauges with increasing applied shear force. It can be seen that two shear cracks formed in the web very suddenly at an applied shear force of 1850 kN, resulting in the sudden increase in strain to approximately 3.5 millistrain at this force. With increasing applied load, the strain increased more gradually until a shear force of 2200 kN, when a third crack formed near the lowest gauge positioned on the web. Again, the strain increased gradually after this point resulting in strains of 3.64, 6.17 and 7.94 millistrain for each of the gauges closest to the crack just before the ultimate shear force of 2739 kN was reached.

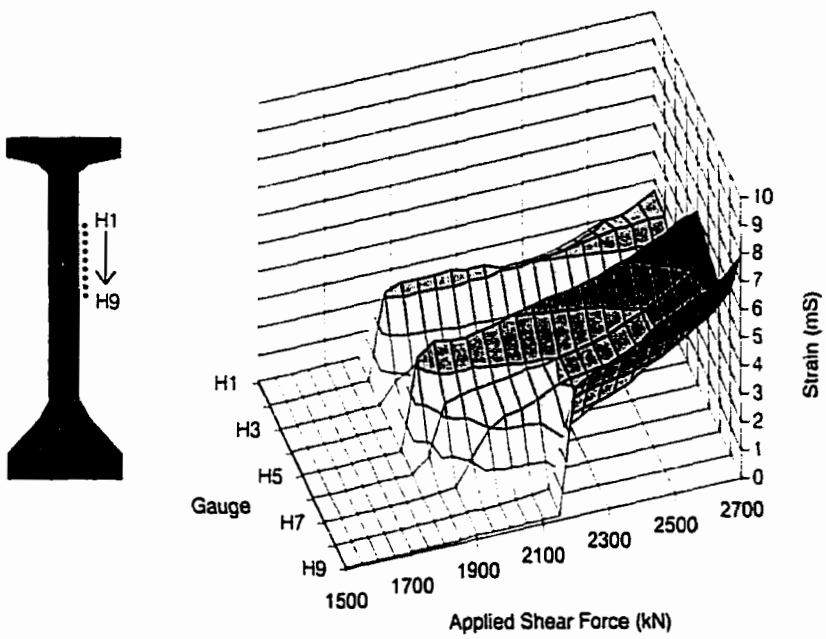

Figure 4.2.4.2b Vertical FRP strain for gauges bonded to the web of beam END-S

The next location of gauges on beam END-S included gauges attached to the web as well as to the two sloped regions of the bottom flange. Gauges I1 to I9 were positioned on the web, gauge I10 was on the first sloped portion of the bottom flange and gauges I11 and I12 were position on the second sloped portion. The strain recorded in these gauges at different load stages is shown in Figure

4.2.4.2c. As can be seen in this figure, cracking occurred at an applied shear force of 1850 kN and resulted in a sudden increase in strain for gauge I2 and a more gradual increase for gauges I3 and I4. The highest strain in these gauges is 7.96 millistrain, but even at this load there is no evidence of debonding which would be marked by a slope of zero between two adjacent gauges. Lower levels of strain were recorded near the bottom of the web in gauge I8 and on the lower sloped portion of the flange in gauge I11. The maximum strain of 3.64 millistrain recorded for gauge I11 was not high enough to induce strain in the adjacent gauge I10, nor to cause visible debonding at the interior corner of the section.

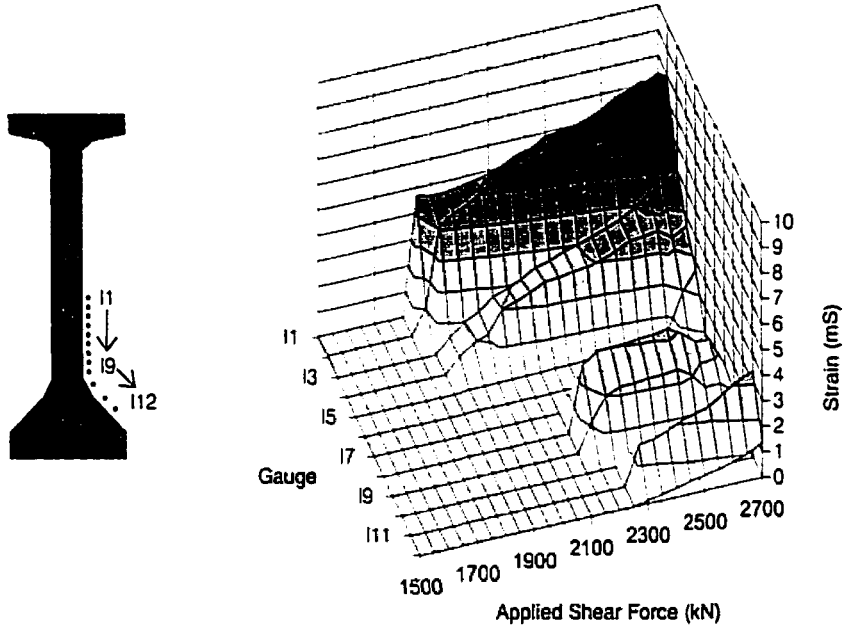

Figure 4.2.4.2c Vertical FRP strain for gauges bonded to the web and bottom flange of beam END-S

The third location of gauges for beam END-S consisted of seven gauges bonded to the web, one gauge on the first sloped part of the bottom flange and two on the lower sloped part of the flange. The strain recorded for these gauges is shown in Figure 4.2.4.2d. An increase in strain in the FRP began at a higher

applied shear force (1900 kN) due to the fact that the web-shear crack required a higher force to propagate down the web to the location of these gauges. In gauges J1 and J3 there is an early peak strain followed by a decrease before rising to ultimate levels. In both cases, this peak occurred just before the adjacent gauge began to strain. Once the force in the sheet could be distributed over a larger area, the strain at the initial locations dropped. A significant level of strain was recorded in the upper part of the bottom flange, but the level of strain was approximately constant as the shear force increased, and did not result in a significant increase in strain in the adjacent gauges. The peak strain reached in gauges J1 and J3 was 7.52 and 7.86 millistrain respectively.

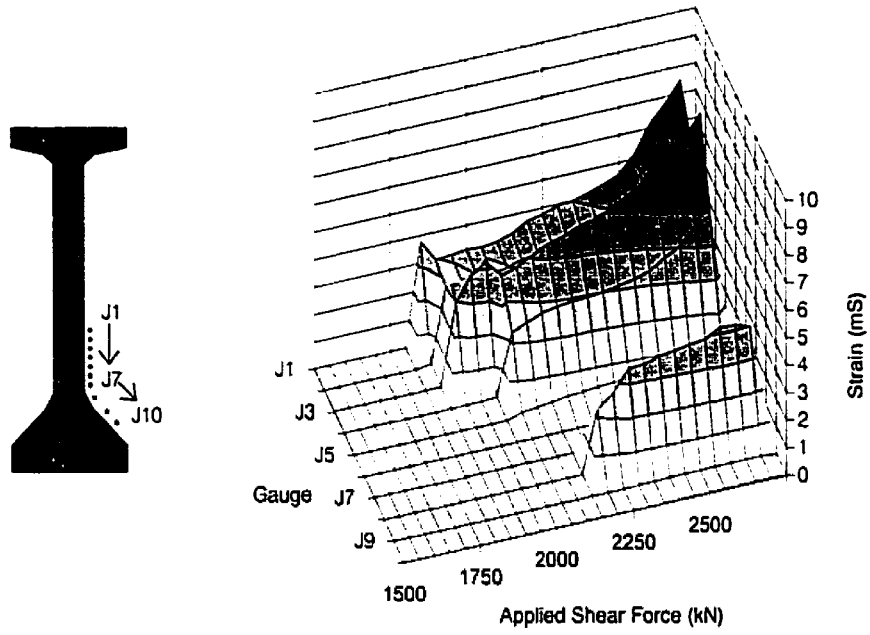

Figure 4.2.4.2d Vertical FRP strain for gauges bonded to the web and bottom flange of beam END-S

4.2.4.3 Beam MID-S

Eight displacement transducers were attached to the concrete surface of beam MID-S or to sheets oriented perpendicular to the direction of the gauge. Thirteen gauges were attached to the vertically oriented CFRP sheets. The average vertical strain at ultimate for these gauges is presented in Table 4.2.4.3a.

Table 4.2.4.3a Average ultimate vertical strain (mS) at different positions on the web of Beam MID-S

Attached to	For all web gauges	For web gauges crossing the failure crack
Concrete	9.17	11.84
CFRP sheet	5.39	5.67
Overall Average	6.82	8.14

The average strain at ultimate for gauges attached to the concrete was higher than for gauges attached to the CFRP sheets, considering all web gauges or just those crossing the failure crack. The highest three vertical strain measurements for the CFRP were 13.29, 10.89 and 7.04 millistrain for gauges occurring directly over the failure crack. Again, this is a significant percentage of the ultimate rupture strain as reported by the manufacturer. However, there was no evidence of rupture for either the horizontally or vertically applied CFRP sheets. The maximum vertical strain for each depth was plotted against the applied shear force to illustrate the distribution of vertical strain within the web along the failure crack in Figure 4.2.4.3a. Vertical strains were highest at the locations of the cut stirrups, just above and below the mid-height of the web.

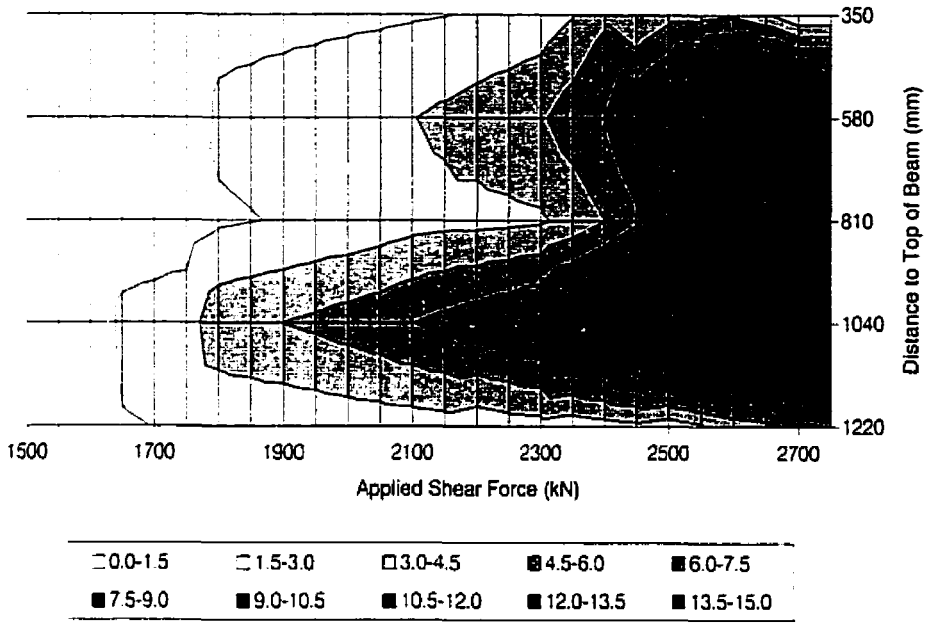

Figure 4.2.4.3a Maximum vertical strain (mS) at five depths on the web of beam MID-S

As with beam END-S, strain gauges with a 6 mm gauge length were positioned at three locations oriented in the direction of the fibres with 50 mm between the gauges to record a profile of the vertical strain in the FRP sheets. The strain in the gauges bonded to the web approximately at mid-height can be seen in Figure 4.2.4.3b. Gauges H5 and H6, which passed directly over the failure crack, recorded the highest strains. The strain at these two locations at ultimate was 8.35 and 8.62 millistrain, respectively. Significant strains were first recorded at an applied shear force of 1650 kN, followed by additional cracking lower on the web at a shear force of 1750 kN. The strain between these two cracks became almost constant, indicating little transfer of force to the concrete through bond action between these two cracks.

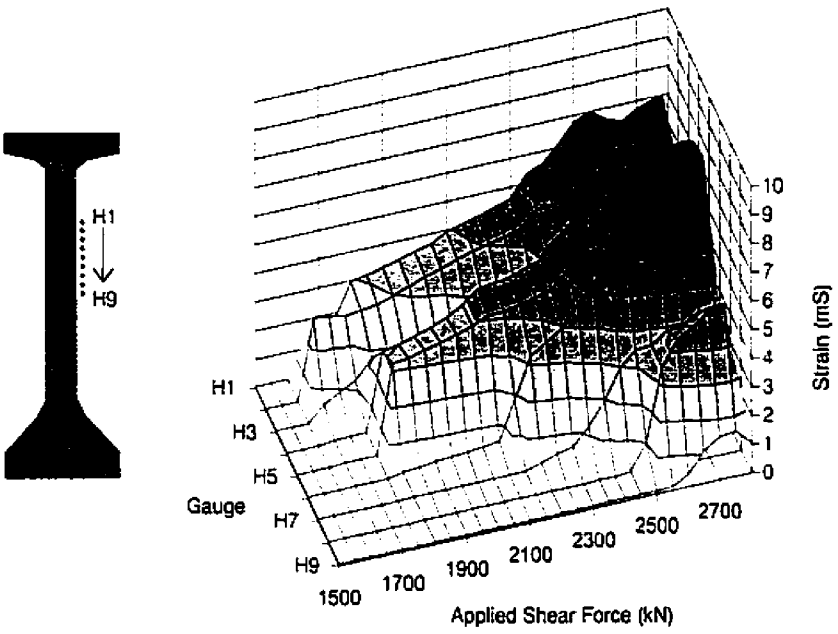

Figure 4.2.4.3b Vertical FRP strain for gauges bonded to the web of beam MID-S

The next series of gauges on beam MID-S included gauges attached to the web as well as to the two sloped regions of the bottom flange in the same arrangement as for beam END-S. The strain recorded in these gauges at different load stages is shown in Figure 4.2.4.3c. Significant strain was recorded starting from an applied shear force of 1650 kN. The maximum strain of 10.07 millistrain was recorded at the location of the failure crack. Strains in the gauges positioned lower on the web increased until an applied shear force of 2250 kN. After this point strains decreased due to debonding.

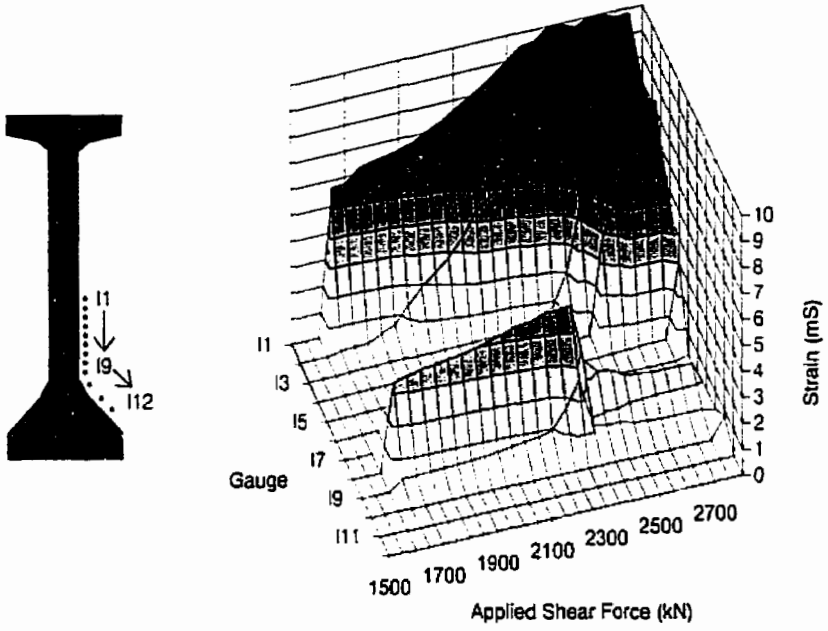

Figure 4.2.4.3c Vertical FRP strain for gauges bonded to the web and bottom flange of beam MID-S

For gauges positioned on the next sheet closer to the support, a similar phenomenon occurred with strain reaching a maximum at an applied shear force of 2300 kN. The strain in these gauges is shown in Figure 4.2.4.3d. At this load level, sheet debonding occurred at the interior corner of the section resulting in a lower strain level in this region while the strain further up the web continued to increase. After debonding, the strains were not completely uniform in the debonded region. This behaviour may be attributed to the fact that the horizontal and vertical sheets remained bonded together and the horizontal sheets remained bonded to the concrete further along the web. Even though the vertical sheet was debonded at the location of the gauge, the portion of the horizontal sheet that remained bonded restrained further straightening.

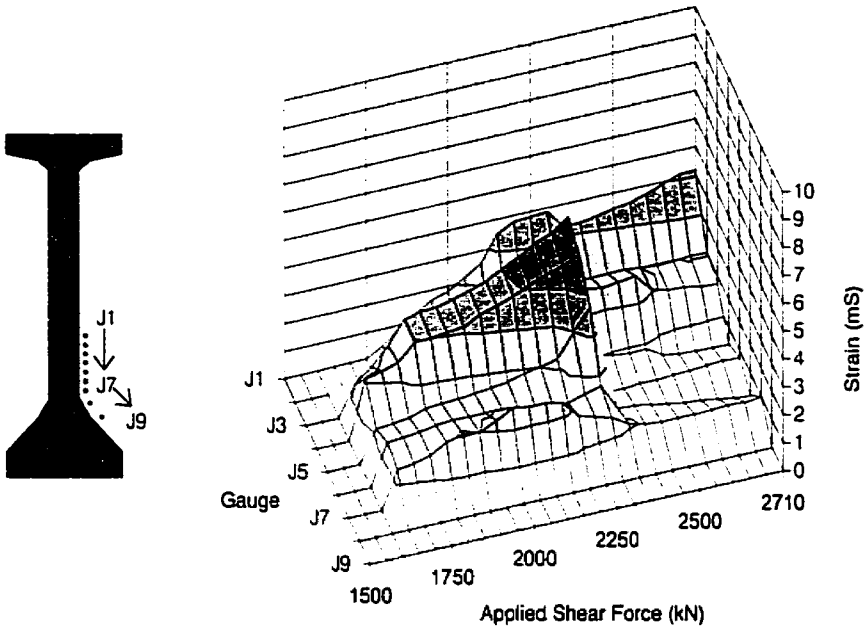

Figure 4.2.4.3d Vertical FRP strain for gauges bonded to the web and bottom flange of beam MID-S

4.2.5 Bond Behaviour

Beam END-S did not exhibit any visible signs of debonding, however a significant proportion of the ultimate tensile strain capacity of the CFRP sheets was developed. With the distance between strain gauges constant, the strain gradient was determined between several pairs of gauges. Values were calculated at the last point in which one gauge was had significant strain, while one of the adjacent gauges had nearly no strain. Following this transition point, the gauge with little strain became significantly strained at the next recorded increase in load. The calculated strain gradients are presented in Table 4.2.5a with references to the figures and gauge labels discussed in the preceding section.

Table 4.2.5a Calculation of strain gradient for beam END-S

Figure	Strained gauge	Unstrained gauge	Applied shear force (kN)	Strain gradient (10^{-6}/mm)
4.2.4.2c	I2	I3	2000	68.98
4.2.4.2c	I4	I5	2500	67.28
4.2.4.2d	J3	J4	2000	82.26
4.2.4.2d	J3	J5	2600	60.23
Average				69.69

Beam MID-S showed visible signs of debonding of both the vertical and horizontal CFRP sheets. The vertical sheets were restrained somewhat by the greater bonding area afforded by the horizontal sheets. The strain gradient was calculated between pairs of gauges in which an increase in strain of one of the gauges was about to occur. These values are presented in Table 4.2.5b. For this beam, the values are much more variable. It is uncertain if this is due to the restraining presence of the horizontal sheet. In this case the highest strain gradient occurred in a region away from the horizontal sheets but immediately over the failure crack.

Table 4.2.5b Calculation of strain gradient for beam MID-S

Figure	Strained gauge	Unstrained gauge	Applied shear force (kN)	Strain gradient (10^{-6}/mm)
4.2.4.3b	H5	H6	2100	72.08
4.2.4.3b	H6	H7	2200	58.80
4.2.4.3c	I8	I9	1650	58.92
4.2.4.3c	I1	I2	1750	120.00
Average				77.45

There were two cases of strain suddenly decreasing shown in Figures 4.2.4.3c and 4.2.4.3d. In the first case strain reached a peak of 5.00 millistrain at gauge I8 before dropping to about 2.0 millistrain then continuing to more slowly decrease to 1.5 millistrain. In the second case, strain reached a peak of 5.74 millistrain before suddenly dropping to approximately 2.5 millistrain. In both cases, this drop did not result in an increase in strain in the adjacent gauges as might be

expected, but a decrease in the highly strained regions with almost no change in the lightly strained regions. In both cases, gauges positioned at the interior corner of the section recorded no increase in strain at this point. This implies that the strain transfer to adjacent gauges due to debonding was equal to the strain reduction due to straightening of the CFRP sheet. The strain gradient that was present after debonding can only be explained by transfer of force to the horizontally oriented CFRP sheet.

4.3 Series B: T-Section Reinforced Concrete Beam Tests

4.3.1 Material Properties

Three concrete cylinders were made for each beam at the time of casting. These cylinders were tested in compression within a day of the beam test for each of the three beam specimens in this series. The results of these tests are presented in Table 4.3.1a.

Table 4.3.1a Results of concrete cylinder tests for Series B beam specimens

Beam	Cylinder	f_c' (MPa)
A-G	1	59.7
	2	55.1
	3	60.0
	average	58.3
B-C	1	51.7
	2	60.2
	3	58.5
	average	56.8
C-C	1	60.7
	2	48.3
	3	56.6
	average	55.2

4.3.2 Load-Deflection Behaviour

Even though the beams were cast from two batches of concrete, their load-deflection behaviour was very similar. As expected, the differences in the external shear reinforcement also had little effect on the stiffness behaviour of the beams, with the addition of a horizontal layer of FRP not increasing the stiffness significantly. Figure 4.3.2a shows the load deflection response at midspan for each of the three beams. Flexural cracking in all three beams occurred at a load of 70-80 kN, corresponding to a moment of 56 kN-m. This compares to a predicted cracking strength corresponding to a moment of 65 kN-m. After cracking the stiffness decreased but remained nearly linear until the late stages of loading.

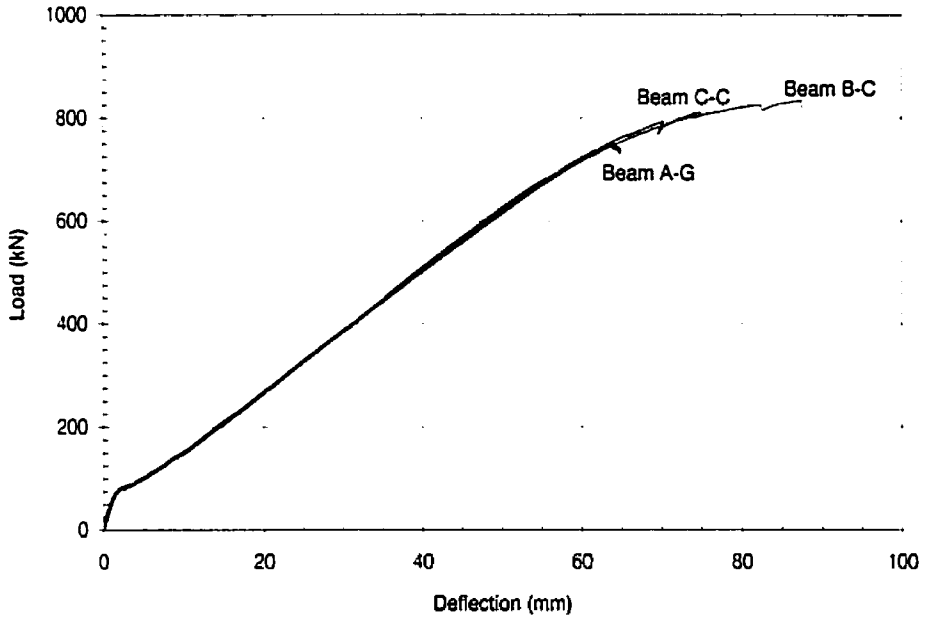

Figure 4.3.2a Load deflection behaviour for Series B beams

The moment-curvature response was also determined assuming a plane section in the constant moment region of the beam and using displacement transducers that were positioned longitudinally 15 mm above the top surface of the beam and on one side of the web approximately at the centre of gravity of the longitudinal

steel reinforcement. Although displacement transducers with a gauge length of 300 mm were used, since the flexural cracks were spaced approximately 250 mm apart in the constant moment region, the gauges were not long enough to average strains over the length of several cracks, and slight discrepancies are evident in the later stages of loading. Of course, this is only a problem on the tension side of the beam. In any event, the response was quite accurately determined using strain compatibility and using the stress-strain response given by Thorenfeldt, Tomaszewicz and Jensen in Collins and Mitchell (1997) as shown in Figure 4.3.2b.

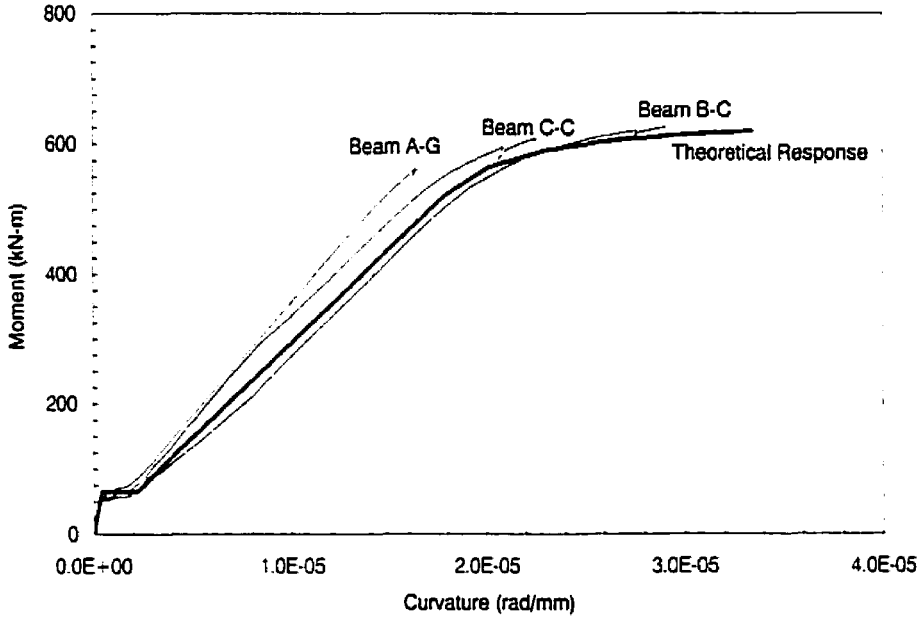

Figure 4.3.2b Moment-curvature response for Series B beams compared to theoretical response

4.3.3 General Behaviour and Failure Modes

Shear compression failure in the strengthened shear span was the mode of failure for each of the three beams as intended. A summary of the experimental results is presented in Table 4.3.3a. Failure was reached before any slip of the flexural reinforcement was observed.

Table 4.3.3a Test results for the Series B tests

Beam	f_c' (MPa)	Shear at flexural-shear cracking (kN)	Failure shear crack angle (degrees)	Ultimate shear strength (kN)
A-G	58	109	36	375
B-C	57	93	52	417
C-C	55	90	35	406

Flexural cracking was first observed in the constant moment region. As the load increased additional flexural cracks, propagating to flexural-shear cracks, occurred in both shear spans. The shear cracking load was determined based on an increase in the steel stirrup strain measured by strain gauges attached to the stirrups and an increase in the concrete strain where the displacement transducers were attached directly to the concrete.

4.3.3.1 Beam A-G

Beam A-G was reinforced for shear using GFRP sheets 250 mm in width spaced at 375 mm on centre. Fibre orientation was perpendicular to the longitudinal axis of the beam and the U shaped stirrup was one continuous sheet. In the strengthened shear span, steel stirrups were spaced at 285 mm (*0.55 d*), whereas in the unstrengthened span stirrups were spaced at 100 mm (*0.19 d*). Cracks were difficult to detect because they are rarely visible through the FRP sheets, only appearing in the gaps between the sheets. But at least three flexural-shear cracks were visible in the strengthened span at a shear force of 200 kN as shown in Figure 4.3.3.1a.

Figure 4.3.3.1a Flexural-shear cracks of beam A-G at an applied shear force of 200 kN (with cracks enhanced)

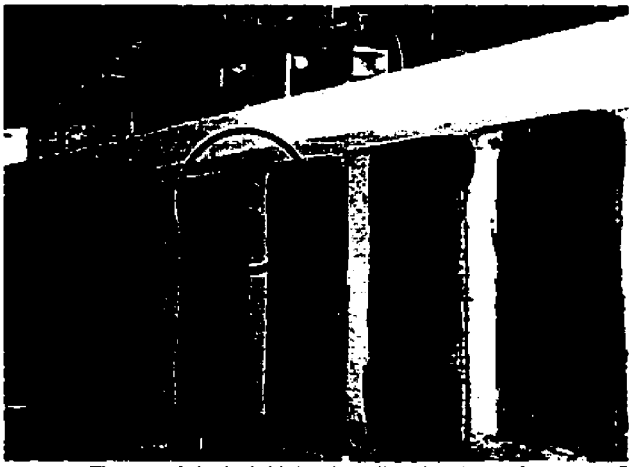

Figure 4.3.3.1b Initial debonding (circled) of beam A-G

As the load continued to increase, the crack width also became larger. At a shear force of 325 kN, debonding began to take place near the region where the shear crack met the compression flange, as shown in Figure 4.3.2.1b. Debonding progressed down the sheet in sudden steps as the debonding stress was reached in a particular area. Two of the stages before failure are shown

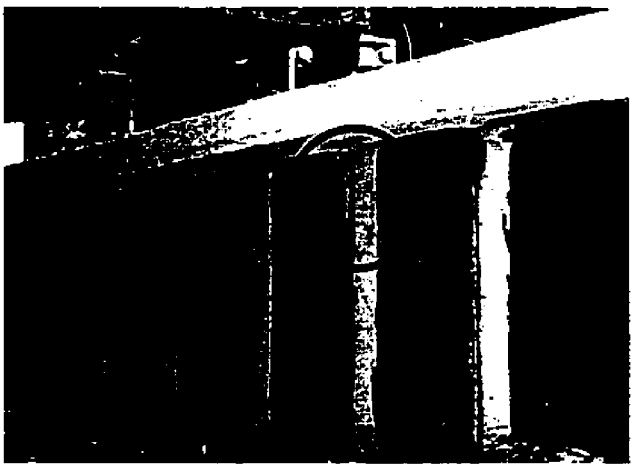

Figure 4.3.3.1c Progression of debonding (circled) of beam A-G

in Figures 4.3.3.1c and 4.3.3.1d. Once debonding had occurred, that region exhibited an increase in the number of cracks while at the same time existing cracks continued to increase in size. Failure occurred due to the sudden and complete debonding of the middle of five of the U-stirrups. Figure 4.3.3.1e shows failure occurring just as the U-stirrup dropped out of view beneath the frame and Figure 4.3.3.1f shows the beam after failure. Note that the primary failure cracks are the same as those viewed at earlier stages of loading. The failure crack was inclined at 36 degrees, passing through the middle of one stirrup and crossing one GFRP sheet.

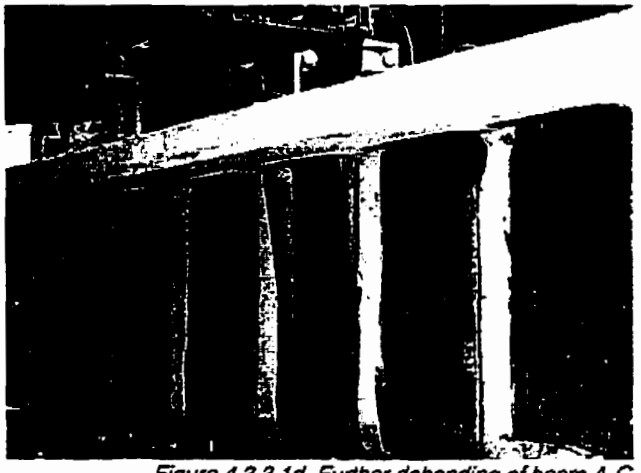

Figure 4.3.3.1d Further debonding of beam A-G

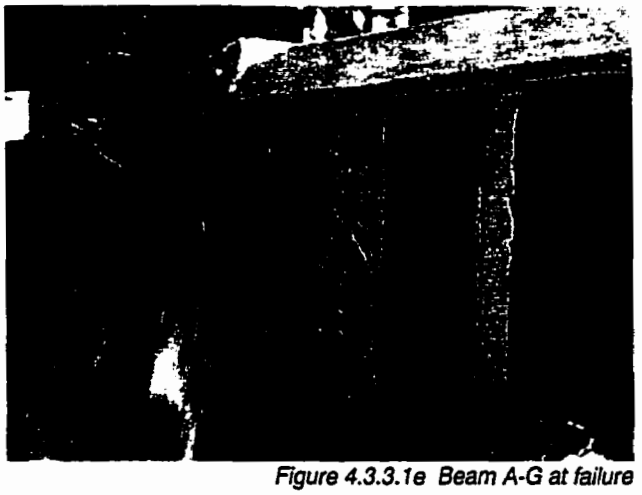

Figure 4.3.3.1e Beam A-G at failure

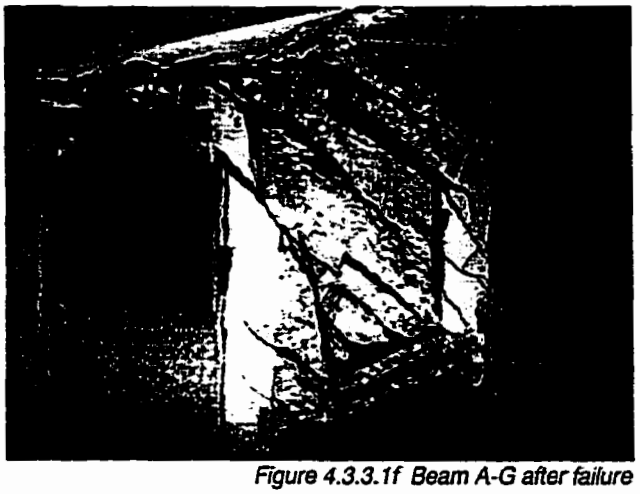

Figure 4.3.3.1f Beam A-G after failure

4.3.3.2 Beam B-C

Beam B-C was reinforced for shear using unidirectional CFRP sheets with the same spacing as the previous beam. Fibre orientation was again perpendicular to the longitudinal axis of the beam. Three cracks were initially visible at a low load level. The first area of debonding occurred at the same location as in the preceding test at the top corner of the second sheet from the left, as seen in Figure 4.3.3.2a. In this case the absence of cracking near the top of the third sheet allowed that sheet to remain fully bonded except for the top right corner. Instead of the failure crack passing through this sheet, a crack at a steeper inclination formed within the area on which the second sheet was bonded, shown in Figure 4.3.3.2b. The failure crack was found to have an angle of 52 degrees.

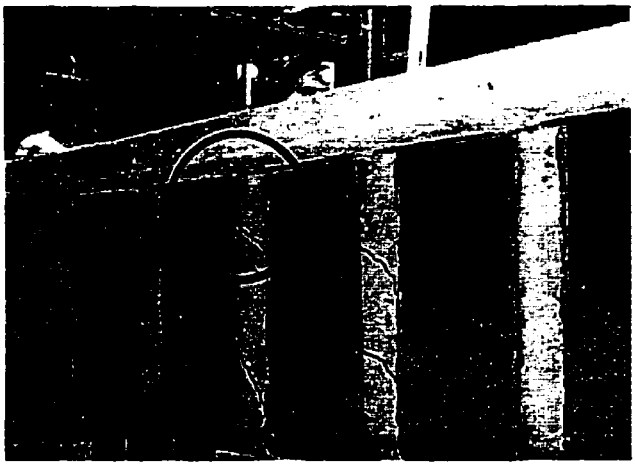

Figure 4.3.3.2a Beam B-C at start of debonding on the second sheet (with cracks enhanced)

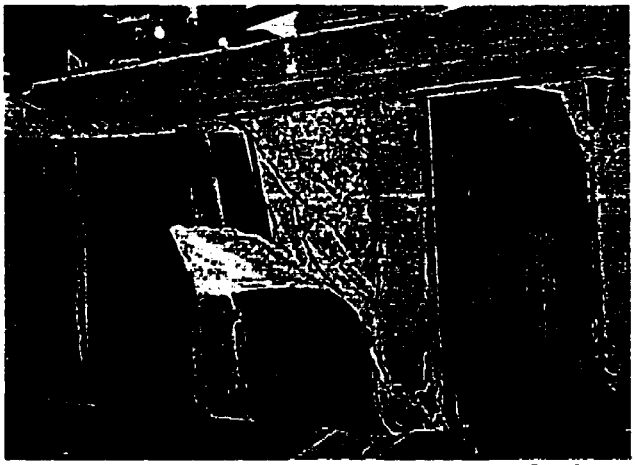

Figure 4.3.3.2b Beam B-C at failure

4.3.3.3 Beam C-C

An additional horizontal sheet of fibres was placed across the top of the web in beam C-C for the purpose of anchoring the vertical sheets and limiting the crack width of the concrete at the top of the web. Figure 4.3.3.3a shows the unusual behaviour as flexural cracks progressed up the web encountering the external reinforcement. This horizontal sheet was not able to improve the shear capacity of the section, with the total shear capacity just lower than beam B-C.

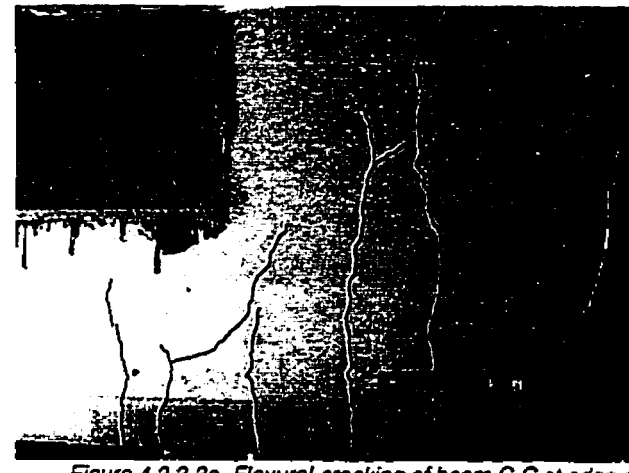

Figure 4.3.3.3a Flexural-cracking of beam C-C at edge of horizontal sheet (with cracks enhanced)

With the addition of a horizontal sheet, cracks were even more difficult to detect and even when a crack was visible near the bottom of the beam in the gaps between the FRP sheets it was difficult if not impossible to determine visually how far the crack continued up the web or whether its inclination varied. Figure 4.3.3.3b shows three visible cracks, one of which lead to the eventual failure shown in Figure 4.3.3.3c. Visual evidence of debonding was also difficult to determine, but at the later stages of loading a large area of debonding was determined under

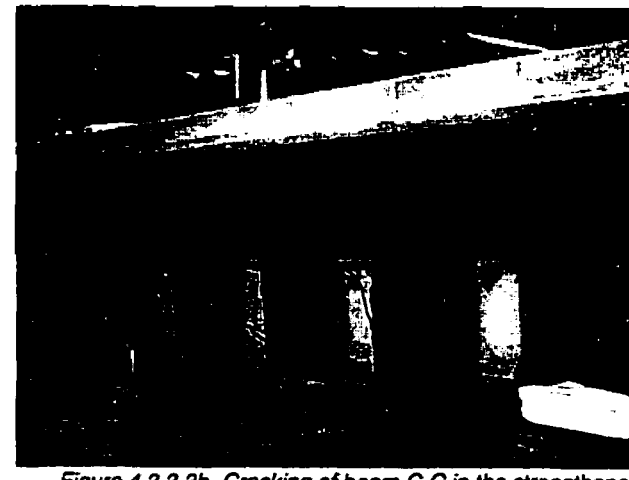

Figure 4.3.3.3b Cracking of beam C-C in the strengthened shear span (with cracks enhanced)

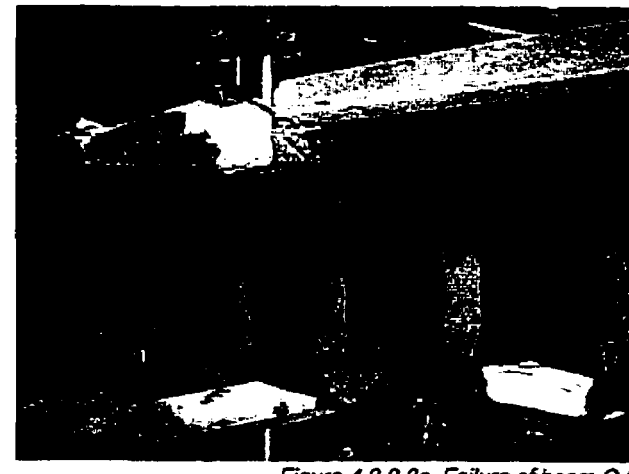

Figure 4.3.3.3c Failure of beam C-C

the third vertical sheet by tapping the sheet with a pencil. Similar to the chain method for determining the extent of spalled concrete, the tapping indicated a very large area of debonding that was at least the full width of the third sheet and down as far as the bottom of the horizontal sheet. It can be seen in Figure 4.3.3.3d that the final failure crack passed immediately through this region at an angle of 35 degrees. Sheets that were removed after failure showed good adhesion of concrete to the sheet, indicating that failure was within the outer layer of concrete as seen in Figure 4.3.3.3e.

Figure 4.3.3.3d Beam C-C showing failure crack passing underneath area of debonding

Figure 4.3.3.3e Underside of removed FRP sheet from beam C-C

4.3.4 Strain Behaviour

4.3.4.1 Average Strain Behaviour

Vertical strain was measured directly on the internal steel stirrups and on the surface of both the concrete and the applied FRP sheets for each beam studied. Six strain gauges were positioned at two depths on four of the internal steel stirrups in the critical shear span. Displacement transducers, at up to sixteen locations on the beam, were used to measure vertical strains on the concrete and the FRP surfaces over a 200 mm gauge length. In addition, localized vertical strain was measured at twenty-one positions for each of the three beams on various positions on the

FRP sheets. The locations of these gauges are described in greater detail in chapter three.

The internal gauges attached to the steel stirrups had a gauge length of 6 mm, and were attached to one leg of the two-legged stirrups. These gauges were found either on the upper part of the stirrup or lower on the leg. The maximum stirrup strains were considerably higher for the stirrups crossing the failure crack than for the remaining stirrups in the critical shear span. Table 4.3.4.1a shows the maximum stirrup strain recorded at the upper and lower levels of the stirrup. The gauge recording the stirrup strain at the upper part of the failure crack for beam C-C was damaged during fabrication so no measurement was possible at this location. The maximum strain in all cases was reached at the instant of failure.

Table 4.3.4.1a Average ultimate strain (mS) for stirrups crossing the failure crack

Location	Beam A-G	Beam B-C	Beam C-C
Upper part of leg	14.73	14.37	-
Lower part of leg	24.24	14.68	17.12
Average	19.48	14.53	-

Displacement transducers with a gauge length of 200 mm were positioned either directly on the concrete surface or on the external FRP reinforcement. The average strains form these gauges were used in this portion of the analysis in addition to local strains which are considered later. In determining the average strain in the shear span, the two highest ultimate strain measurements from the top half of the web were used together with the two highest strain measurements from gauges on the bottom half of the web. These results can be seen in Table 4.3.4.1b. In all cases where the gauge was bonded to the FRP sheets the strain for the gauges in the lower half of the web was higher than the gauges in the top half of the web. This was the result of debonding occurring at the top of the sheet reducing the average strain measurement at the top of the web.

There was no such pattern for gauges bonded to the concrete. Clearly, the vertical strain in the exposed concrete between the FRP sheets is significantly higher than the adjacent strain in the sheet. This was similar to the finding of the Series A beams where vertical strains were lower at stirrup locations than in between stirrup locations as well as locations in between the vertical FRP sheets. To take advantage of the non-discrete reinforcement provided by the FRP sheets, it may be beneficial to apply the FRP sheets with no gaps between them to improve the shear-cracking characteristics of the entire web.

Table 4.3.4.1b Average ultimate strain (mS) for 200 mm gauge length displacement transducers

Bonded to	Location	Beam A-G	Beam B-C	Beam C-C
FRP sheet	Upper web	5.45	6.59	6.24
	Lower web	9.45	9.42	8.87
	Average	7.45	8.00	7.56
Concrete	Upper web	13.10	12.74	11.73
	Lower web	12.58	7.56	13.53
	Average	12.84	10.15	12.63

As with the internal steel stirrups, gauges bonded directly to the concrete typically recorded their highest strain at the moment before failure. However, the gauges bonded to the FRP sheets showed a different response, with only the gauges on the lower part of the web recording their highest strain at the moment before failure. This is due to debonding of the sheets occurring near the top of the web before failure is reached. The point in the loading history when the strain reached its highest level was determined as a percent of the beam ultimate displacement. These values are included in Table 4.3.4.1c for the gauges attached to the FRP sheets.

Table 4.3.4.1c Point of maximum recorded strain as a percent of ultimate beam displacement for 200 mm gauge length displacement transducers

Bonded to	Location	Beam A-G	Beam B-C	Beam C-C
FRP sheet	Upper web	94.5%	87.7%	81.9%
	Lower web	99.3%	100%	100%
	Average	96.9%	93.9%	91.0%

4.3.4.2 Local Strain Behaviour

Localized strain measurements, occurring over a gauge length of 6 mm were used in determining an effective FRP sheet strain as well as behaviour near the shear crack locations. Typically the highest strains were found at mid-height of the sheet, but this varied somewhat in relation to the exact location of the shear cracks. Vertical strain measured near the bottom of the beam was lower due to the more vertical inclination of the flexural-shear cracks at this location. The lowest ultimate strain was measured over the region within 150 mm below the underside of the top flange. In this region, the highest strains were recorded some time before failure as observed with the large gauge length displacement transducers. After this point strains decreased because of debonding originating at the top of the sheet while strains over the lower portion of the sheet continued to increase.

Appendix A shows the progression of vertical strain over a series of load steps from just after cracking to just before failure for each of the three beams. For each beam, initially one diagonal crack is formed at an applied shear force between 100 and 125 kN. A second crack develops by an applied shear force of 200 kN and is located away from the first crack a distance equal to the stirrup spacing. It can be seen that the highest vertical strains in the FRP sheets at any load step are at the crack locations and that the strain is approximately constant along that crack. The strain distribution along the crack can be approximated by taking the maximum strain across each of the five rows instrumented with strain gauges. This allows a continuous record of vertical strain and applied shear force to be obtained.

Figure 4.3.4.2a shows the maximum strain in the GFRP sheets at five depths on the web of beam A-G. At least four gauges for each depth, across three different sheets, were used to determine the maximum strain. Initially, the vertical strain was first recorded at the middle of the web followed by straining at the top and

bottom of the web. Peak strains were reached at the top of the sheets at a shear force well below ultimate. After this, strain decreased at the top of the sheets, while increasing over the lower portion of the web. The highest strains recorded on the GFRP sheets were 11.23 and 12.33 millistrain. These strains were recorded at depths of 325 and 425 mm, respectively.

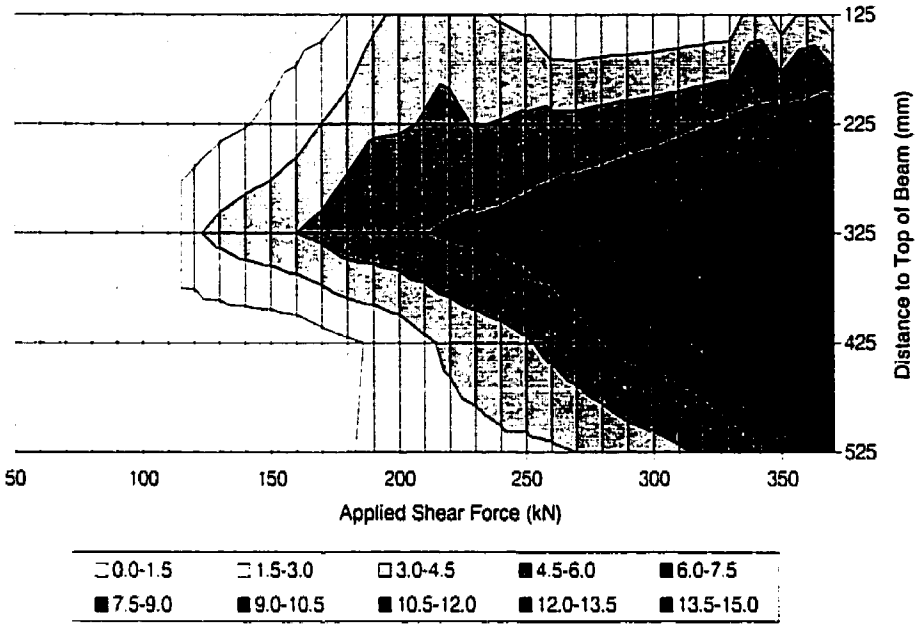

Figure 4.3.4.2a Maximum vertical strain (mS) at five depths on the web of beam A-G

The same procedure was used for used to determine the maximum strain for the CFRP sheets bonded to the web of beam B-C, shown in Figure 4.3.4.2b. Straining of the CFRP sheets began at a lower applied shear force than for beam A-G, just after flexural cracking began in the shear span. The peak strain in the gauges closest to the top of the sheet was 3.71 millistrain occurring at an applied shear force of 260 kN. The highest strains were again located at depths of 325 and 425 mm below the top of the beam, with strains of 11.74 and 11.56 millistrain. This is comparable to the strain reached in beam A-G.

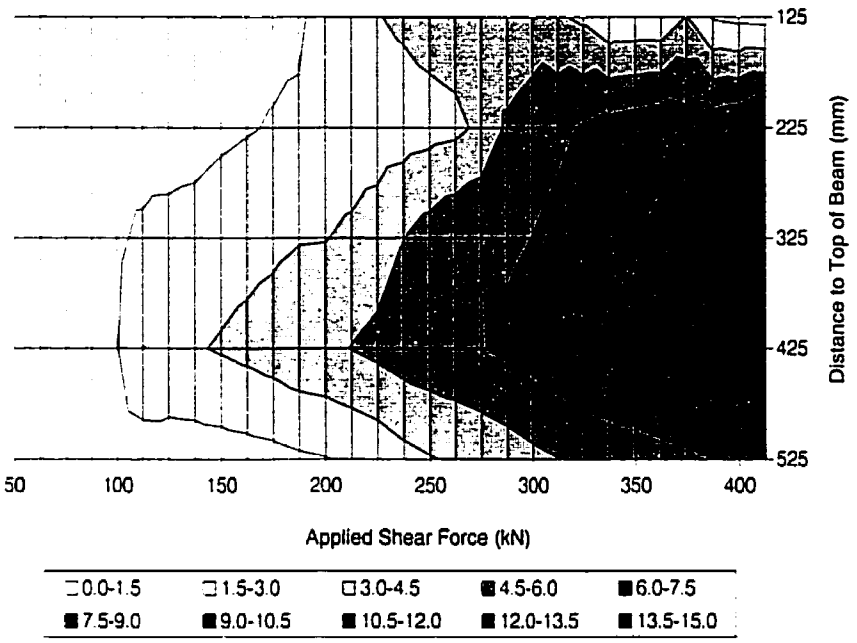

Figure 4.3.4.2b Maximum vertical strain (mS) at five depths on the web of beam B-C

Maximum vertical strain for the CFRP sheets bonded to the web of beam C-C is shown in Figure 4.3.4.2c. Vertical strain began to be recorded after 100 kN of applied shear force, as with beam B-C. However, unlike beam B-C, the strain at a depth of 225 mm did not begin to increase significantly until a load of 220 kN. One possible reason for the delay in vertical strain may be that the horizontal sheet may have further restrained the shear crack from progressing up the web. Maximum strain at the top of the sheet was higher than for the other beams indicating that the presence of a horizontal sheet may improve the bond in this location. However, bond failure was not completely prevented, as the sheet debonded after reaching its maximum strain at an applied shear force of 350 kN.

Very high strain measurements were observed at a depth of 325 mm, some of which were above the maximum tensile elongation reported by the manufacturer. It was unclear how this happened, but there may have been some effect due to the position of these gauges. All the gauges on this row and above

were bonded to the horizontal CFRP sheet that was placed over the vertical sheets. The results for the top two rows were consistent with the other tests. However, the gauges on at a depth of 325 mm were positioned just above the bottom of the horizontal sheet. Transfer of the longitudinal strain into the vertical sheets and subsequently into the concrete may have resulted in higher strains than typical due to the edge discontinuity of the horizontal sheet. These very high strains were only recorded near failure at an applied shear force above 360 kN.

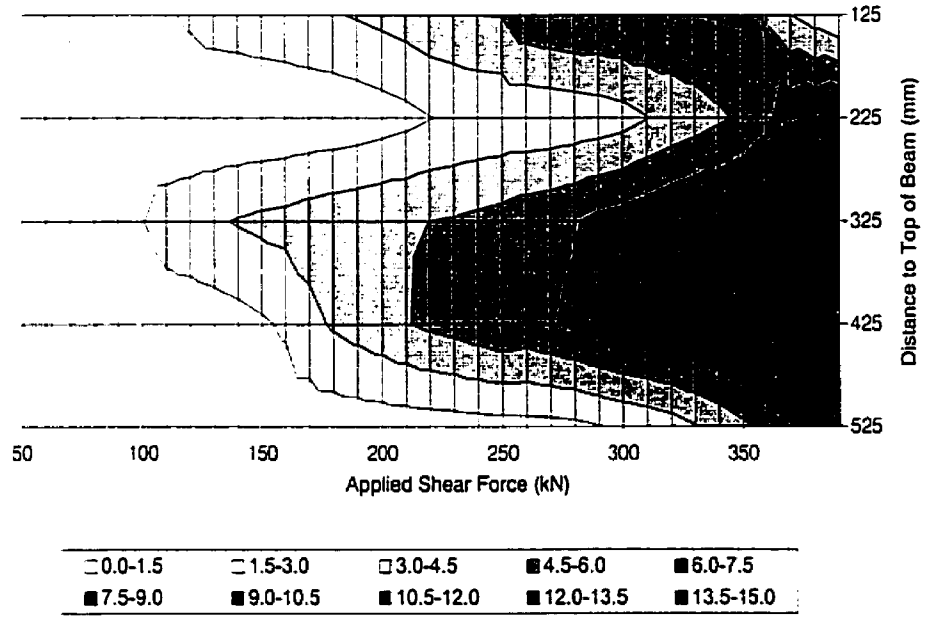

Figure 4.3.4.2c Maximum vertical strain (mS) at five depths on the web of beam C-C

To facilitate comparison of FRP strain measurements among the three beams, the average strain across each row for beams A-G, B-C and C-C was plotted except for the gauges positioned at the top of the sheets. These rows are located at depths of 225 mm, 325 mm, 425 mm and 525 mm and are shown as Figures 4.3.4.2d, 4.3.4.2e, 4.3.4.2f, and 4.3.4.2g. The strain across the top row at a depth of 125 mm is discussed later in the bond behaviour section.

Significant vertical strain was recorded at an applied shear force of about 100 kN for gauges at middle of the web, at a depth of 325 mm straining first, and gauges near the top of the beam, at a depth of 225 mm, straining last. The FRP strain in beam A-G was typically greater than the strain in the other two beams at higher load levels. It can also be seen that at a depth of 225 mm from the top, the vertical strain peaked prior to failure. Only in beam C-C did the strain increase again after the first peak.

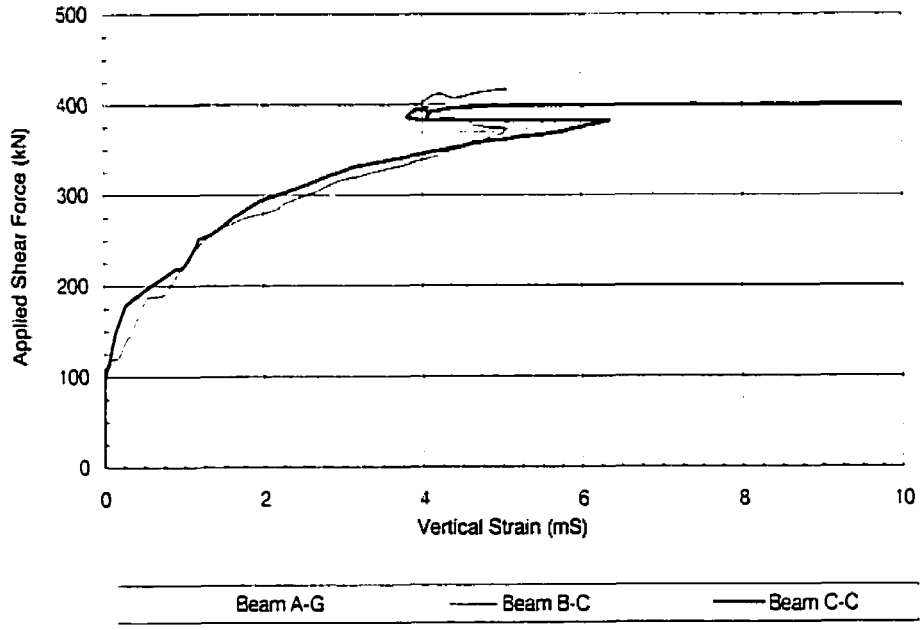

Figure 4.3.4.2d Average vertical strain at a depth of 225 mm for each of the Series B beams

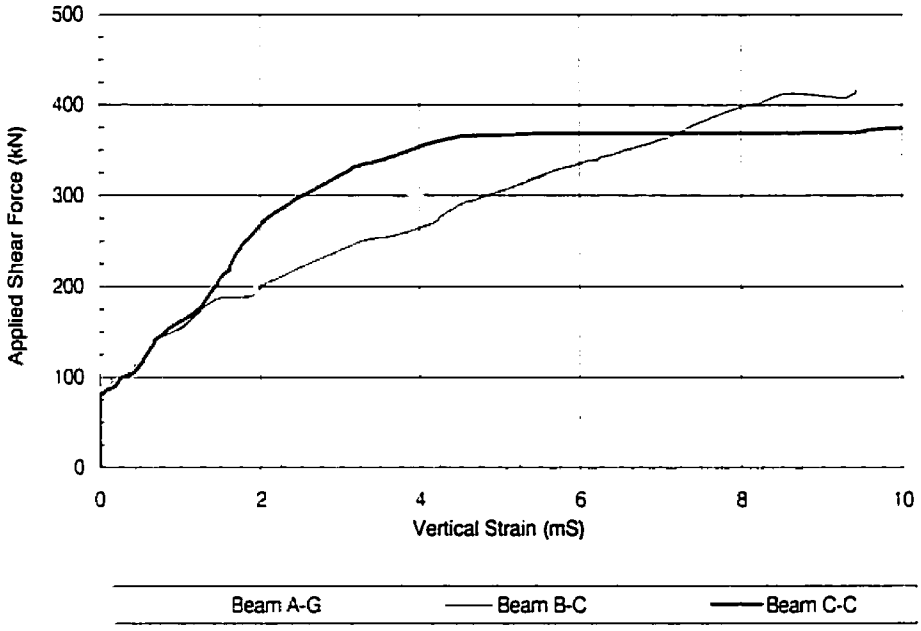

Figure 4.3.4.2e Average vertical strain at a depth of 325 mm for each of the Series B beams

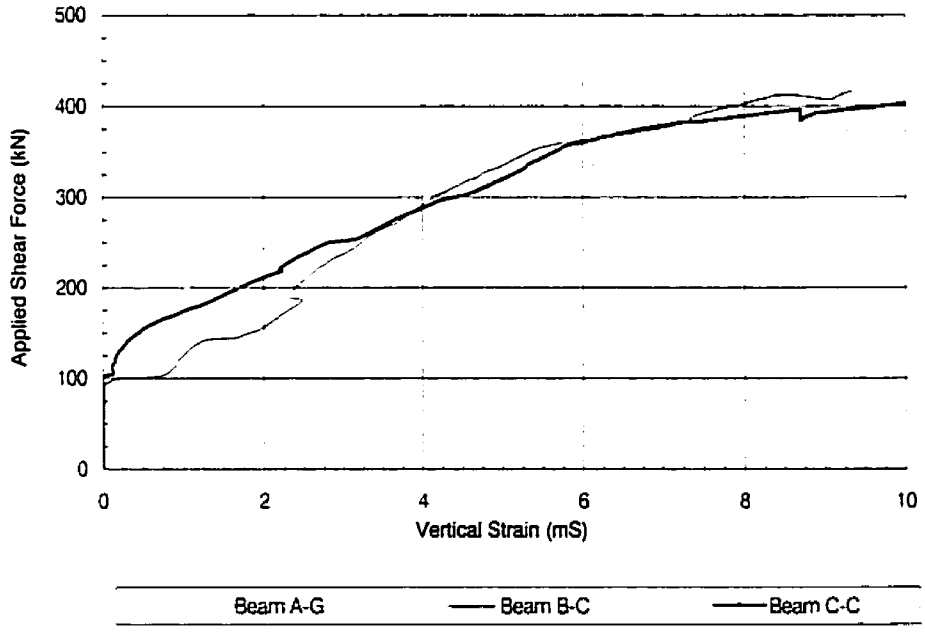

Figure 4.3.4.2f Average vertical strain at a depth of 425 mm for each of the Series B beams

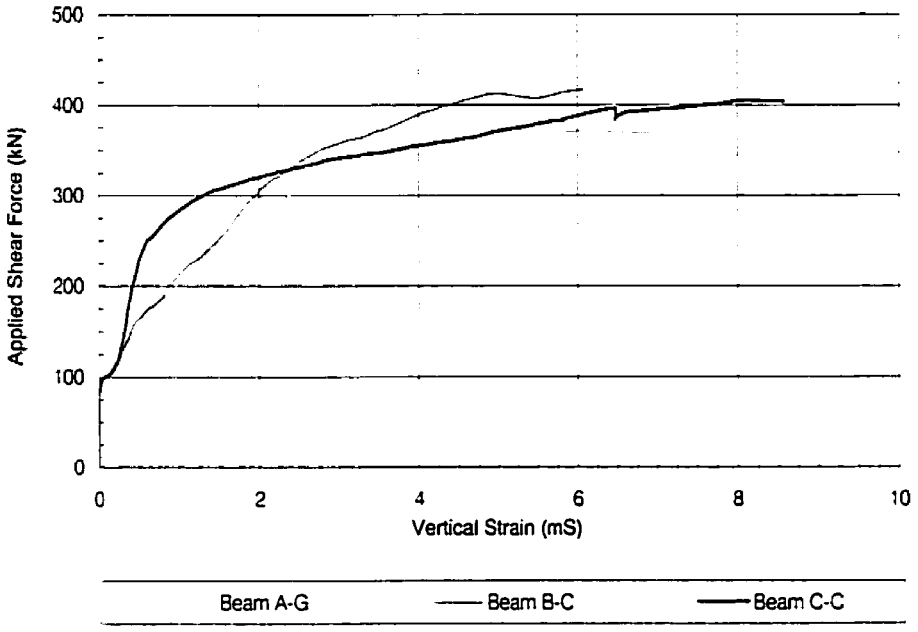

Figure 4.3.4.2g Average vertical strain at a depth of 525 mm for each of the Series B beams

4.3.5 Bond Behaviour

In places on the beam where the primary shear crack is likely to be toward the top of the sheet, debonding is likely to occur. Debonding will not occur all at once, but will progress in a series of steps from the top of the beam down to the first crack, then from the first crack to the next crack and so on. As a portion of the sheet is debonded, the effective length must shift down the web. For the sheets closer to the support, debonding is not likely to occur. In this region the full tensile capacity of the sheets can be reached since the strain is low enough in the anchorage zone of that sheet that debonding may occur only locally around the crack, without the entire sheet debonding.

Before debonding occurs, each of the components of the beam, the concrete, steel and FRP carry a portion of the shear load. Debonding of FRP over a certain region requires that the force across the crack be carried by other adjacent fibres that remain bonded, or be transferred to the internal steel stirrups. When a

sheet completely debonds, the load must be transferred to the only other material that can carry the tensile force, the steel. Failure is very sudden after complete sheet debonding, since if the steel is yielding it can only take a modest increase in load directly related to its plastic stiffness. Thus, overloading of the stirrups results in excessive elongation and causes the shear crack to open very wide, which eliminates any remaining aggregate interlock in the concrete and results in failure. This series of steps happens nearly instantaneously, but not before considerable warning through excessive cracking and areas of partial sheet debonding.

Debonding was examined by plotting the vertical strain of four gauges at a depth of 125 mm or 50 mm from the top of the FRP sheets. The strain at debonding for each beam was nearly constant for two of the beams studied. The strain in gauges closest to the top of the sheet was plotted against the applied shear in Figure 4.3.5a for beam A-G. These gauges were located 50 mm from the top of the sheet at the underside of the compression flange. Of the four gauges bonded to the top of two different sheets, the maximum strain at which debonding takes place is evident. The average peak strain for gauges B1, C1 and E1 was 4.26 millistrain. This corresponds to a maximum strain gradient of $85.2\ (10)^{-6}$/mm.

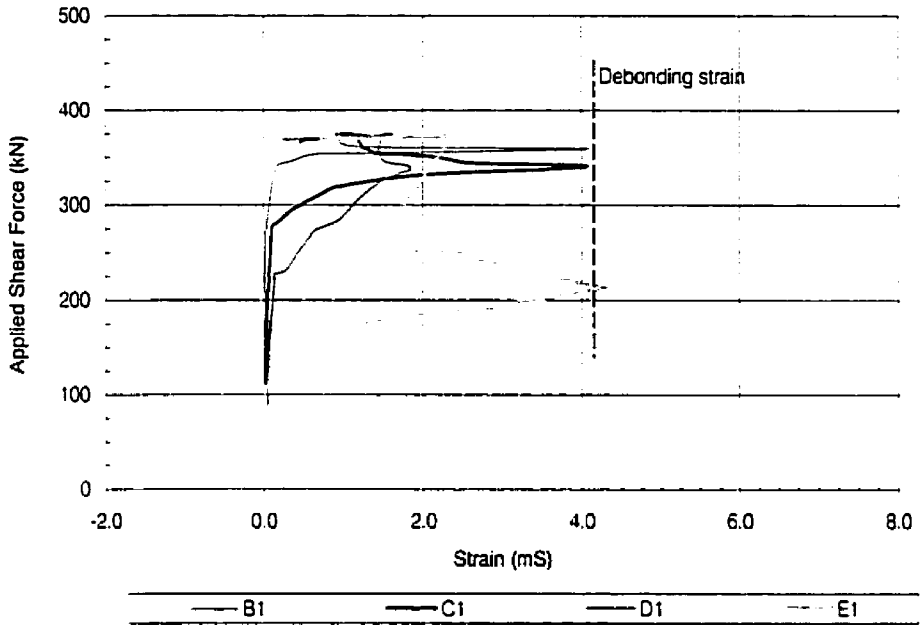

Figure 4.3.5a Vertical FRP strain at a depth of 125 mm for beam A-G

Figure 4.3.5b shows the initial sequence of debonding for beam A-G. The first region of debonding corresponds to the location of gauge E1 in which debonding occurred at an applied shear force of 215 kN. The following two regions of debonding correspond to gauge locations C1 and B1. Figures 4.3.5a and 4.3.5b indicate that the strain at which debonding occurs is constant and the load at which debonding occurs is related to the distance between the edge of the sheet and the failure crack. Once these regions had debonded, complete debonding of the entire middle sheet occurred simultaneously with failure. Complete debonding was due to the close spacing of the shear cracks especially at the top of the sheet.

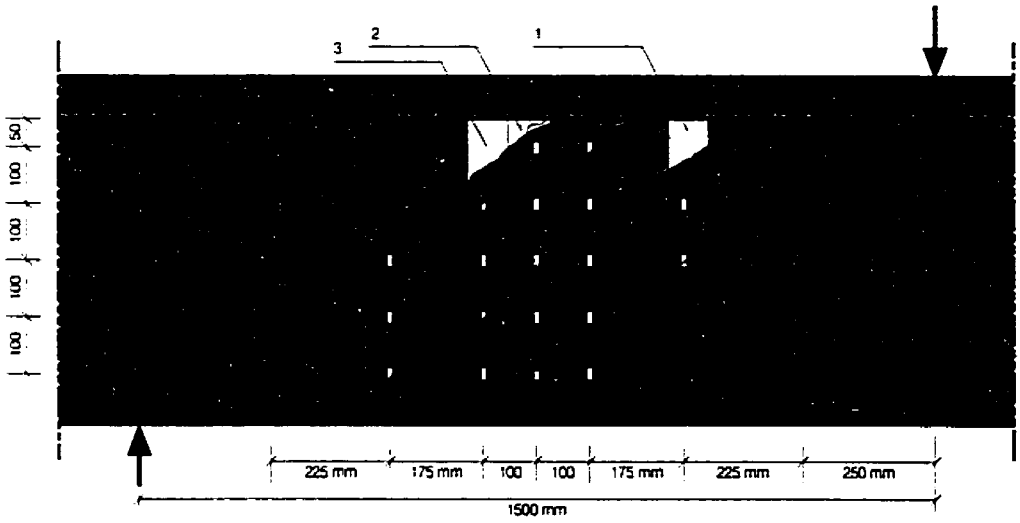

Figure 4.3.5b Sequence of debonding and cracking in relation to the strain gauges on beam A-G

The vertical strain for gauges attached to the same locations on beam B-C is shown in Figure 4.3.5c. Of the three gauges that debonded, the average strain at debonding was 3.68 millistrain corresponding to a strain gradient of 73.6 $(10)^{-6}$ /mm. This lies in between the values of 69.7 $(10)^{-6}$ and 77.5 $(10)^{-6}$/mm found in the Series A beams END-S and MID-S. Once the debonding strain was reached, the strain at these locations gradually or suddenly decreased with increasing load. The debonding can be seen in Figure 4.3.5d in relation to the cracking at failure.

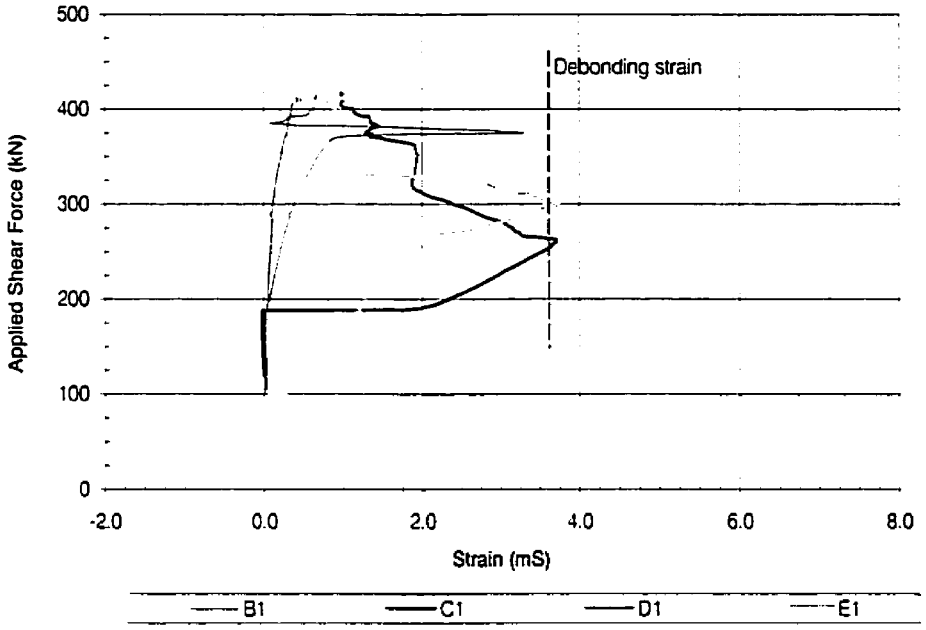

Figure 4.3.5c Vertical FRP strain at a depth of 125 mm for beam B-C

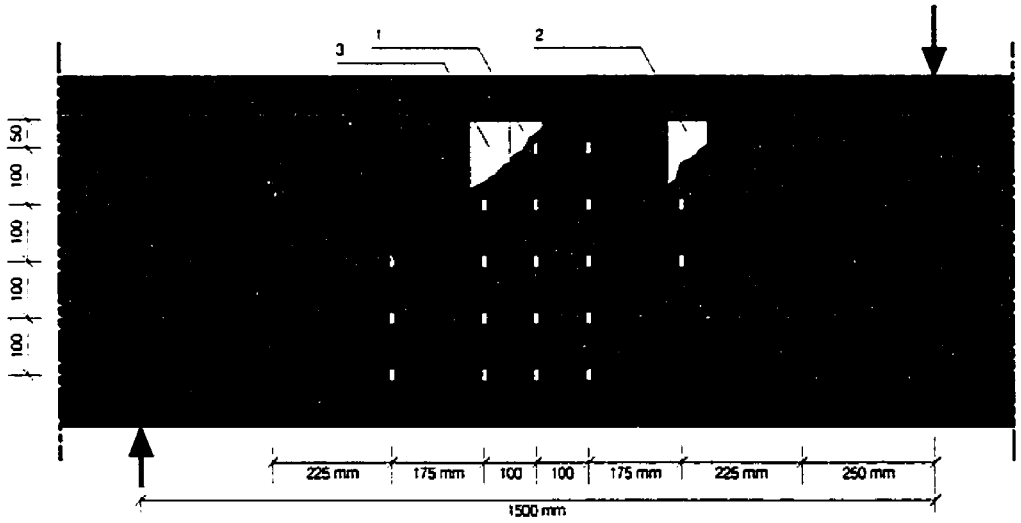

Figure 4.3.5d Sequence of debonding and cracking in relation to the strain gauges on beam B-C

The vertical strain 50 mm from the top of the CFRP sheet for beam C-C is shown in Figure 4.3.5e. Here the debonding strain is uncertain. For two of the gauges, B1 and D1, there is debonding at a strain of 2.8 millistrain. However,

gauge E1 sustains a strain of up to 6.25 millistrain over a considerable range of load before debonding. It is uncertain why the presence of the horizontal CFRP sheet could potentially decrease or increase the strain at debonding. One possible reason for the decrease in strain at debonding is that the concrete might be subjected to biaxial bonding stresses. Vertical bonding stress would result from the shear being carried by the vertical sheets, as with the other beams. Perpendicular to this stress would be the bonding stress resulting from flexure since the horizontal sheet was located below the neutral axis of the beam. Since bond failure is governed by the concrete surface shear strength, it is probable that the surface shear strength of the concrete decreases if it is subjected to biaxial shear as opposed to uniaxial shear.

Due to the horizontally applied sheet, no visual observations of the sequence or exact location of debonding could be made.

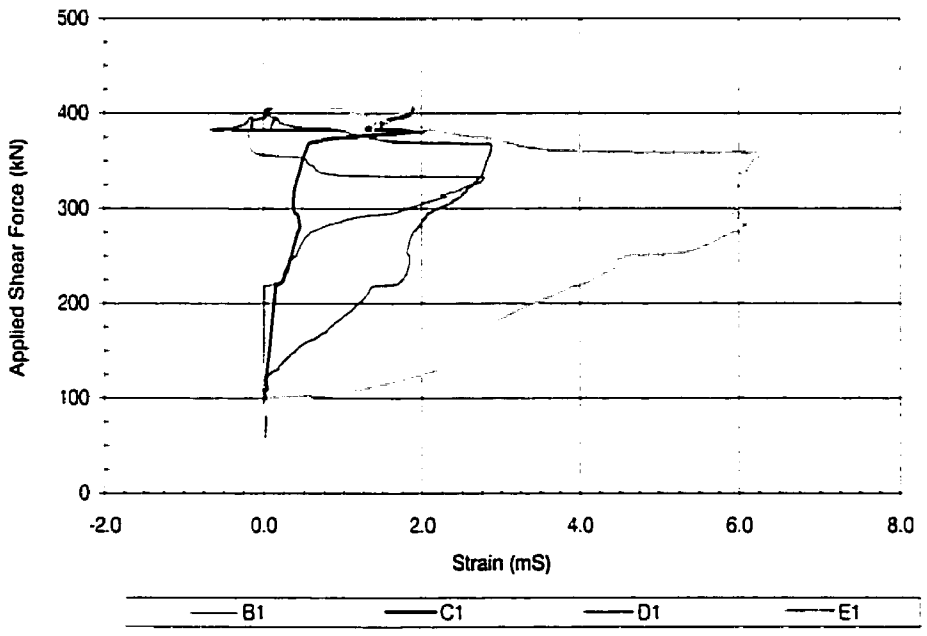

Figure 4.3.5e Vertical FRP strain at a depth of 125 mm for beam C-C

5. EFFECTIVE STRAIN MODEL

5.1 Introduction

Unlike the design of steel stirrups, there is not a clearly defined stress value that may be used in the design of FRP sheets for shear strengthening applications. This is due in part to the many choices available in design. Different FRP types, geometrical layouts and concrete strength all influence the maximum strain in the sheets at failure. Since Triantafillou (1998a) first proposed using an effective stress method for the analysis and design of beams reinforced with FRP sheets for shear, other researchers have extended this model to include the effect of bond strength (Khalifa *et al.*, 1998). New work has also been introduced utilising the strip method for FRP in conjunction with the shear friction method for the concrete and steel stirrups (Deniaud and Cheng, 2000).

However, these models do not account for many important factors in determining the capacity of an FRP shear strengthening scheme. Although size, the degree of internal steel reinforcement and the effect of pseduo-isotropic laminates have been found qualitatively to affect strengthening, their effects have been neglected in models developed to date. With an increased number of tests from different researchers available to use for analysis, the factors influencing effective stress and their relative importance have become more clearly defined. Following the general procedure of Khalifa *et al.* (1998) and realising that bond governs failure for nearly all beams that are not fully wrapped, a model is proposed to better account for additional factors influencing FRP shear strengthening. These additional factors include: the beam width, the transverse steel reinforcement ratio, the concrete strength, the effect of pseudo-isotropic laminates and the available anchorage of the FRP sheets.

5.2 Development of the Proposed Equation

Fifty-six tests of beams strengthened for shear were included in the analysis to develop a model for determining the effective strain in the FRP sheets. Fifty-

three of these were beams found in the literature and the remaining three were from the Series B tests described earlier. Only previously uncracked beams strengthened with sheets attached to each side of the web or in the form of U-jackets were included in the analysis since debonding typically governs the failure of this type of beams, whereas for beams fully wrapped with FRP sheets the bond strength is not as important and sheet rupture is dominant.

It is conceivable that a fully wrapped beam could be strengthened in shear even if there was no bond between the FRP and the concrete substrate. The same could not be said for beams with sheets on the side or in the form of U-jackets. In addition, the practicality of fully wrapped beams is limited when considering rehabilitation or strengthening since most beams are typically cast together with the deck slab.

All of the beams included in this analysis failed in shear. Beams that failed in flexure were not included since the effective FRP strain could have been greater had the beams failed in shear. Beams with special mechanical anchorage of the ends were not included in this analysis but the model could account for different anchorage systems as more tests are conducted. However, beams that improved bond due to additional bonded length were included. Including the tests which involved wrapping of I-section beams was not possible since peeling of the sheets at the interior corner of the section typically results in a different failure mechanism with lower effective strains, particularly for smaller beams.

Results of tests done by the following researchers were included in the analysis: Chajes *et al.* (1995), Deniaud and Cheng (2000), Khalifa *et al.* (2000a), Khalifa *et al.* (2000b), Khalifa *et al.* (2000c), Sato *et al.* (1997a), Triantafillou (1998a) and Uji, (1992). Also included are four tests by Sato *et al.* (1996) reported in both Khalifa *et al.* (1998) and Deniaud and Cheng (2000). In this analysis, each data point represents a single beam test. Section and material properties for each of the

included beams are listed in Table 5.2a. This table lists the following properties: beam width or web width (b_w), overall beam height (h), the effective depth of the longitudinal reinforcement (d), the concrete strength (f'_c), the yield strength of the transverse reinforcement (f_y), the cross-sectional area of the stirrups, the spacing of the stirrups, and the transverse steel reinforcement ratio (ρ_v).

The geometrical and material properties of the FRP strengthening schemes are included in Table 5.2b. These properties include the type of fibre, where *A* represents aramid fibre, *C* represents carbon fibre and *G* represents glass fibre. Two application types were included, sheets bonded to the two sides of the beam separately (*Sides*) or where the sheets are wrapped underneath the soffit (*U-wrap*). The effective depth of the FRP reinforcement (d_{frp}) is defined as the distance from the top of the sheet to the centroid of the longitudinal reinforcement. The width to spacing ratio $(w/s)_{frp}$ indicates tests in which the sheets were applied continuously or a gap left between the sheets. The thickness (t_{frp}) and stiffness (E_{frp}) of the FRP is included in addition to the FRP shear reinforcement ratio (ρ_{frp}). The shear reinforcement ratio is calculated as,

$$\rho_{frp} = \left(\frac{2\,t_{frp}}{b_w}\right)\left(\frac{w}{s}\right)_{frp} \qquad (5.1)$$

Material properties of the sheets are included as the rupture stress (f_{fu}) and the fibre elongation at ultimate (ε_{fu}). The orientation of the primary fibre orientation is listed as (β_1) and if there is a secondary fibre direction it is given as (β_2).

Table 5.2a Section and material properties for beams from the literature

No. (-)	Researcher (-)	Beam (-)	b_w (mm)	h (mm)	d (mm)	f'_c (MPa)	f_y (MPa)	A_v (mm^2)	s (mm)	ρ_v (-)
1	Chajes *et al.*	E1	63.5	190.5	152.4	41.8	0	0.0	∞	0.000%
2	Chajes *et al.*	E2	63.5	190.5	152.4	48.3	0	0.0	∞	0.000%
3	Chajes *et al.*	A1	63.5	190.5	152.4	45.5	0	0.0	∞	0.000%
4	Chajes *et al.*	A2	63.5	190.5	152.4	48.3	0	0.0	∞	0.000%
5	Chajes *et al.*	45G2	63.5	190.5	152.4	41.8	0	0.0	∞	0.000%
6	Chajes *et al.*	G1	63.5	190.5	152.4	43.9	0	0.0	∞	0.000%
7	Chajes *et al.*	G2	63.5	190.5	152.4	47.1	0	0.0	∞	0.000%
8	Chajes *et al.*	45G1	63.5	190.5	152.4	47.1	0	0.0	∞	0.000%
9	Triantafillou	S1a	70	110	100.0	30.0	0	0.0	∞	0.000%
10	Triantafillou	S1b	70	110	100.0	30.0	0	0.0	∞	0.000%
11	Triantafillou	S1-45	70	110	100.0	30.0	0	0.0	∞	0.000%
12	Triantafillou	S2a	70	110	100.0	30.0	0	0.0	∞	0.000%
13	Triantafillou	S2b	70	110	100.0	30.0	0	0.0	∞	0.000%
14	Triantafillou	S2-45	70	110	100.0	30.0	0	0.0	∞	0.000%
15	Triantafillou	S3a	70	110	100.0	30.0	0	0.0	∞	0.000%
16	Triantafillou	S3b	70	110	100.0	30.0	0	0.0	∞	0.000%
17	Triantafillou	S3-45	70	110	100.0	30.0	0	0.0	∞	0.000%
18	Sato *et al.*	No. 2	150	300	240.0	35.7	387	63.4	100	0.423%
19	Uji	5	100	200	170.0	24.1	0	0.0	∞	0.000%
20	Uji	6	100	200	170.0	26.9	0	0.0	∞	0.000%
21	Uji	7	100	200	170.0	26.9	0	0.0	∞	0.000%
22	Deniaud & Cheng	T4S2C45	140	400	354.0	29.4	520	56.5	200	0.202%
23	Deniaud & Cheng	T4S2Tri	140	400	354.0	30.4	520	56.5	200	0.202%
24	Deniaud & Cheng	T4S4G90	140	400	354.0	30.0	520	56.5	400	0.101%
25	Deniaud & Cheng	T4NSG90	140	400	354.0	30.2	0	0.0	∞	0.000%
26	Deniaud & Cheng	T4S2G90	140	400	354.0	30.3	520	56.5	200	0.202%
27	Khalifa *et al.*	A-SO3-2	150	305	253.3	27.5	0	0.0	∞	0.000%
28	Khalifa *et al.*	A-SO3-3	150	305	253.3	27.5	0	0.0	∞	0.000%
29	Khalifa *et al.*	A-SW3-2	150	305	253.3	19.3	350	78.5	125	0.419%
30	Khalifa *et al.*	A-SO3-4	150	305	253.3	27.5	0	0.0	∞	0.000%
31	Khalifa *et al.*	A-SO3-5	150	305	253.3	27.5	0	0.0	∞	0.000%
32	Khalifa *et al.*	B-CO2	150	305	254.2	20.5	0	0.0	∞	0.000%
33	Khalifa *et al.*	B-CO3	150	305	254.2	20.5	0	0.0	∞	0.000%
34	Khalifa *et al.*	B-CW2	150	305	254.2	27.5	350	78.5	125	0.419%
35	Khalifa *et al.*	A-SO4-2	150	305	255.0	27.5	0	0.0	∞	0.000%
36	Khalifa *et al.*	A-SW4-2	150	305	255.0	19.3	350	78.5	125	0.419%
37	Khalifa *et al.*	A-SO4-3	150	305	255.0	27.5	0	0.0	∞	0.000%
38	Khalifa *et al.*	BT5	150	405	356.7	35.0	0	0.0	∞	0.000%
39	Khalifa *et al.*	BT4	150	405	356.7	35.0	0	0.0	∞	0.000%
40	Khalifa *et al.*	A2	150	405	356.7	32.0	0	0.0	∞	0.000%
41	Khalifa *et al.*	A3	150	405	356.7	32.0	0	0.0	∞	0.000%
42	Khalifa *et al.*	A4	150	405	356.7	32.0	0	0.0	∞	0.000%
43	Khalifa *et al.*	BT2	150	405	356.7	35.0	0	0.0	∞	0.000%
44	Khalifa *et al.*	BT3	150	405	356.7	35.0	0	0.0	∞	0.000%
45	Khalifa *et al.*	A5	150	405	356.7	32.0	0	0.0	∞	0.000%
46	Sato *et al.*	S3	200	300	260.0	41.3	0	0.0	∞	0.000%
47	Sato *et al.*	S2	200	300	260.0	45.2	0	0.0	∞	0.000%
48	Sato *et al.*	S4	200	300	260.0	37.5	0	0.0	∞	0.000%
49	Sato *et al.*	S5	200	300	260.0	39.7	0	0.0	∞	0.000%
50	Deniaud & Cheng	T6NSC45	140	600	554.0	44.1	0	0.0	∞	0.000%
51	Deniaud & Cheng	T6S4C90	140	600	554.0	44.1	520	56.5	400	0.101%
52	Deniaud & Cheng	T6S4Tri	140	600	554.0	44.1	520	56.5	400	0.101%
53	Deniaud & Cheng	T6S4G90	140	600	554.0	44.1	520	56.5	400	0.101%
54	Schnerch	C-C	180	615	516.0	55.2	400	200.0	285	0.390%
55	Schnerch	B-C	180	615	516.0	56.8	400	200.0	285	0.390%
56	Schnerch	A-G	180	615	516.0	58.3	400	200.0	285	0.390%

Table 5.2b FRP configuration and FRP material properties for the beams from the literature

No.	Researcher	Beam	Type	Application	d_{frp}	$(w/s)_{frp}$	t_{frp}	E_{frp}	ρ_{frp}	f_{fu}	ε_{fu}	β_1	β_2
(-)	(-)	(-)	(-)	(-)	(mm)	(-)	(mm)	(GPa)	(-)	(MPa)	(mS)	(deg)	(deg)
1	Chajes *et al.*	E1	G	U-wrap	88.9	1.000	0.457	14.3	1.440%	172	12.0	90	0
2	Chajes *et al.*	E2	G	U-wrap	88.9	1.000	0.457	14.3	1.440%	172	12.0	90	0
3	Chajes *et al.*	A1	A	U-wrap	88.9	1.000	1.041	11.0	3.280%	224	20.3	90	0
4	Chajes *et al.*	A2	A	U-wrap	88.9	1.000	1.041	11.0	3.280%	224	20.3	90	0
5	Chajes *et al.*	45G2	C	U-wrap	88.9	1.000	0.584	21.0	1.840%	186	8.9	45	135
6	Chajes *et al.*	G1	C	U-wrap	88.9	1.000	0.584	21.0	1.840%	186	8.9	90	0
7	Chajes *et al.*	G2	C	U-wrap	88.9	1.000	0.584	21.0	1.840%	186	8.9	90	0
8	Chajes *et al.*	45G1	C	U-wrap	88.9	1.000	0.584	21.0	1.840%	186	8.9	45	135
9	Triantafillou	S1a	C	Sides	100.0	0.500	0.154	235	0.220%	3300	14.0	90	
10	Triantafillou	S1b	C	Sides	100.0	0.500	0.154	235	0.220%	3300	14.0	90	
11	Triantafillou	S1-45	C	Sides	100.0	0.500	0.154	235	0.220%	3300	14.0	45	
12	Triantafillou	S2a	C	Sides	100.0	0.750	0.154	235	0.330%	3300	14.0	90	
13	Triantafillou	S2b	C	Sides	100.0	0.750	0.154	235	0.330%	3300	14.0	90	
14	Triantafillou	S2-45	C	Sides	100.0	0.750	0.154	235	0.330%	3300	14.0	45	
15	Triantafillou	S3a	C	Sides	100.0	1.000	0.154	235	0.440%	3300	14.0	90	
16	Triantafillou	S3b	C	Sides	100.0	1.000	0.154	235	0.440%	3300	14.0	90	
17	Triantafillou	S3-45	C	Sides	100.0	1.000	0.154	235	0.440%	3300	14.0	45	
18	Sato *et al.*	No. 2	C	U-wrap	140.0	1.000	0.111	230	0.148%	3480	15.0	90	
19	Uji	5	C	Sides	170.0	1.000	0.097	230	0.194%	2650	11.5	90	
20	Uji	6	C	Sides	170.0	1.000	0.097	230	0.194%	2650	11.5	45	
21	Uji	7	C	Sides	170.0	1.000	0.194	230	0.388%	2650	11.5	90	
22	Deniaud & Cheng	T4S2C45	C	U-wrap	204.0	0.500	0.700	44.8	0.500%	422	9.5	45	
23	Deniaud & Cheng	T4S2Tri	G	U-wrap	204.0	1.000	2.100	8.1	3.000%	124	12.9	90	30,150
24	Deniaud & Cheng	T4S4G90	G	U-wrap	204.0	1.000	1.800	17.7	2.571%	250	14.1	90	
25	Deniaud & Cheng	T4NSG90	G	U-wrap	204.0	1.000	1.800	17.7	2.571%	250	14.1	90	
26	Deniaud & Cheng	T4S2G90	G	U-wrap	204.0	1.000	1.800	17.7	2.571%	250	14.1	90	
27	Khalifa *et al.*	A-SO3-2	C	U-wrap	253.3	0.400	0.165	228	0.088%	3790	15.0	90	
28	Khalifa *et al.*	A-SO3-3	C	U-wrap	253.3	0.600	0.165	228	0.132%	3790	15.0	90	
29	Khalifa *et al.*	A-SW3-2	C	U-wrap	253.3	1.000	0.165	228	0.220%	3790	15.0	90	0
30	Khalifa *et al.*	A-SO3-4	C	U-wrap	253.3	1.000	0.165	228	0.220%	3790	15.0	90	
31	Khalifa *et al.*	A-SO3-5	C	U-wrap	253.3	1.000	0.165	228	0.220%	3790	15.0	90	0
32	Khalifa *et al.*	B-CO2	C	U-wrap	254.2	0.400	0.165	228	0.088%	3790	15.0	90	
33	Khalifa *et al.*	B-CO3	C	U-wrap	254.2	1.000	0.165	228	0.220%	3790	15.0	90	
34	Khalifa *et al.*	B-CW2	C	U-wrap	254.2	1.000	0.165	228	0.220%	3790	15.0	90	0
35	Khalifa *et al.*	A-SO4-2	C	U-wrap	255.0	0.400	0.165	228	0.088%	3790	15.0	90	
36	Khalifa *et al.*	A-SW4-2	C	U-wrap	255.0	1.000	0.165	228	0.220%	3790	15.0	90	0
37	Khalifa *et al.*	A-SO4-3	C	U-wrap	255.0	1.000	0.165	228	0.220%	3790	15.0	90	
38	Khalifa *et al.*	BT5	C	Sides	256.7	0.400	0.165	228	0.088%	3790	15.0	90	
39	Khalifa *et al.*	BT4	C	U-wrap	256.7	0.400	0.165	228	0.088%	3790	15.0	90	
40	Khalifa *et al.*	A2	C	U-wrap	256.7	1.000	0.165	228	0.220%	3790	15.0	90	
41	Khalifa *et al.*	A3	C	U-wrap	256.7	1.000	0.165	228	0.220%	3790	15.0	90	
42	Khalifa *et al.*	A4	C	U-wrap	256.7	1.000	0.165	228	0.220%	3790	15.0	90	
43	Khalifa *et al.*	BT2	C	U-wrap	256.7	1.000	0.165	228	0.220%	3790	15.0	90	
44	Khalifa *et al.*	BT3	C	U-wrap	256.7	1.000	0.165	228	0.220%	3790	15.0	90	0
45	Khalifa *et al.*	A5	C	U-wrap	256.7	1.000	0.165	372	0.220%	3520	8.0	90	
46	Sato *et al.*	S3	C	U-wrap	260.0	0.500	0.111	230	0.056%	3480	15.1	90	
47	Sato *et al.*	S2	C	Sides	260.0	0.500	0.111	230	0.056%	3480	15.1	90	
48	Sato *et al.*	S4	C	Sides	260.0	1.000	0.111	230	0.111%	3480	15.1	90	
49	Sato *et al.*	S5	C	U-wrap	260.0	1.000	0.111	230	0.111%	3480	15.1	90	
50	Deniaud & Cheng	T6NSC45	C	U-wrap	404.0	0.500	0.700	44.8	0.500%	422	9.5	45	
51	Deniaud & Cheng	T6S4G90	C	U-wrap	404.0	0.500	0.700	44.8	0.500%	422	9.5	90	
52	Deniaud & Cheng	T6S4Tri	G	U-wrap	404.0	1.000	2.100	8.1	3.000%	124	12.9	90	30,150
53	Deniaud & Cheng	T6S4G90	G	U-wrap	404.0	1.000	1.800	17.7	2.571%	250	14.1	90	
54	Schnerch	C-C	C	U-wrap	441.0	0.667	0.111	230	0.082%	3400	15.0	90	
55	Schnerch	S-C	C	U-wrap	441.0	0.667	0.111	230	0.082%	3400	15.0	90	
56	Schnerch	A-G	G	U-wrap	441.0	0.667	0.353	72.4	0.261%	1730	20.0	90	

The FRP contribution to shear capacity ($V_{frp,exp}$) for each beam was calculated as the difference between the total shear capacity of a strengthened beam (V_{exp}) and the total shear capacity of an equivalent unstrengthened beam. For the Series B beams included in this analysis, the strength of an equivalent control beam was calculated for each of the three beams using the software program Response that utilises the Modified Compression Field Theory (Collins and Mitchell, 1997). The calculated FRP shear contribution for each beam is given in Table 5.2c.

Wherever possible, the observed maximum strain in the FRP sheets ($\varepsilon_{frp,o}$) was also recorded. For the beams tested by Khalifa *et al.* (2000a, 2000b and 2000c), this is the maximum observed strain at mid-height at one of several gauge locations in the shear span. For the tests completed by the author, the observed maximum strain is the average strain along the failure crack at their highest strain before failure. These values are given in Table 5.2c.

The method used to calculate the effective strain in the FRP sheets is the equation proposed by Khalifa *et al.* (1998) in ACI format, which includes the definition for the depth of the FRP sheets and the width to spacing ratio for beams with sheets that are not continuous,

$$\varepsilon_{frp} = \frac{V_{frp}\, s_{frp}}{2\, t_{frp}\, w_{frp}\, E_{frp} \left(\sin\beta_1 + \cos\beta_1\right) d_{frp}} \qquad (5.2)$$

The effective FRP strain was calculated from this equation since it is more obviously related to the FRP strengthening configuration than the equation proposed by Triantafillou (1998a) as discussed further in Section 5.3. The effective FRP strain for each beam resulting from this equation is presented in Table 5.2c. Also included in this table is the failure mode as defined by the researcher. The dominant mode of failure is debonding.

Table 5.2c Failure mode and calculation of the experimental effective FRP strain

No.	Researcher	Beam	V_{exp}	$V_{frp,exp}$	(observed) $\varepsilon_{frp,o}$	(5.2) ε_{frp}	Failure
(-)	(-)	(-)	(kN)	(kN)	(mS)	(mS)	(-)
1	Chajes *et al.*	E1	36.7	17.9	6.00	12.02	Rupture
2	Chajes *et al.*	E2	34.0	15.1		12.02	Rupture
3	Chajes *et al.*	A1	38.7	19.9		9.75	Rupture
4	Chajes *et al.*	A2	30.0	11.2		5.49	Rupture
5	Chajes *et al.*	45G2	47.3	28.4		8.86	Rupture
6	Chajes *et al.*	G1	35.5	16.7		7.66	Rupture
7	Chajes *et al.*	G2	36.4	17.6		8.09	Rupture
8	Chajes *et al.*	45G1	37.5	18.7		6.08	Rupture
9	Triantafillou	S1a	21.8	13.6		3.74	Debond
10	Triantafillou	S1b	19.5	11.3		3.11	Debond
11	Triantafillou	S1-45	22.3	14.1		2.75	Debond
12	Triantafillou	S2a	24.1	15.9		2.92	Debond
13	Triantafillou	S2b	21.1	12.9		2.38	Debond
14	Triantafillou	S2-45	23.7	15.5		2.01	Debond
15	Triantafillou	S3a	21.4	13.2		1.82	Debond
16	Triantafillou	S3b	18.8	10.6		1.46	Debond
17	Triantafillou	S3-45	20.4	12.2		1.19	Debond
18	Sato *et al.*	No. 2	223.0	24.0		3.36	Debond
19	Uji	5	44.6	20.1		2.65	Debond
20	Uji	6	56.9	32.4		3.07	Debond
21	Uji	7	44.6	20.1		1.33	Debond
22	Deniaud & Cheng	T4S2C45	219.1	17.8		1.97	Debond
23	Deniaud & Cheng	T4S2Tri	242.7	41.4		5.97	Rupture
24	Deniaud & Cheng	T4S4G90	205.6	48.7		3.74	Unzipping
25	Deniaud & Cheng	T4NSG90	159.0	43.6		3.35	Unzipping
26	Deniaud & Cheng	T4S2G90	225.6	24.4		1.87	Unzipping
27	Khalifa *et al.*	A-SO3-2	131.0	54.0	4.70	7.08	Debond
28	Khalifa *et al.*	A-SO3-3	133.5	56.5	5.20	4.94	Debond
29	Khalifa *et al.*	A-SW3-2	177.0	50.5	2.30	2.65	Splitting
30	Khalifa *et al.*	A-SO3-4	144.5	67.5	4.50	3.54	Debond
31	Khalifa *et al.*	A-SO3-5	169.5	92.5	4.30	4.85	Splitting
32	Khalifa *et al.*	B-CO2	88.0	40.0	4.70	5.23	Debond
33	Khalifa *et al.*	B-CO3	113.0	65.0	3.70	3.40	Debond
34	Khalifa *et al.*	B-CW2	214.0	39.0	2.70	2.04	Splitting
35	Khalifa *et al.*	A-SO4-2	127.5	62.5	6.20	8.14	Debond
36	Khalifa *et al.*	A-SW4-2	180.5	80.5	1.90	4.20	Splitting
37	Khalifa *et al.*	A-SO4-3	155.0	90.0	4.30	4.69	Splitting
38	Khalifa *et al.*	BT5	121.5	31.5		4.08	Debond
39	Khalifa *et al.*	BT4	162.0	72.0	10.00	9.32	Debond
40	Khalifa *et al.*	A2	154.0	65.5	4.50	3.39	Debond
41	Khalifa *et al.*	A3	161.5	73.0	4.00	3.78	Debond
42	Khalifa *et al.*	A4	152.5	64.0	4.10	3.31	Debond
43	Khalifa *et al.*	BT2	155.0	65.0	4.50	3.37	Debond
44	Khalifa *et al.*	BT3	157.5	67.5		3.50	Debond
45	Khalifa *et al.*	A5	186.0	97.5	3.60	3.09	Debond
46	Sato *et al.*	S3	202.1	110.0		15.10	Debond
47	Sato *et al.*	S2	160.5	68.4		10.30	Debond
48	Sato *et al.*	S4	156.3	64.2		4.84	Debond
49	Sato *et al.*	S5	198.2	106.1		7.99	Debond
50	Deniaud & Cheng	T6NSC45	213.6	103.5		5.78	Debond
51	Deniaud & Cheng	T6S4C90	272.8	85.3		6.73	Debond
52	Deniaud & Cheng	T6S4Tri	316.7	129.2		9.40	Debond
53	Deniaud & Cheng	T6S4G90	297.5	109.9		4.27	Debond
54	Schnerch	C-C	406.0	126.5	9.09	8.43	Debond
55	Schnerch	B-C	417.0	138.1	7.05	9.20	Debond
56	Schnerch	A-G	375.0	95.7	8.35	6.37	Debond

Non-linear regression analysis was used to determine a simplified equation that best fit the available data. After many trials, the following equation was developed to calculate the predicted effective FRP strain in units of millistrain,

$$\varepsilon_{frp} = 0.0012 \frac{k_L}{\rho_v + 0.0065} \left(\frac{f'_c}{\rho_{frp} E_{frp}} \right)^{\frac{1}{4}} \sqrt{\frac{\sin \beta_1}{k_e} \frac{d_{frp}}{d}} \qquad (5.3)$$

This equation includes the contribution of the reinforcement ratio of both the FRP and the steel stirrups (if any), the concrete strength, the angle of the FRP sheets with respect to the longitudinal axis of the beam, the ratio of the depth of the FRP to the depth of longitudinal steel, the effect of multidirectional fibre orientation and the effect of the sheet configuration. The predicted effective FRP strain is limited to the ultimate tensile strain reported by the manufacturer.

The results of the proposed effective strain equation (5.3) were compared with the calculated experimental effective FRP strain. These results are shown in Figure 5.2a, indicating good agreement between the predicted and experimental results.

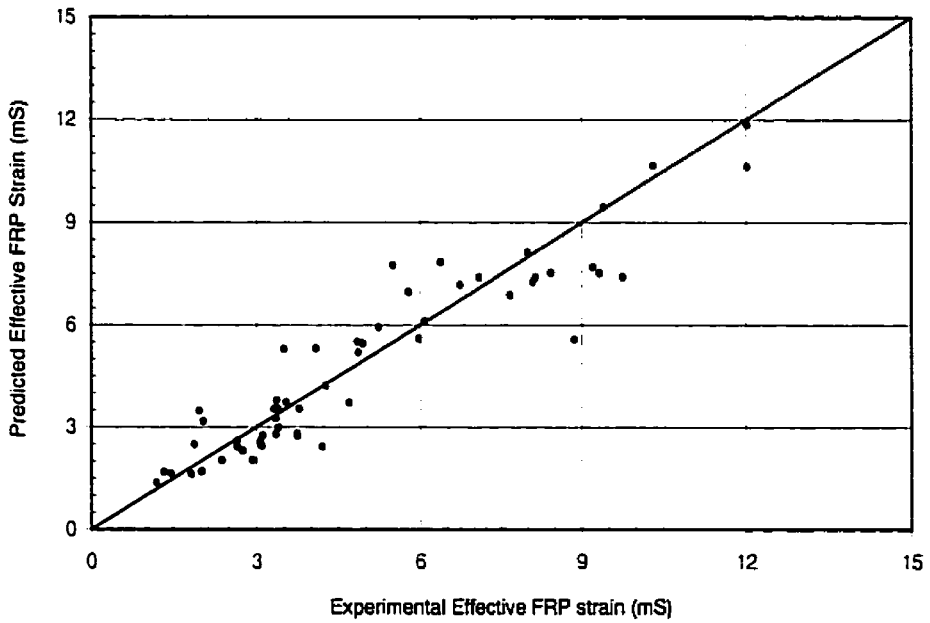

Figure 5.2a Comparison of predicted and experimental effective FRP strain using equation proposed by the author

With the predicted effective FRP strain, the FRP contribution to shear capacity was calculated by rearranging equation (5.2). The concrete and steel shear contributions were calculated using the ACI equations,

$$V_c = \frac{\sqrt{f'_c}\, b_w\, d}{6} \qquad (5.4) \text{ and } (5.5)$$

$$V_s = \frac{A_v\, f_y\, d}{s}$$

The predicted shear capacity was calculated to be the sum of the FRP, concrete and steel stirrup shear contributions. Using this value, the ratio of the experimental to the predicted shear capacity was calculated for each beam. These values are presented in Table 5.2d.

For design, certain limits must be adhered to in strengthening using FRP sheets. Just a beam can be over-reinforced with steel stirrups, the standard check should be made to ensure that the sum of the steel and FRP shear contributions do not exceed the level where concrete crushing failure of the concrete struts would occur. Also, to avoid a shear crack from developing between two sheets, the maximum centre to centre spacing of the sheets should be limited a length of one sheet width plus one quarter the effective depth as recommended by Khalifa *et al.* (1998).

Table 5.2d Predicted shear strength using the proposed model for effective FRP strain

No.	Researcher	Beam	k_e	k_L	$\varepsilon_{frp,p}$	$\varepsilon_{frp}/\varepsilon_{frp,p}$	$V_{frp,pred}$	V_c	V_s	V_{pred}	V_{exp}/V_{pred}
(-)	(-)	(-)	(-)	(-)	(mS)	(-)	(kN)	(kN)	(kN)	(kN)	(-)
1	Chajes *et al.*	E1	1.0	1.4	10.63	1.13	12.3	10.4	0.0	22.8	1.61
2	Chajes *et al.*	E2	1.0	1.4	11.85	1.01	13.8	11.2	0.0	25.0	1.36
3	Chajes *et al.*	A1	1.0	1.4	7.41	1.32	15.1	10.9	0.0	26.0	1.49
4	Chajes *et al.*	A2	1.0	1.4	7.76	0.71	15.8	11.2	0.0	27.1	1.11
5	Chajes *et al.*	45G2	1.0	1.4	5.58	1.59	17.2	10.4	0.0	27.6	1.71
6	Chajes *et al.*	G1	1.0	1.4	6.88	1.11	15.0	10.7	0.0	25.7	1.38
7	Chajes *et al.*	G2	1.0	1.4	7.26	1.11	15.8	11.1	0.0	26.9	1.36
8	Chajes *et al.*	45G1	1.0	1.4	6.10	1.00	18.8	11.1	0.0	29.9	1.26
9	Triantafillou	S1a	2.0	1	2.74	1.36	9.9	6.4	0.0	16.3	1.33
10	Triantafillou	S1b	2.0	1	2.74	1.13	9.9	6.4	0.0	16.3	1.19
11	Triantafillou	S1-45	2.0	1	2.31	1.19	11.8	6.4	0.0	18.2	1.22
12	Triantafillou	S2a	2.0	1	2.02	1.44	11.0	6.4	0.0	17.4	1.38
13	Triantafillou	S2b	2.0	1	2.02	1.17	11.0	6.4	0.0	17.4	1.21
14	Triantafillou	S2-45	2.0	1	1.70	1.18	13.1	6.4	0.0	19.5	1.22
15	Triantafillou	S3a	2.0	1	1.63	1.12	11.8	6.4	0.0	18.2	1.18
16	Triantafillou	S3b	2.0	1	1.63	0.89	11.8	6.4	0.0	18.2	1.03
17	Triantafillou	S3-45	2.0	1	1.37	0.86	14.0	6.4	0.0	20.4	1.00
18	Sato *et al.*	No. 2	1.0	1	2.80	1.20	20.0	35.8	58.9	114.8	1.94
19	Uji	5	2.0	1	2.60	1.02	19.7	13.9	0.0	33.6	1.33
20	Uji	6	2.0	1	2.57	1.19	27.1	14.7	0.0	41.8	1.36
21	Uji	7	2.0	1	1.68	0.79	25.5	14.7	0.0	40.2	1.11
22	Deniaud & Cheng	T4S2C45	1.0	1	3.49	0.56	31.5	44.8	52.0	128.4	1.71
23	Deniaud & Cheng	T4S2Tri	1.0	1.4	5.60	1.07	38.9	45.5	52.0	136.5	1.78
24	Deniaud & Cheng	T4S4G90	1.0	1	2.81	1.33	36.5	45.2	26.0	107.7	1.91
25	Deniaud & Cheng	T4NSG90	1.0	1	3.26	1.03	42.4	45.4	0.0	87.7	1.81
26	Deniaud & Cheng	T4S2G90	1.0	1	2.49	0.75	32.4	45.5	52.0	129.9	1.74
27	Khalifa *et al.*	A-SO3-2	1.0	1	7.40	0.96	56.4	33.2	0.0	89.6	1.46
28	Khalifa *et al.*	A-SO3-3	1.0	1	5.46	0.91	62.4	33.2	0.0	95.6	1.40
29	Khalifa *et al.*	A-SW3-2	1.0	1.4	2.43	1.09	46.3	27.8	55.7	129.8	1.36
30	Khalifa *et al.*	A-SO3-4	1.0	1	3.72	0.95	70.9	33.2	0.0	104.1	1.39
31	Khalifa *et al.*	A-SO3-5	1.0	1.4	5.21	0.93	99.3	33.2	0.0	132.5	1.28
32	Khalifa *et al.*	B-CO2	1.0	1	5.93	0.88	45.4	28.8	0.0	74.2	1.19
33	Khalifa *et al.*	B-CO3	1.0	1	2.98	1.14	57.1	28.8	0.0	85.8	1.32
34	Khalifa *et al.*	B-CW2	1.0	1.4	3.17	0.64	60.6	33.3	55.9	149.8	1.43
35	Khalifa *et al.*	A-SO4-2	1.0	1	7.40	1.10	56.8	33.4	0.0	90.2	1.41
36	Khalifa *et al.*	A-SW4-2	1.0	1.4	2.43	1.73	46.6	28.0	56.1	130.7	1.38
37	Khalifa *et al.*	A-SO4-3	1.0	1	3.72	1.26	71.4	33.4	0.0	104.8	1.48
38	Khalifa *et al.*	BT5	2.0	1	5.32	0.77	41.1	52.8	0.0	93.8	1.30
39	Khalifa *et al.*	BT4	1.0	1	7.52	1.24	58.1	52.8	0.0	110.8	1.46
40	Khalifa *et al.*	A2	1.0	1	3.54	0.96	68.3	50.4	0.0	118.7	1.30
41	Khalifa *et al.*	A3	1.0	1	3.54	1.07	68.3	50.4	0.0	118.7	1.36
42	Khalifa *et al.*	A4	1.0	1	3.54	0.94	68.3	50.4	0.0	118.7	1.28
43	Khalifa *et al.*	BT2	1.0	1	3.78	0.89	73.0	52.8	0.0	125.8	1.23
44	Khalifa *et al.*	BT3	1.0	1.4	5.29	0.66	102.2	52.8	0.0	155.0	1.02
45	Khalifa *et al.*	A5	1.0	1	2.45	1.26	77.2	50.4	0.0	127.6	1.46
46	Sato *et al.*	S3	1.0	1	14.08	1.07	93.5	55.7	0.0	149.2	1.35
47	Sato *et al.*	S2	2.0	1	10.66	0.97	70.7	58.3	0.0	129.0	1.24
48	Sato *et al.*	S4	2.0	1	5.51	0.88	73.1	53.1	0.0	126.2	1.24
49	Sato *et al.*	S5	1.0	1	8.13	0.98	107.9	54.6	0.0	162.5	1.22
50	Deniaud & Cheng	T6NSC45	1.0	1	6.97	0.83	124.8	85.8	0.0	210.7	1.01
51	Deniaud & Cheng	T6S4C90	1.0	1	7.17	0.94	90.9	85.8	40.7	217.4	1.25
52	Deniaud & Cheng	T6S4Tri	1.0	1.4	9.45	0.99	129.8	85.8	40.7	256.4	1.24
53	Deniaud & Cheng	T6S4G90	1.0	1	4.21	1.01	108.5	85.8	40.7	235.1	1.27
54	Schnerch	C-C	1.0	1	7.53	1.12	113.1	115.0	144.8	372.9	1.09
55	Schnerch	B-C	1.0	1	7.70	1.20	115.5	116.7	144.8	377.1	1.11
56	Schnerch	A-G	1.0	1	7.84	0.81	117.9	118.2	144.8	380.9	0.98

The ratio of experimental shear capacity to predicted shear capacity was plotted for each of the beams included in this analysis. These are presented in order of decreasing depth of FRP reinforcement, then by decreasing FRP shear reinforcement ratio multiplied by FRP elastic modulus. These results are shown in Figure 5.2b.

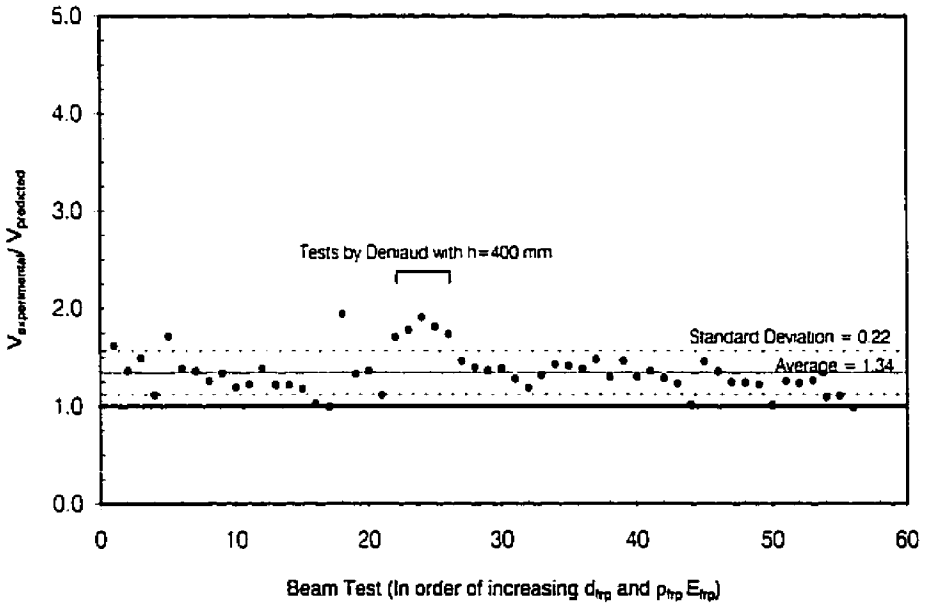

Figure 5.2b Ratio of experimental to predicted total shear capacity using model proposed by the author

It can be seen that most results are well predicted with only one result that is unconservative, and no experimental results that are over twice the predicted shear capacity. For the beams tested by Deniaud and Cheng (2000) that have a height of 400 mm the model is somewhat more conservative than for other tests. It is suspected that this is because the FRP sheets were extended underneath the flange to provide additional anchorage through greater bonded length. In conjunction with the fact that these beams had a very thick top flange in proportion to their height, it is suspected that this anchorage had a beneficial effect on the shear capacity of the tested beams that the model is unable to account for in its current form. For the larger, 600 mm height, beams tested by

Deniaud and Cheng (2000), the model predicts the experimental results quite well since these beams have a more realistic flange thickness to height ratio.

5.3 Definitions Important to the Model

A consensus has not been reached in defining important variables needed to determine the effective strain. The primary difference between the FRP shear contribution equation of Triantafillou (1998a) and the FRP shear contribution equation of Khalifa *et al.* (1998) is in their definition of the depth. Triantafillou defines the depth over which the FRP is effective in shear resistance as 0.9 times the depth from the top of the beam to the centroid of the longitudinal reinforcement. Khalifa *et al.* (1998), define d_{frp} as the effective depth of FRP shear reinforcement, usually equal to d for rectangular sections and $d - h_f$ for T-sections. The method Triantafillou (1998a) uses to define the effective depth of the FRP reinforcement is largely invalid for use in T-section beams since for beams with thick flanges, the actual height of FRP bonded to the web might be even less than what is accounted for using this definition.

In a later work by Deniaud and Cheng (2000), an alternate method for defining the effective depth of the FRP reinforcement is used. The effective depth of the FRP, d_{frp}, is defined by Deniaud and Cheng (2000) as the FRP sheet height along the side of the web. Thus, the effective depth includes the length of sheet that extends below the level of the flexural reinforcement. If one considers the truss model for shear, it is not clear how this part of the sheet can be effective in contributing to shear resistance.

In this thesis, h_{frp} is used to denote the FRP sheet height along the side of the web, and the precedent set by Khalifa *et al.* (1998) is followed in defining the effective depth of the FRP shear reinforcement, d_{frp}.

5.4 Findings

As with the original model proposed by Triantafillou (1998a) and modified by Khalifa *et al.* (1998), the FRP shear reinforcement ratio has been found to be important in describing the effective FRP strain. The FRP shear reinforcement ratio is the term with the greatest significance in determining the effective FRP strain, based on the t-ratio obtained during the statistical analysis. In this thesis, the FRP shear reinforcement ratio used is that proposed by Khalifa *et al.* (1998), which includes the sheet spacing, defined by equation (5.1). In the proposed equation for effective FRP strain (5.3), the effective FRP strain was found to be inversely proportional to $\rho_{frp} E_{frp}$ to the ¾ power. This produces a curve similar to the models of Triantafillou (1998a) and Khalifa *et al.* (1998) where increasing $\rho_{frp} E_{frp}$ results in less of a decrease in effective strain at large values of $\rho_{frp} E_{frp}$.

The effective strain equation proposed by Deniaud and Cheng (2000) does not include variables to describe the effect of the beam width or the width to spacing ratio of the FRP sheets. However, in this analysis the effect of these variables was found to be significant. Increases in beam width increase the effective strain almost proportionally. This may be attributed to increasing improvement of the shear behaviour of the concrete due to the addition of FRP sheets with increases in beam width. For narrow beams, the improvement in concrete shear resistance by providing non-discreet shear reinforcement is likely to be small in comparison with wide beams, or beams lightly reinforced for shear. This is due to crack spacing, and therefore crack widths, becoming larger as the distance away from the reinforcement increases, reducing aggregate interlock action. The inclusion of the width to spacing ratio reflects the fact that beams with a low reinforcement ratio exhibit higher strains than for those that have a high reinforcement ratio.

The shear reinforcement ratio of the steel stirrups was also found to affect the strain in the FRP sheets. As the reinforcement ratio increases from zero, the

effective strain is decreased. This reflects the findings of Deniaud and Cheng (2000) that FRP sheets are less effective for beams that are heavily reinforced internally. This is also reflected in the findings of Khalifa *et al.* (2000a) that the contribution of FRP benefits the shear capacity for beams without steel shear reinforcement more greatly than for beams with moderate amounts of steel shear reinforcement. Furthermore, this effect has also been described in the work of Araki *et al.* (1997) in utilising an effective shear reinforcement ratio that accounts for the reinforcement provided by the steel as well as the FRP sheets in predicting shear strength.

Concrete compressive strength has been found by Horiguchi and Saeki (1997) and reported by Izumo *et al.* (1997) to have a high correlation with the bond strength since bond failure is typically controlled by the surface shear strength of the concrete which can be related to its compressive strength. Horiguchi and Saeki (1997) found the bond strength to be proportional to the 2/3 power of the concrete compressive strength in following the JSCE Standard Specification for Design and Construction of Concrete Structures for bond strengths of deformed bars and tensile strength of concrete. In the proposed equation, the effective FRP strain was found to be proportional to a power somewhat greater than 2/3 power. It was therefore assumed to be proportional to the ¾ power of the concrete compressive strength for simplicity of the equation.

For sheets with unidirectional fibres, the failure mode reported in nearly all the cases was debonding. In sheets with fibres woven in two or more directions, the failure typically results in rupture of the fibres. It is unclear in many cases whether rupture occurs at the peak stress or whether it occurred because of extreme geometry changes after failure. It is also unclear if the rupture is of the fibres carrying the tension required for the truss model, or the secondary fibres.

In the proposed equation, it was found that the effect of a sheet with at least two fibre orientations was significant in improving the effective strain in the direction of the tensile shear force. Khalifa et al. (1998) first recognized the benefit of using pseudo-isotropic sheets and recommended their use, but the effect was not quantifiable at that time. The term k_L in the proposed equation accounts for pseudo-isotropic FRP reinforcement. If there is only one fibre direction, k_L is set equal to 1.0 and if there are at least two fibre orientations that have an equal fibre content as the first, k_L may be increased to 1.4. Of the fifty-six tests included in the model, fifteen utilised pseudo-isotropic fibres oriented at either 45 or 90 degrees to the longitudinal axis of the beam. Only two tests utilised a triaxial fibre arrangement. More study is required to determine if the angle of secondary fibres is significant or if there is any benefit in having more than two fibre orientations.

The remaining parameters in the proposed equation for effective FRP strain account for the configuration of the sheets on the beam. The term $sin\,\beta$ was included to account for a lower effective FRP strain in beams with sheets oriented at an angle. However, this lower strain is offset by the improvement in FRP shear contribution due to their optimum orientation as described in the following example. For two equivalent beams with the same reinforcement ratio, one with sheets oriented at 45 degrees and the other at 90 degrees, the first beam is predicted to have an effective strain that is 84% of the second beam, but have a 19% greater FRP shear contribution than the second beam due to the $(sin\,\beta_l + cos\,\beta_l)$ term in equation (5.2). In comparison with the model predictions, Uji (1992) found a 27% greater FRP shear contribution in two tests of beams with the same reinforcement ratio but at a 45-degree fibre inclination as compared with vertical sheets.

The term k_e has been used to account for the number of free edges of the FRP sheet on one side of the beam. For beams with U-jackets k_e is equal to 1.0 and for

beams that are strengthened separately on each web k_c is equal to 2.0. Deniaud and Cheng (2000) use the term k_a to describe this effect. For fully wrapped beams, k_a is set to zero, so that the predicted effective FRP strain goes to infinity and is limited by the ultimate rupture strain of the sheet. Unfortunately, the observed strain in the FRP sheet for fully wrapped beams is usually much lower than the ultimate strain reported by the manufacturer, as mentioned previously. No attempt was made in this study to determine a k_c value for fully wrapped beams.

Furthermore, Deniaud and Cheng (2000) allow non-integer values of k_a for their T-section beams to account for an additional 100 mm bonded length attached to the underside of the flange. No attempt in the proposed model was made to account for the improvement in performance due to this additional bonded area. With further experimental data, one would expect that the term k_c in the proposed effective FRP strain equation could be used to account for improvements made to the free edge by additional bonded length or by anchorage. Furthermore, the k_c term could also be used to modify the effective strain when small I-section beams are used where the effective strain is lowered due to straightening of the sheets at the interior corners of the section. Due to the limited number of tests of beams with improved anchorage (Sato *et al.*, 1997b) and only one size of I-section beam found in the literature (Hutchinson, 1999) no recommendations for refining the k_c term can be made at this time.

The ratio d_{frp}/d is a term that quantifies the available anchorage of the sheets. The maximum possible value for this term is 1.0 when the FRP sheets are applied contiguously over the entire shear depth. This ratio is low for T-section beams with thick flanges, where there is a limited length to develop strain on the web of the beam. Size effect is also accounted for in this term since smaller beams are more likely to have a small d_{frp}/d ratio, reducing the effective strain capacity of the sheets.

5.5 Effect of FRP Shear Reinforcement on Concrete Contribution

The difficulty of analysing the data by calculating the effective strain based on the difference between the shear contribution of a strengthened beam and an unstrengthened beam is that included in the effective strain term is the beneficial effect of the sheets in increasing the concrete shear contribution. The benefit of limiting crack width with the addition of stirrups is recognised in the Modified Compression Field Theory. However, this aspect is neglected when the individual shear contributions are added together as separate entities. The Modified Compression Field Theory accounts for this by separating beams with stirrups apart from beams without stirrups and providing different coefficients for each case in calculating shear contribution. Models based on the constant angle truss approach have a constant concrete contribution regardless of the transverse reinforcement provided.

For beams strengthened with gaps between individual FRP sheets, shear cracks were observed to have smaller crack spacing within the strengthened area as compared to the exposed concrete area. The smaller crack spacing results in smaller crack widths, theoretically improving the concrete shear aggregate interlock. By calculating the effective FRP strain as the difference between the strengthened and unstrengthened beams, the beneficial effect of smaller crack spacing results in a greater calculated effective FRP strain than what may be observed. This would be particularly significant in beams without stirrups where the crack spacing is larger and determined largely by the longitudinal reinforcement ratio.

Determining the FRP shear contribution by direct observation of the effective strain in the sheets at failure would be preferable. This is not without problems since effective FRP strains have been found to be localised to the failure shear crack (Hutchinson, 1999 and Deniaud and Cheng, 2000). If a gauge is not placed directly at the failure shear crack location, the validity of using that strain may

be questioned. This would result in a calculated effective FRP strain that is higher than the observed effective FRP strains, since there may not be a gauge at the locations of peak strain. Furthermore, most of the experimental data does not include observations of effective strain. However, the more recent tests by Khalifa *et al.* (2000a, 2000b and 2000c) do include this data.

For the twenty-one tests that do report an observed effective FRP strain, this value was compared to the calculated FRP strain. Taking the ratio of calculated to observed effective FRP strain, it was found that while the median of all observations was found to be 0.95, the average was 1.09. This means that, most often, the calculated strain is lower than the observed effective FRP strain, but when the calculated strain is greater than the observed strain the difference may be large. Figure 5.5a shows the relationship between the observed and calculated effective strains. Direct observation of FRP strain along the failure crack is preferable in directly accounting for the FRP shear contribution separately from any enhancement to the concrete contribution.

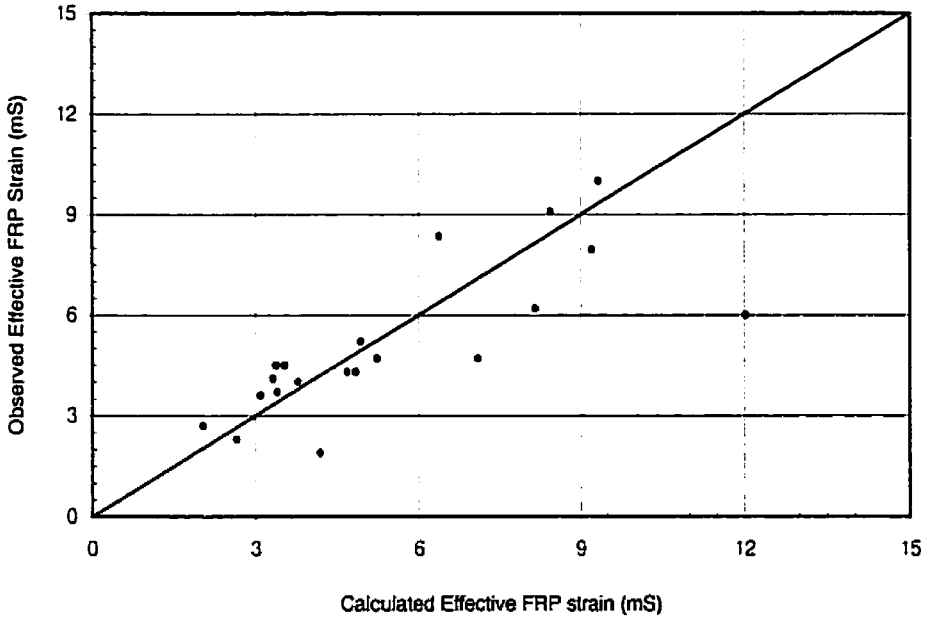

Figure 5.5a The relationship between observed and calculated effective FRP strain for tests reporting an observed strain

5.6 Limit of Vertical Strain

The proposed model sets no limit on the maximum vertical strain in the sheets, other than the maximum ultimate tensile strain reported by the manufacturer. Some previous work has proposed a limiting effective FRP strain value in order to limit crack width and maintain concrete integrity (Khalifa *et al.*, 1998). However, observation of FRP behaviour has shown that the sheets, in providing non-discrete shear reinforcement, prevent the formation of large shear cracks that are few in number. Instead, many shear cracks are formed and they are distributed closely together. This considerably limits the crack width and implies that aggregate interlock would not be lost even at high effective strains in the FRP sheet. In addition, high strains are very localised as was previously discussed.

5.7 Comparison with Other Models

5.7.1 Model Proposed by Khalifa *et al.*

The results of the proposed effective strain model were compared with those proposed by Khalifa *et al.* (1998). This model requires that the shear capacity be limited to the lowest of three values calculated based on the effective stress in the FRP sheets, the available bond strength and a limitation on the maximum strain to prevent loss of concrete integrity due to large crack widths. A more detailed description this model is presented in Section 2.4.4.

The equation proposed by Khalifa *et al.* (1998) was used to predict the effective FRP strain for each of the beams considered.

$$\varepsilon_{frp} = \varepsilon_{fu}\left[0.5622-\left(\rho_{frp}\,E_{frp}\right)^2-1.2188\left(\rho_{frp}\,E_{frp}\right)+0.778\right] \qquad (5.6)$$

The effective FRP strain calculated using this equation was compared to the experimental effective FRP strain that was calculated from the FRP contribution resulting from strengthening. The results for each of the beams included in the analysis are given in Table 5.7.1a. Here the effective length, L_e, is calculated

using equation (2.24) developed by Maeda *et al.* (1997). The effective width, w_{fe}, was calculated using either equation (2.22) or (2.23). Figure 5.7.1a compares the predicted with the experimental effective strain.

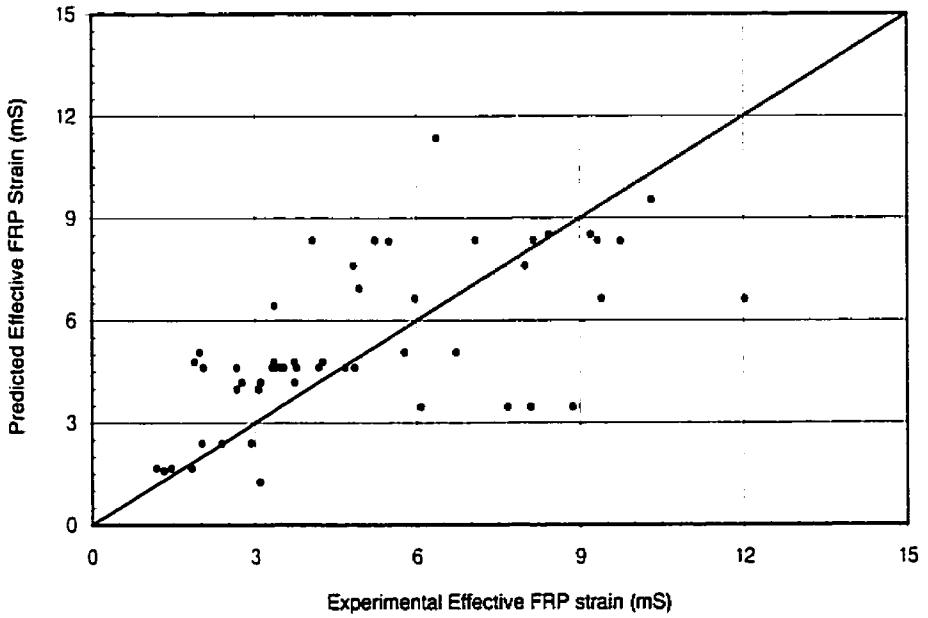

Figure 5.7.1a Comparison of predicted and experimental effective FRP strain using equation proposed by Khalifa et al. (1998)

Table 5.7.1a Predicted shear strength using the model of Khalifa et al. (1998)

No.	Researcher	Beam	(5.6) $\varepsilon_{fe,p}$	(2.24) L_e	(2.22.23) w_{fe}	$V_{f,\,stress}$	$V_{f,\,bond}$	$V_{f,\,govern}$	(5.4) V_c	(5.5) V_s	V_{pred}
(-)	(-)	(-)	(mS)	(mm)	(mm)	(kN)	(kN)	(kN)	(kN)	(kN)	(kN)
1	Chajes *et al.*	E1	6.63	155.4	-66.5	7.0	0.0	0.0	10.4	0.0	10.4
2	Chajes *et al.*	E2	6.63	155.4	-66.5	7.0	0.0	0.0	11.2	0.0	11.2
3	Chajes *et al.*	A1	8.32	111.9	-23.0	17.0	0.0	0.0	10.9	0.0	10.9
4	Chajes *et al.*	A2	8.32	111.9	-23.0	17.0	0.0	0.0	11.2	0.0	11.2
5	Chajes *et al.*	45G2	3.47	107.9	-19.0	10.7	0.0	0.0	10.4	0.0	10.4
6	Chajes *et al.*	G1	3.47	107.9	-19.0	7.6	0.0	0.0	10.7	0.0	10.7
7	Chajes *et al.*	G2	3.47	107.9	-19.0	7.6	0.0	0.0	11.1	0.0	11.1
8	Chajes *et al.*	45G1	3.47	107.9	-19.0	10.7	0.0	0.0	11.1	0.0	11.1
9	Triantafillou	S1a	4.19	57.5	-15.1	15.2	0.0	0.0	6.4	0.0	6.4
10	Triantafillou	S1b	4.19	57.5	-15.1	15.2	0.0	0.0	6.4	0.0	6.4
11	Triantafillou	S1-45	4.19	57.5	-15.1	21.4	0.0	0.0	6.4	0.0	6.4
12	Triantafillou	S2a	2.40	57.5	-15.1	13.0	0.0	0.0	6.4	0.0	6.4
13	Triantafillou	S2b	2.40	57.5	-15.1	13.0	0.0	0.0	6.4	0.0	6.4
14	Triantafillou	S2-45	2.40	57.5	-15.1	18.4	0.0	0.0	6.4	0.0	6.4
15	Triantafillou	S3a	1.67	57.5	-15.1	12.1	0.0	0.0	6.4	0.0	6.4
16	Triantafillou	S3b	1.67	57.5	-15.1	12.1	0.0	0.0	6.4	0.0	6.4
17	Triantafillou	S3-45	1.67	57.5	-15.1	17.1	0.0	0.0	6.4	0.0	6.4
18	Sato *et al.*	No. 2	6.42	70.4	69.6	46.3	24.7	24.7	35.8	58.9	119.5
19	Uji	5	3.99	76.2	17.6	30.2	4.6	4.6	13.9	0.0	18.5
20	Uji	6	3.99	76.2	17.6	42.0	4.9	4.9	14.7	0.0	19.6
21	Uji	7	1.59	51.0	68.1	24.1	25.4	24.1	14.7	0.0	38.8
22	Deniaud & Cheng	T4S2C45	5.07	62.5	141.5	42.6	24.1	24.1	44.8	52.0	120.9
23	Deniaud & Cheng	T4S2Tri	6.64	89.2	114.8	53.1	30.9	30.9	45.5	52.0	128.5
24	Deniaud & Cheng	T4S4G90	4.79	62.0	142.0	62.4	49.4	49.4	45.2	26.0	120.6
25	Deniaud & Cheng	T4NSG90	4.79	62.0	142.0	62.4	49.6	49.6	45.4	0.0	95.0
26	Deniaud & Cheng	T4S2G90	4.79	62.0	142.0	62.4	49.7	49.7	45.5	52.0	147.2
27	Khalifa *et al.*	A-SO3-2	8.34	56.3	197.1	63.4	27.7	27.7	33.2	0.0	60.9
28	Khalifa *et al.*	A-SO3-3	6.93	56.3	197.1	87.9	41.6	41.6	33.2	0.0	74.8
29	Khalifa *et al.*	A-SW3-2	4.62	56.3	197.1	97.6	54.7	54.7	27.8	55.7	138.3
30	Khalifa *et al.*	A-SO3-4	4.62	56.3	197.1	97.6	69.3	69.3	33.2	0.0	102.5
31	Khalifa *et al.*	A-SO3-5	4.62	56.3	197.1	97.6	69.3	69.3	33.2	0.0	102.5
32	Khalifa *et al.*	B-CO2	8.34	56.3	197.9	63.6	22.9	22.9	28.8	0.0	51.7
33	Khalifa *et al.*	B-CO3	4.62	56.3	197.9	97.9	57.2	57.2	28.8	0.0	86.0
34	Khalifa *et al.*	B-CW2	4.62	56.3	197.9	97.9	69.6	69.6	33.3	55.9	158.8
35	Khalifa *et al.*	A-SO4-2	8.34	56.3	198.7	63.8	28.0	28.0	33.4	0.0	61.4
36	Khalifa *et al.*	A-SW4-2	4.62	56.3	198.7	98.3	55.2	55.2	28.0	56.1	139.3
37	Khalifa *et al.*	A-SO4-3	4.62	56.3	198.7	98.3	69.9	69.9	33.4	0.0	103.3
38	Khalifa *et al.*	BT5	8.34	56.3	144.1	64.2	23.8	23.8	52.8	0.0	76.6
39	Khalifa *et al.*	BT4	8.34	56.3	200.4	64.2	33.1	33.1	52.8	0.0	85.9
40	Khalifa *et al.*	A2	4.62	56.3	200.4	98.9	78.0	78.0	50.4	0.0	128.4
41	Khalifa *et al.*	A3	4.62	56.3	200.4	98.9	78.0	78.0	50.4	0.0	128.4
42	Khalifa *et al.*	A4	4.62	56.3	200.4	98.9	78.0	78.0	50.4	0.0	128.4
43	Khalifa *et al.*	BT2	4.62	56.3	200.4	98.9	82.8	82.8	52.8	0.0	135.5
44	Khalifa *et al.*	BT3	4.62	56.3	200.4	98.9	82.8	82.8	52.8	0.0	135.5
45	Khalifa *et al.*	A5	1.26	42.4	214.3	46.8	102.4	46.8	50.4	0.0	97.3
46	Sato *et al.*	S3	9.54	70.4	189.6	50.2	37.2	37.2	55.7	0.0	92.8
47	Sato *et al.*	S2	9.54	70.4	119.1	50.2	24.8	24.8	58.3	0.0	83.1
48	Sato *et al.*	S4	7.60	70.4	119.1	100.4	43.8	43.8	53.1	0.0	96.8
49	Sato *et al.*	S5	7.60	70.4	189.6	100.4	72.4	72.4	54.6	0.0	127.0
50	Deniaud & Cheng	T6NSC45	5.07	62.5	341.5	84.4	76.2	76.2	85.8	0.0	162.1
51	Deniaud & Cheng	T6S4C90	5.07	62.5	341.5	59.7	76.2	59.7	85.8	40.7	186.2
52	Deniaud & Cheng	T6S4Tri	6.64	89.2	314.8	105.2	108.7	105.2	85.8	40.7	231.8
53	Deniaud & Cheng	T6S4G90	4.79	62.0	342.0	123.5	153.7	123.5	85.8	40.7	250.1
54	Schnerch	C-C	8.51	70.4	370.6	111.0	117.5	111.0	115.0	144.8	370.8
55	Schnerch	B-C	8.51	70.4	370.6	111.0	119.8	111.0	116.7	144.8	372.5
56	Schnerch	A-G	11.35	70.4	370.6	179.5	121.9	121.9	118.2	144.8	385.0

The FRP contribution to shear capacity was calculated based on the governing mode of failure based on stress in the FRP, bond between the concrete and FRP, and limiting the allowable crack width. The concrete and steel shear contributions were calculated using the ACI equations (5.4) and (5.5). The calculated values for each test are given in Table 5.7.1a. The ratio of experimental shear capacity to predicted shear capacity was plotted for each beam included in the analysis in order of decreasing depth of FRP reinforcement, then by decreasing FRP shear reinforcement ratio multiplied by FRP elastic modulus. These results are shown in Figure 5.7.1b.

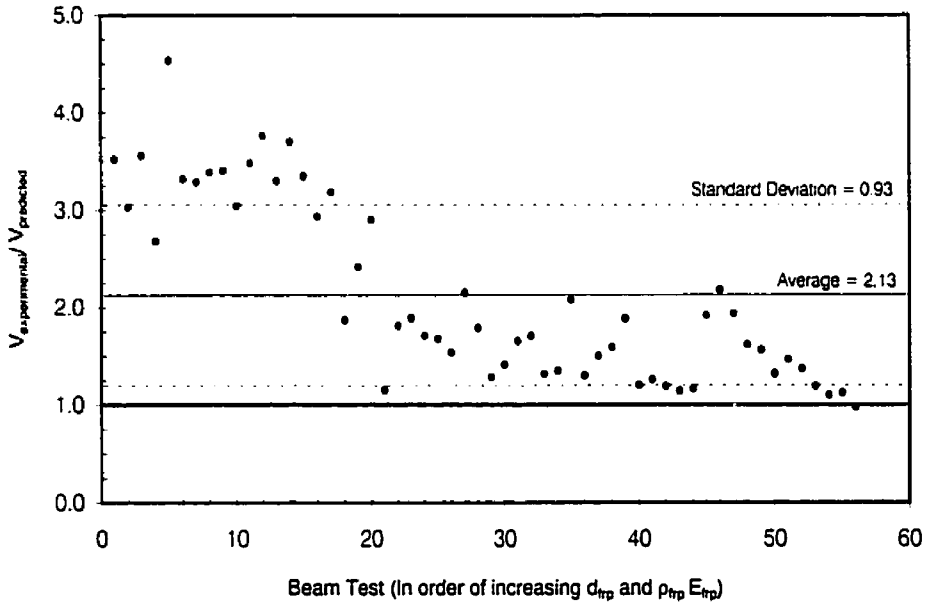

Figure 5.7.1b Ratio of experimental to predicted total shear capacity using model proposed by Khalifa et al. (1998)

While all but one prediction is conservative, for very small beams the model is quite conservative. This is due to the use of effective width in limiting the effective FRP strain because of the bonded surface configuration. For the beams included in the analysis the effective length ranged from a minimum of 42.4 mm to a maximum of 155.4 mm. For tests done by Chajes *et al.* (1995) and Triantafillou (1998a) the effective depth of the FRP was only 88.9 and 100 mm

respectively. This means that the effective width of the sheets, as defined in equations (2.26) and (2.27), became less than zero. Since the effective width became less than zero, there is effectively no bonded area with the result that no strengthening can be attributed to the FRP shear reinforcement. However, from the experimental results, the FRP reinforcement did provide considerable strengthening. The FRP contribution averaged 48.4 % of the experimental shear strength for the beams tested by Chajes *et al.* (1995) and 61.5 % of the experimental shear strength for the beams tested by Triantafillou (1998a). Therefore, even small beams can be significantly strengthened in shear particularly when they lack any internal reinforcement. This can be explained by the fact that the FRP sheets do not need to develop their full bond strength to be effective. Even at low levels of strain in the sheets, they are able to significantly restrain large cracks and distribute cracking. These effects are particularly beneficial in beams without transverse reinforcement in which the only other means of controlling crack width is through the longitudinal reinforcement. The small beams of Khalifa *et al.* (1998) and Triantafillou (1998a) had no transverse reinforcement.

5.7.2 Model Proposed by Deniaud and Cheng

The results of the proposed effective strain model were compared with those proposed by Deniaud and Cheng (2000). This model is based on the shear friction method for the concrete, using a continuous shear friction design equation and the strip method for the FRP strengthening. By using a continuous equation, the iterations that are required to find the minimum shear strength for the discrete equation are eliminated. The reduction in computational effort results in the continuous equation being more conservative than the results for the discrete equation. Further description of the model is given in Section 2.4.4.

The effective FRP strain equation, defined by Deniaud and Cheng (2000) as the maximum FRP strain, was developed using a parametric study involving the use

of five parameters. Two equations were proposed to determine the effective FRP strain, an exact equation and a simplified equation. The exact equation was used for this comparison. This equation takes the following form with the units of effective strain in millistrain,

$$\varepsilon_{frp} = 30.3318\, f'^{\,0.51503}_{c}\; h_{frp}^{\,0.160524} \left(t_{frp}\, E_{frp}\right)^{-1.53175} \left(\sin\beta_1\right)^{-0.09557} \left(k_a\right)^{-0.111054} \qquad (5.7)$$

Note that some of the variable names were changed to reflect the definitions used in this thesis.

The effective FRP strain calculated using this equation was compared with the experimental effective FRP strain that was calculated from the FRP contribution resulting from strengthening. The results of these calculations for each of the beams included in the analysis are given in Table 5.7.2a. Figure 5.7.2a compares the predicted with the experimental effective strain.

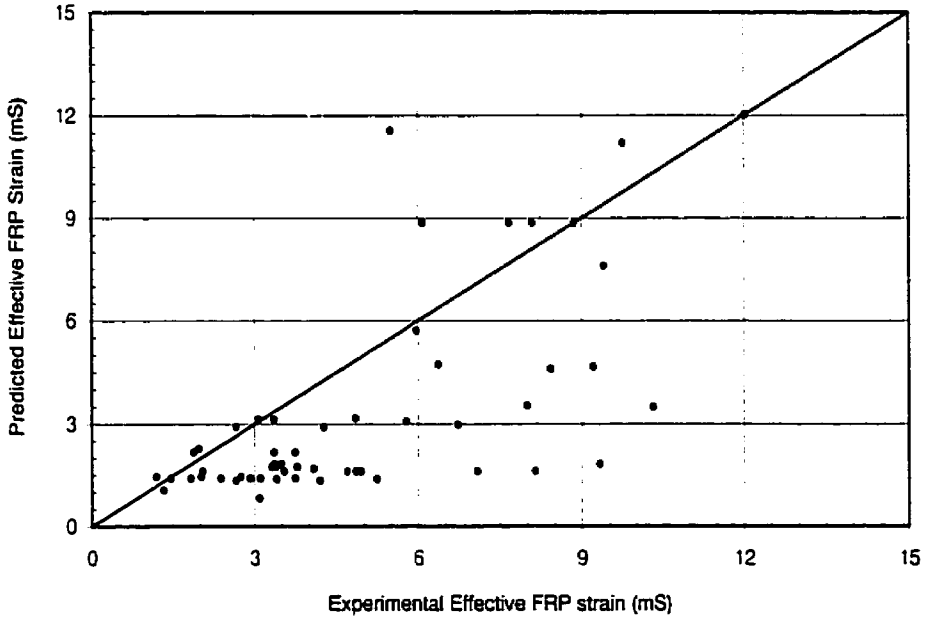

Figure 5.7.2a Comparison of predicted and experimental effective FRP strain using equation proposed by Deniaud and Cheng (2000)

Table 5.7.2a Predicted shear strength using the model of Deniaud and Cheng (2000)

No. (-)	Researcher (-)	Beam (-)	k_a (-)	$\varepsilon_{frp,p}$ (5.7) (mS)	$\varepsilon_{frp}/\varepsilon_{frp,p}$ (-)	V_{pred} (kN)	V_{exp}/V_{pred} (-)
1	Chajes *et al.*	E1	1.00	12.02	1.00	38.40	0.96
2	Chajes *et al.*	E2	1.00	12.02	1.00	38.40	0.88
3	Chajes *et al.*	A1	1.00	11.20	0.87	52.70	0.73
4	Chajes *et al.*	A2	1.00	11.56	0.47	52.70	0.57
5	Chajes *et al.*	45G2	1.00	8.86	1.00	43.00	1.10
6	Chajes *et al.*	G1	1.00	8.86	0.86	47.90	0.74
7	Chajes *et al.*	G2	1.00	8.86	0.91	47.90	0.76
8	Chajes *et al.*	45G1	1.00	8.86	0.69	43.00	0.87
9	Triantafillou	S1a	2.00	1.41	2.65	10.50	2.07
10	Triantafillou	S1b	2.00	1.41	2.20	10.50	1.85
11	Triantafillou	S1-45	2.00	1.46	1.88	9.40	2.37
12	Triantafillou	S2a	2.00	1.41	2.07	14.00	1.72
13	Triantafillou	S2b	2.00	1.41	1.68	14.00	1.51
14	Triantafillou	S2-45	2.00	1.46	1.38	12.30	1.92
15	Triantafillou	S3a	2.00	1.41	1.29	21.00	1.02
16	Triantafillou	S3b	2.00	1.41	1.03	21.00	0.89
17	Triantafillou	S3-45	2.00	1.46	0.81	18.40	1.11
18	Sato *et al.*	No. 2	1.00	3.13	1.07		
19	Uji	5	2.00	2.91	0.91	52.40	0.85
20	Uji	6	2.00	3.14	0.98	53.70	1.06
21	Uji	7	2.00	1.07	1.24	48.30	0.92
22	Deniaud & Cheng	T4S2C45	0.79	2.27	0.87	176.80	1.24
23	Deniaud & Cheng	T4S2Tri	0.79	5.71	1.04	213.00	1.14
24	Deniaud & Cheng	T4S4G90	0.79	2.17	1.73	163.10	1.26
25	Deniaud & Cheng	T4NSG90	0.79	2.18	1.54	139.60	1.14
26	Deniaud & Cheng	T4S2G90	0.79	2.18	0.86	205.00	1.10
27	Khalifa *et al.*	A-SO3-2	1.00	1.62	4.38		
28	Khalifa *et al.*	A-SO3-3	1.00	1.62	3.05		
29	Khalifa *et al.*	A-SW3-2	1.00	1.35	1.97		
30	Khalifa *et al.*	A-SO3-4	1.00	1.62	2.19		
31	Khalifa *et al.*	A-SO3-5	1.00	1.62	3.00		
32	Khalifa *et al.*	B-CO2	1.00	1.39	3.76		
33	Khalifa *et al.*	B-CO3	1.00	1.39	2.44		
34	Khalifa *et al.*	B-CW2	1.00	1.62	1.26		
35	Khalifa *et al.*	A-SO4-2	1.00	1.62	5.03		
36	Khalifa *et al.*	A-SW4-2	1.00	1.35	3.11		
37	Khalifa *et al.*	A-SO4-3	1.00	1.62	2.90		
38	Khalifa *et al.*	BT5	2.00	1.70	2.40		
39	Khalifa *et al.*	BT4	1.00	1.83	5.09		
40	Khalifa *et al.*	A2	1.00	1.75	1.94		
41	Khalifa *et al.*	A3	1.00	1.75	2.16		
42	Khalifa *et al.*	A4	1.00	1.75	1.90		
43	Khalifa *et al.*	BT2	1.00	1.83	1.84		
44	Khalifa *et al.*	BT3	1.00	1.83	1.91		
45	Khalifa *et al.*	A5	1.00	0.83	3.75		
46	Sato *et al.*	S3	1.00	3.60	4.19	86.20	2.34
47	Sato *et al.*	S2	2.00	3.49	2.95	83.20	1.93
48	Sato *et al.*	S4	2.00	3.17	1.52	138.20	1.13
49	Sato *et al.*	S5	1.00	3.53	2.26	157.10	1.26
50	Deniaud & Cheng	T6NSC45	0.79	3.08	1.88	133.10	1.60
51	Deniaud & Cheng	T6S4C90	0.79	2.98	2.26	214.40	1.27
52	Deniaud & Cheng	T6S4Tri	0.79	7.60	1.24	332.50	0.95
53	Deniaud & Cheng	T6S4G90	0.79	2.91	1.47	310.40	0.96
54	Schnerch	C-C	1.00	4.60	1.83		
55	Schnerch	B-C	1.00	4.66	1.97		
56	Schnerch	A-G	1.00	4.72	1.35		

The ratio of experimental shear capacity to predicted shear capacity was plotted for each beam that Deniaud and Cheng (2000) analysed that was also included in this analysis. In total thirty-three tests were compared. These are presented in order of decreasing depth of FRP reinforcement, then by decreasing FRP shear reinforcement ratio multiplied by FRP elastic modulus, shown in Figure 5.7.2b.

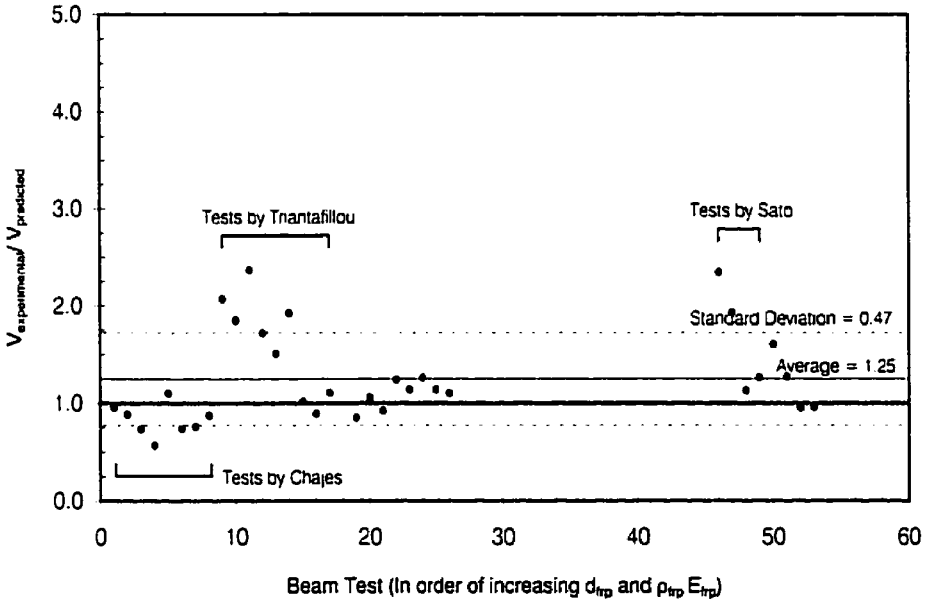

Figure 5.7.2b Ratio of experimental to predicted total shear capacity using model proposed by Deniaud and Cheng (2000)

The model proposed by Deniaud and Cheng (2000) is more conservative for beams that have a width to spacing ratio of the FRP sheets less than one since the method does not include the effect of this type of sheet configuration. This is apparent for six of the beams tested by Triantafillou (1998a) as well as two of the beams tested by Sato *et al.* (1997a). This model is unconservative for seven of the eight beams tested by Chajes *et al.* (1995), likely due to their small size, and unconservative for five others.

5.7.3 Statistical Comparisons

Comparing the models, Table 5.7.3a shows the improvement in predicting the effective FRP strain using the proposed equation. By improving the prediction of the effective strain, the prediction of the total shear capacity is also improved. The model proposed by Deniaud and Cheng (2000), in spite of being more computationally intensive, does not predict the results better than either of the other two models judging by the value of R^2 and is unconservative for a considerable number of the tests.

Table 5.7.3a Statistical comparisons among the three models for fifty-three beam tests from the literature and the three Series B tests

	Model	Khalifa *et al.*	Deniaud and Cheng	Schnerch
$\varepsilon_{frp,e}/\varepsilon_{frp,p}$	R^2	38.8 %	41.4 %	89.8 %
	Average	1.01	1.95	1.02
	Median	0.86	1.84	1.04
	Standard Deviation	0.51	1.09	0.22
V_{exp}/V_{pred}	R^2	92.3 %	90.5 % *	92.8 %
	Average	2.13	1.25 *	1.34
	Median	1.80	1.11 *	1.32
	Standard Deviation	0.93	0.47 *	0.22
	# of unconservative predictions	1	12 *	1
	lowest unconservative prediction	97 %	57 % *	98 %

* For the prediction of shear capacity, the model proposed by Deniaud and Cheng (2000) includes thirty-three tests

Further improvement to the proposed model could be made through developing the effect of the k_e term in describing not only the number of free edges, but also using this term to describe the anchorage provided at the free edges, if any. This term could also be modified to account for the reduction in effective FRP strain due to peeling at the interior corners of smaller I-section beams.

5.8 Model Predictions

5.8.1 Series A Beams

The proposed model has been used to confirm the results of the tests of the Series A beams. These calculations are shown in Table 5.8a. Although these were I-section beams, due to their large size peeling at the interior corners was observed to be insignificant. It can be seen that both the effective FRP strain equation reported by Khalifa *et al.* (1998) and the proposed effective FRP strain equation predict the observed FRP strain of each beam well. It should be noted that the observed effective FRP strain for beam END-S is expected to be somewhat lower than might be anticipated since the beam failed prematurely in flexure.

Table 5.8.1a Statistical comparisons among the three models for two Series A tests

	Model	Khalifa *et al.*		Deniaud and Cheng		Schnerch	
	Beam	END-S	MID-S	END-S	MID-S	END-S	MID-S
$\varepsilon_{frp,o}$	Observed strain (mS)	7.78	10.41	7.78	10.41	7.78	10.41
$\varepsilon_{frp,p}$	Predicted strain (mS)	7.18	7.57	4.26	4.26	8.18	8.45
$\varepsilon_{frp,o}/\varepsilon_{frp,p}$	Ratio	1.08	1.37	1.83	2.45	0.95	1.23
V_{exp}	Experimental Shear Capacity (kN)	2740 +	2710	2740 +	2710	2740 +	2710
V_{pred}	Predicted Shear Capacity (CSA) (kN)	2980.5	2991.2	-	-	3036.8	3044.8
V_{exp}/V_{pred}	Ratio	0.92 +	0.91	-	-	0.90 +	0.89

The effective FRP strain equation of Deniaud and Cheng (2000) does not predict the observed strain very well. It is thought that this is because equation (5.7) gives too much strength to the FRP sheet thickness and stiffness terms, t_{frp} E_{frp}. The effect of this term is modified by the exponent -1.53175. If a power equation trend line is used to describe the parabolic equation of Khalifa *et al.* (1998), its

power is −0.874, using the data between 0.05 < $\rho_{frp} E_{frp}$ < 1.00 GPa. In the proposed effective FRP strain model the effect of the reinforcement ratio multiplied by the sheet stiffness, $\rho_{frp} E_{frp}$ is to the exponent −0.75. Thus, for the large beams strengthened with a relatively low value of $t_{frp} E_{frp}$, the FRP strain equation of Deniaud and Cheng (2000) is conservative.

5.8.2 Series B Beams

For the Series B beams, the predicted effective FRP strains and predicted shear capacity for each beam is shown in Table 5.8b. Although the FRP strain is accounted for quite well, the overall shear capacity is unconservative for both models. It is suspected that this is due to the unconservative effect of the high strength concrete on the concrete contribution. Both the proposed effective FRP equation and equation (5.7) of Khalifa *et al.* (1998) are somewhat unconservative in predicting the strain in the GFRP sheets. The model of Deniaud and Cheng (2000) is not unconservative in predicting the strain in the GFRP, but is more conservative in predicting the other strains suggesting that the overall model is conservative with a similar poor prediction of the GFRP sheet strain.

Table 5.8.2a Statistical comparisons among the three models for the three Series B tests

	Model	Khalifa *et al.*			Deniaud and Cheng			Schnerch		
	Beam	A-G	B-C	C-C	A-G	B-C	C-C	A-G	B-C	C-C
$\varepsilon_{frp,e}$	Experimental strain (mS)	6.37	9.20	8.43	6.37	9.20	8.43	6.37	9.20	8.43
$\varepsilon_{frp,p}$	Predicted strain (mS)	13.56	8.39	8.39	4.72	4.66	4.60	7.84	7.70	7.53
$\varepsilon_{frp,e}/\varepsilon_{frp,p}$	Ratio	0.47	1.10	1.00	1.35	1.97	1.83	0.81	1.20	1.12
V_{exp}	Experimental Shear Capacity (kN)	375	417	406	375	417	406	375	417	406
V_{pred}	Predicted Shear Capacity (ACI) (kN)	385	372	371	-	-	-	381	377	373
V_{exp}/V_{pred}	Ratio	0.97	1.12	1.09	-	-	-	0.98	1.11	1.09

The overall shear contribution for the model of Khalifa *et al.* (1998) and the proposed model are very similar. The unconservative prediction of GFRP strain in beam A-G by Khalifa *et al.* (1998) does not adversely affect the prediction of the shear capacity for this beam since the bond strength rather than the effective stress governs in this case.

6. SUMMARY AND CONCLUSIONS

6.1 Summary

Most research to this point has consisted of beams with a small height in comparison to the effective bond length of the FRP sheets they are strengthened with. Two series of beams were tested in order to develop a better understanding of the behaviour of large-scale beams strengthened in shear with FRP sheets. The first series consisted of three prestressed concrete beam specimens that were cut from a larger girder. One of these beams was tested as a control specimen. The other two were strengthened with CFRP sheets with fibres primarily oriented in the vertical direction. The second series of specimens consisted of three reinforced concrete specimens that were constructed to examine debonding as a potential failure mode in large-scale specimens. One of these was strengthened for shear using GFRP sheets, while the remaining two used CFRP sheets.

6.2 Conclusions

While size effects are detrimental to concrete shear contribution, they are beneficial in enhancing the FRP shear contribution. For the Series A beams the large area available for bonding of the FRP to the concrete was responsible for restraining peeling forces generated at the interior corners of the I-section from the web-shear and flexural-shear cracks occurring near the tension flange. Unlike in smaller beams, peeling was not responsible for failure and the strain in the FRP sheets along the failure crack was observed to be much higher than the smaller beams. For the Series B beams, which failed by debonding, their size was sufficient to allow significantly higher strains than typically recorded in the literature.

Failure of the Series B, T-section beams strengthened in shear with FRP was not sudden, but the large-scale beams exhibited progressive debonding starting at the top of a sheet above a primary shear crack. The strain in the FRP is critical in

determining when the sheets will debond. Debonding did not occur simultaneously with failure, but rather load was transferred away from debonded regions for a significant time in the load history. Local areas of debonding may be significant in providing additional warning of failure as compared to unstrengthened beams, particularly those that are not reinforced in shear.

Vertical strains in the web were found to be highest in the concrete away from either steel or FRP shear reinforcement. Continuous FRP reinforcement may be superior to FRP reinforcement with gaps between the sheets in maintaining a uniform stress field in the concrete. This would have the effect of distributing shear cracks and minimizing their width over the entire web rather than just at the sheet locations. Strains in the FRP sheets were found to be extremely localized to the crack location in both series of beams. For the Series B beams, the vertical strain was found to be approximately constant along the primary shear cracks.

Calculation of shear capacity through addition of shear contribution of individual components may not be the most accurate method of calculating shear capacity. Just as the shear behaviour of beams without stirrups is significantly different than the behaviour of beams with stirrups, beams strengthened with FRP have more distributed cracking with cracks smaller in width. This behaviour improves the shear contribution of the concrete since aggregate interlock forces can be more effectively activated. If addition of components is to be used for simplicity, it must be understood that the FRP contribution includes not only the effect of strain in the FRP sheets, but must also include the enhanced behaviour of the concrete. There is a synergistic effect in shear strengthening with FRP sheets, greater than the sum of the individual material contributions.

An equation was developed from experimental results in the literature as well as from this study. With the understanding that beams that are not fully wrapped typically fail by debonding of the sheets, this model was able to predict effective strains for all sizes of beams studied. Even beams that are small in height relative to the effective bond length of the FRP can be strengthened significantly in shear. In conjunction with observations of the concrete behaviour in regions strengthened with FRP sheets, it was found that limiting the effective strain in the FRP sheets to maintain shear integrity of the concrete is not necessary. This is due to the beneficial effect of the FRP sheets in improving the cracking behaviour of the concrete, limiting crack width and improving crack distribution.

Factors influencing the effectiveness of the FRP strengthening scheme are: the concrete strength, the end anchorage of the sheets, the steel reinforcement ratio, the axial stiffness of the FRP sheets, the angle of the fibres, use of FRP sheets with more than one fibre orientation, and the ratio of the FRP effective depth to the effective depth of the section. Higher concrete strength improves the effectiveness of the bond of the FRP sheets since the concrete cylinder strength is related to the surface shear strength of the beam. As found in previous studies, the effective strain is decreased with increasing axial stiffness of the FRP sheets. Also, the end condition was found to affect the effective strain in the FRP sheets. The effect of different anchorages could be included in the model with more tests conducted to determine its effect. The effect of steel reinforcement ratio, pseudo-isotropic FRP sheets and the ratio of the FRP effective depth to effective depth were all quantified in the model.

6.3 Notes for Further Research

Better understanding is needed of what fraction of strengthening is developed through load carried by the fibres and what fraction is developed through enhancement of the aggregate interlock behaviour of the concrete on large scale

beams. One technique by which this could be accomplished is by comparing beams with the same shear reinforcement ratio but different application methods. Continuous FRP sheets should provide the greatest improvement of concrete capacity, followed by FRP sheets with gaps between them, FRP strips and FRP rods applied as near-surface mounted reinforcement. Differences may also be observed in beams having similar steel shear reinforcement ratios but either closely spaced small diameter reinforcement or large diameter reinforcement spaced further apart.

Observation of strain in the sheets is necessary to define their performance, however much of the research to date does not include this information. More beams, of different configurations than already tested should include observations of FRP strain. This should be done so that models are based on strains that are observed, rather than inferred. It would be preferable if the reported strain was not the strain at one location on the FRP sheets, but the average strain as measured by several different gauges along the failure crack.

The proposed model allows for the effect of the end condition to be simply described. However, more and more methods of anchoring the ends have been developed by different researchers. The effectiveness of a particular method of end anchorage could be accounted for through non-integer values for the term accounting for the number of free edges on one side of the beam. This term could also be modified to account for I-section geometry where peeling limits the effective stress in small beams. More sizes of I-section beams should be studied, with different interior corner dimensions to determine at what size peeling is critical in limiting the effective strain in the sheets.

Debonding tests have been completed on samples loaded in one direction. However the stress state on the web of a beam is biaxial. While the FRP sheets primarily resist load in the direction of the fibres, the concrete to which they are

bonded may be in biaxial tension (near the bottom of the web) or some combination of tension and compression. Since bond strength is governed by the surface shear strength of the concrete, and this strength may be different depending on the biaxial stress state of the concrete, investigations should be made to measure this effect.

This research found that the pseudo-isotropic fibres are more effective than unidirectional fibres for shear strengthening. More work is required to determine the effect of varying the secondary fibre orientation, or the benefit of a third fibre direction. These fibres likely further improve the cracking characteristics of the concrete, enhancing the concrete contribution rather than directly contributing to the load carried by the fibres.

Various aspects of durability of the FRP sheets need to be considered. While the material itself is durable provided ultraviolet exposure is limited, in particular the long-term effect of moisture at the bonding surface needs to be examined. While several field applications have taken place, accelerated durability tests would be able to determine the effects of long-term exposure more quickly. This is of particular concern for bridge girders, where moisture may be introduced at the top of the girder through deficiencies in the deck, but not allowed to escape due to sealing of three sides of the girder with epoxy. Even if the epoxy and concrete behaviour is adequate with long-term exposure to moisture, the change in moisture gradients within the beam may influence the corrosion of the internal steel reinforcement. Moisture effects may also be aggravated by freeze-thaw action. Performance in fire also needs to be addressed in addition to the interaction of protective or intumescent coatings applied to the surface of the FRP.

Strengthening of bridges in the field has occurred while the bridge is subjected to cyclic loading. However in most experimental work, the beam is subject only

to its own self-weight, and sometimes the member is even inverted to make strengthening easier. Testing should be completed on beams strengthened while they are carrying load, or subject to load cycling while the epoxy is curing, to more accurately simulate field strengthening conditions.

Finally, the effects different ratios of shear to moment should be examined. Most tests completed have been done on beams using three or four point loading. These tests have a low shear to moment ratio, with the critical location for shear usually occurring near the load point. More common application of load, particularly in buildings, is by distributed loading. With this type of loading there is a higher shear to moment ratio at the end of the beam. Although this type of test is more difficult to conduct, the results would be more applicable to actual structures.

REFERENCES

Adhikary, Bimal Babu, Hiroshi Mutsuyoshi, and Masashi Sano. "Shear strengthening of reinforced concrete beams using steel plates bonded on the beam web: Experiments and analysis," Construction and Building Materials, v. 14, no. 5, July 2000, pp. 237-244.

Ahmad, Shuaib H., A. R. Khaloo, and A. Poveda. "Shear capacity of reinforced high-strength concrete beams," Journal of the American Concrete Institute, v. 83, no. 2, March-April 1996, pp. 297-305.

Al-Sulaimani, Ghazi J., Alfarabi Sharif, Istem A. Basunbul, Mohhamed H. Baluch, and Bader N. Ghaleb. "Shear repair for reinforced concrete by fiberglass plate bonding," ACI Structural Journal, v. 91, no. 3, July-August 1994, pp. 458-464.

Araki, Nobuhiro, Yasuhiro Matsuzaki, Katsuhiko Nakano, Takahiro Kataoka and Hiroshi Fukuyama. "Shear capacity of retrofitted RC members with continuous fiber sheets," Japan Concrete Institute. Non-metallic (FRP) Reinforcement for Concrete Structures: Proceedings of the Third International Symposium, v. 1, October 1997, pp. 512-522.

ASCE-ACI Task Committee 426, "The shear strength of reinforced concrete members," ASCE Journal of the Structural Division, Proceedings of the American Society of Civil Engineers, v. 99, no. ST6, June 1973, pp. 1091-1187.

Bartlett, F. Michael and James G. MacGregor. "Cores from high-performance beams," ACI Materials journal, v. 91, no. 6, November-December 1994, pp. 460-469.

Bažant, Zden.k P. and Jin-Keun Kim. "Size effect in shear failure of longitudinally reinforced beams," Journal of the American Concrete Institute, v. 81, no. 5, September-October 1984, pp. 456-468.

Bažant, Zden.k P. and Zhiping Cao. "Size effect of shear failure in prestressed concrete beams," Journal of the American Concrete Institute, v. 83, no. 2, March-April 1986, pp. 260-268.

Bažant, Zden.k P. and Hsu-Huei Sun. "Size effect in diagonal shear failure: Influence of aggregate size and stirrups," ACI Materials Journal, v. 84, no. 4, September-October 1987, pp. 259-272.

Belarbi, Abdeldjelil and Thomas T. C. Hsu. "Constitutive laws of concrete in tension and reinforcing bars stiffened by concrete," ACI Structural Journal, v. 91, no. 4, July-August 1994, pp. 465-474.

Bizindavyi, L. and K. W. Neale. "Transfer lengths and bond strengths for composites bonded to concrete," Journal of Composites for Construction, v. 3, no. 4, November 1999, pp. 153-160.

Chajes, Michael J., Ted F. Januszka, Dennis R. Mertz, Theodore A. Thomson, Jr., and William W. Finch, Jr. "Shear strengthening of reinforced concrete beams using externally applied composite fabrics," ACI Structural Journal, v. 92, no. 3, May-June 1995, pp. 295-303.

Chajes, Michael J., William W. Finch, Jr., Ted F. Januszka, and Theodore A. Thomson, Jr. "Bond and force transfer of composite material plates bonded to concrete," ACI Structural Journal, v. 93, no. 2, March-April, 1996, pp. 208-217.

Collins, Michael P. and Denis Mitchell. "Shear and torsion design of prestressed and non-prestressed concrete beams," Journal of the Prestressed Concrete Institute, v. 25, no. 5, September-October 1980, pp. 32-100.

Collins, Michael P., Denis Mitchell, Perry Adebar and Frank J. Vecchio. "A general shear design method," ACI Structural Journal, v. 93, no. 1, January-February 1996, pp. 36-45.

Collins, Michael P. and Denis Mitchell. Prestressed Concrete Structures. Response Publications, Canada, 1997, 766 p.

Collins, Michael P. and Daniel Kuchma. "How safe are our large, lightly reinforced concrete beams, slabs, and footings?" ACI Structural Journal, v. 96, no. 4, July-August 1999, pp. 482-490.

Deniaud, Christophe and J. J. Roger Cheng. "Behaviour of reinforced concrete beams strengthened in shear with FRP sheets," University of Alberta Department of Civil and Environmental Engineering: Structural Engineering Report No. 234, October 2000, 265 p.

Dolan, Brendan E., H. R. Hamilton III, and Charles W. Dolan. "Strengthening with bonded FRP laminate," Concrete International: Design and Construction. v. 20, no. 6, June 1998, pp. 51-55.

Elzanaty, Ashraf H., Arthur H. Nilson, and Floyd O. Slate. "Shear capacity of reinforced concrete beams using high-strength concrete," Journal of the American Concrete Institute, v. 83, no. 2, March-April 1986, pp. 290-296.

Funakawa, Isao, Kazuyuki Shimono, Tadatomo Watanabe, Shiro Asada, and Sakae Ushijima. "Experimental study on shear strengthening with continuous fiber reinforcement sheet and methyl methacrylate resin," Japan Concrete Institute. Non-metallic (FRP) Reinforcement for Concrete Structures: Proceedings of the Third International Symposium, v. 1, October 1997, pp. 475-482.

Horiguchi, Takashi and Noboru Saeki. "Effect of test methods and quality of concrete on bond strength of CFRP sheet," Japan Concrete Institute. Non-metallic (FRP) Reinforcement for Concrete Structures: Proceedings of the Third International Symposium, v. 1, October 1997, pp. 265-270.

Hutchinson, Robin L. "The use of externally bonded CFRP sheets for shear strengthening of I-Shaped prestressed concrete bridge girders," Ph. D. Thesis, University of Manitoba, Winnipeg, 1999, 270 p.

Izumo, Kenji, Toshihiro Asamizu, Noboru Saeki and Kazunori Shimura. "Shear strengthening of PRC members by fiber sheets," Transactions of the Japan Concrete Institute, v. 19, 1997, pp. 105-112.

Izumo, Kenji, Toshihiro Asamizu, Noboru Saeki and Kazunori Shimura. "Bond behaviour of aramid and carbon fiber sheeting," Transactions of the Japan Concrete Institute, v. 20, 1998, pp. 269-278.

Kani, G. N. J. "How safe are our large reinforced concrete beams?," ACI Journal Proceedings, v. 64, no. 3, March 1967, pp. 128-141.

Karbhari, V. M. "Characteristics of adhesion between composites and concrete as related to infrastructure rehabilitation," International Society for the Advancement of Material and Process Engineering, Proceedings of the 27th International SAMPE Technical Conference, v. 27, Albuquerque, New Mexico, October 9-12, 1995, pp. 1083-1094.

Khalifa, Ahmed, William J. Gold, Antonio Nanni, and Abdel Aziz M. I., "Contribution of externally bonded FRP to shear capacity of RC flexural members," Journal of Composites for Construction, v. 2, no. 4, November 1998, pp.195-203.

Khalifa, A. and A. Nanni. "Rehabilitation of rectangular simply supported RC beams with shear deficiencies using CFRP composites," Construction and Building Materials (Submitted for publication), April 1999.

Khalifa, A., A. Belarbi and A. Nanni. "Shear performance of RC members strengthened with externally bonded FRP wraps," Proceedings of the 12th World Conference on Earthquake Engineering, Auckland, New Zealand, paper 305, Jan. 30-Feb. 04, 2000a, 10pp.

Khalifa, Ahmed and Antonio Nanni. "Improving shear capacity of existing RC T-section beams using CFRP composites," Cement and Concrete Composites, v. 22, no. 3, June 2000b, pp. 165-174.

Khalifa, A., L. De Lorenzis, and A. Nanni, "FRP composites for shear strengthening of RC beams," Proceedings 3rd International Conference on Advanced Composite Materials in Bridges and Structures, Ottawa, Canada, J. Humar and A. G. Razaqpur, editors, August 15-18, 2000c, pp. 137-144.

Kim, Jin-Keun and Yon-Dong Park. "Shear strength of reinforced high strength concrete beams without web reinforcement," Magazine of Concrete Research, v. 46, no. 166, March 1994, pp. 7-16.

Lee, Y. J., T. E. Boothby, C. E. Bakis, and A. Nanni. "Slip modulus of FRP sheets bonded to concrete," Journal of Composites for Construction, v. 3, no. 4, November 1999, pp. 161-167.

Limberger, E. and J. Vielhaber. "Experimental investigations on the behavior of CFRP-prepreg strengthened structural elements," Proceedings ACMBS-II, 2nd International Conf. on Advanced Composite Materials in Bridges and Structures, M. M. El-Badry, ed., Canadian Soc. for Civil Engineering, Montreal, Quebec, Canada, 1996, pp. 597-604.

MacGregor, James G. Reinforced Concrete: Mechanics and Design. Prentice-Hall, Englewood Cliffs, New Jersey, 1988.

MacGregor, James G and F. Michael Bartlett. Reinforced Concrete: Mechanics and Design. First Canadian edition. Prentice-Hall Canada Inc., Scarborough, Ontario, 2000.

Maeda, Toshiya, Yasuyuki Asano, Yasuhiko Sato, Tamon Ueda and Yoshio Kakuta. "A study on bond mechanism of carbon fiber sheet," Japan Concrete Institute. Non-metallic (FRP) Reinforcement for Concrete Structures: Proceedings of the Third International Symposium, v. 1, October 1997, pp. 279-286.

Master Builders Technologies. "MBrace composite strengthening system," Product information brochure, 2001.

McIntyre, M. and A. Scanlon. "Interpretation and application of core test data in strength evaluation of existing concrete bridge structures," Canadian Journal of Civil Engineering, v. 17, no. 3, June 1990, pp. 471-480.

McKenna, J. K. and M. A. Erki. "Strengthening of reinforced concrete flexural members using externally applied steel plates and fibre composite sheets – A survey," Canadian Journal of Civil Engineering, v. 21, no. 1, February 1994, pp. 16-24.

Mitsubishi Chemical Corporation, Composite Materials Department, http://www.m-kagaku.co.jp/english/aboutmcc/division/prod/carbonfiber/replark.htm, 2001.

Nilson, Arthur H., and George Winter. Design of Concrete Structures. Eleventh edition. Mc-Graw-Hill, Inc., New York, 1991.

Polak, Maria Anna and Jaroslaw J. Dubas. "Shear design of high strength concrete beams – Canadian code perspective," Canadian Journal of Civil Engineering, v. 23, no. 4, August 1996, pp. 809-819.

Rahal, Khaldoun N. and Michael P. Collins. "Background to the general method of shear design in the 1994 CSA-A23.3 standard," Canadian Journal of Civil Engineering, v. 26, no.6, December 1999, pp. 827-839.

Ramirez, Julio A. and John E. Breen. "Evaluation of a modified truss-model approach for beams in shear," ACI Structural Journal, v. 88, no. 5, September-October 1991, pp. 562-571.

Sato, Yasuhiko, Tamon Ueda, Yoshio Kakuta and Sadamu Ono. "Ultimate shear capacity of reinforced concrete beams with carbon fiber sheet," Japan Concrete Institute. Non-metallic (FRP) Reinforcement for Concrete Structures: Proceedings of the Third International Symposium, v. 1, October 1997, pp. 499-506.

Sato, Yasuhiko, Hideo Katsumata and Yoshiro Kobatake. "Shear strengthening of existing reinforced concrete beams by CFRP sheet," Japan Concrete Institute. Non-metallic (FRP) Reinforcement for Concrete Structures: Proceedings of the Third International Symposium, v. 1, October 1997, pp. 507-514.

Täljsten, Björn. "Defining anchor lengths of steel and CFRP plates bonded to concrete," International Journal of Adhesion and Adhesives, v. 17, no. 4, November 1997, pp. 319-327.

Täljsten, B. and L. Elfgren. "Strengthening concrete beams for shear using CFRP-materials: Evaluation of different application methods," Composites Part B: Engineering, v. 31, no. 2, 2000, pp. 87-96.

Triantafillou, Thanasis C. "Shear strengthening of reinforced concrete beams using epoxy-bonded FRP composites," ACI Structural Journal, v. 95, no. 2, March-April 1998a, pp. 107-115.

Triantafillou, Thanasis C., "Composites: A new possibility for the shear strengthening of concrete, masonry and wood," Composites Science and Technology, v. 85, no 8, August 1998b, pp. 1285-1295.

Uji, Kimitaka. "Improving shear capacity of existing reinforced concrete members by applying carbon fiber sheets," Transactions of the Japan Concrete Institute, v. 14, 1992, pp. 253-266.

Umezu, Kenji, Manabu Fujita, Hiroshi Nakai, Kazukiyo Tamaki. "Shear behavior of RC beams with aramid fiber sheet," Japan Concrete Institute. Non-metallic (FRP) Reinforcement for Concrete Structures: Proceedings of the Third International Symposium, v. 1, October 1997, pp. 491-498.

Vecchio, Frank J., M. P. Collins, and Jim Aspiotis. "High-strength concrete elements subjected to shear," ACI Structural Journal, v. 91, no. 4, July-August 1994, pp. 423-433.

Volnyy, Vladimir A. and Chris P. Pantelides. "Bond length of CFRP composites attached to precast concrete walls," Journal of Composites for Construction, v. 3, no. 4, November 1999, pp. 168-176.

Xie, Ming and Vistasp M. Karbhari. "Peel test for characterization of polymer composite/concrete interface," Journal of Composite Materials, v. 32, no 21, 1998, pp. 1894-1913.

Yoshizawa, Hiroyuki, Toru Myojo, Masayoshi Okoshi, Mutuki Mizukoshi and Howard S. Kilger. "Effect of sheet bonding condition on concrete members having externally bonded carbon fiber sheet," Proceedings of the 1996 4th Materials Engineering Conference. Part 2 (of 2), Washington, DC, Nov 10-14, 1996, pp. 1608-1616.

APPENDIX

A. Vertical Strain in the Web of Series B Beams

A.1 Beam A-G

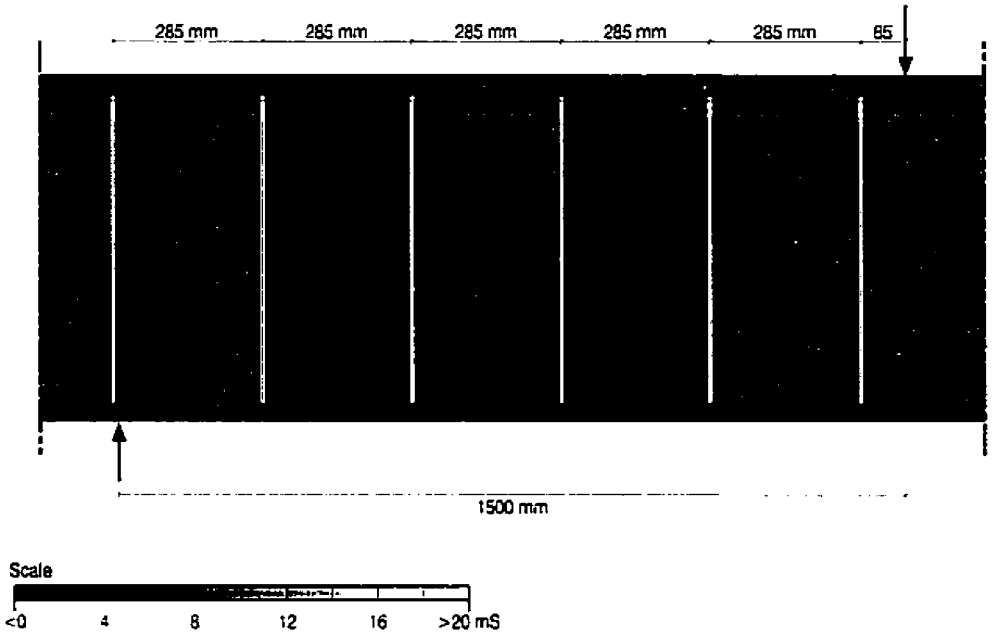

Figure A.1a Vertical strain in web of beam A-G at applied shear force of 125 kN

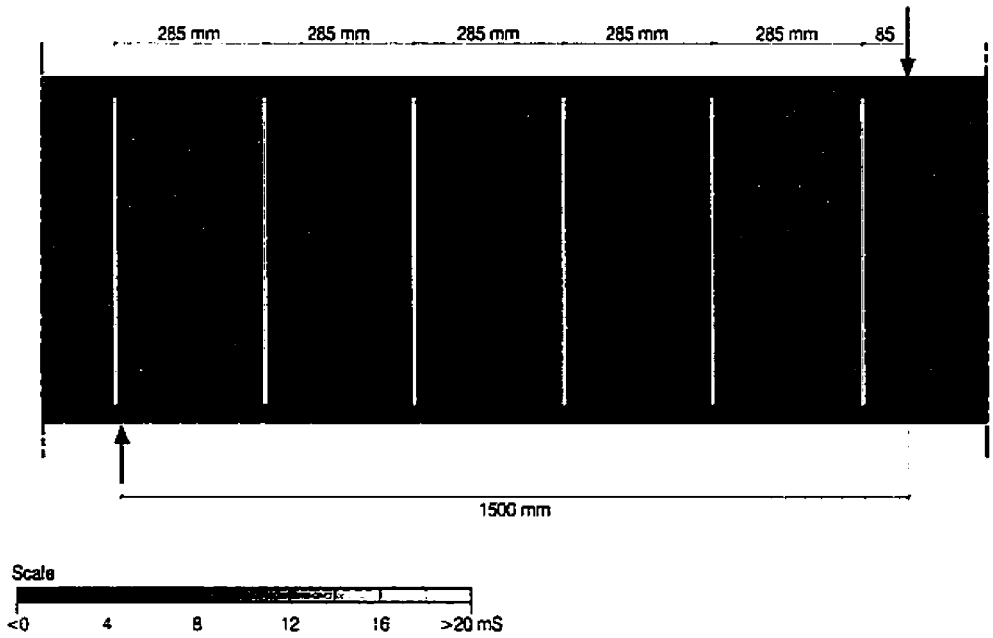

Figure A.1b Vertical strain in web of beam A-G at applied shear force of 200 kN

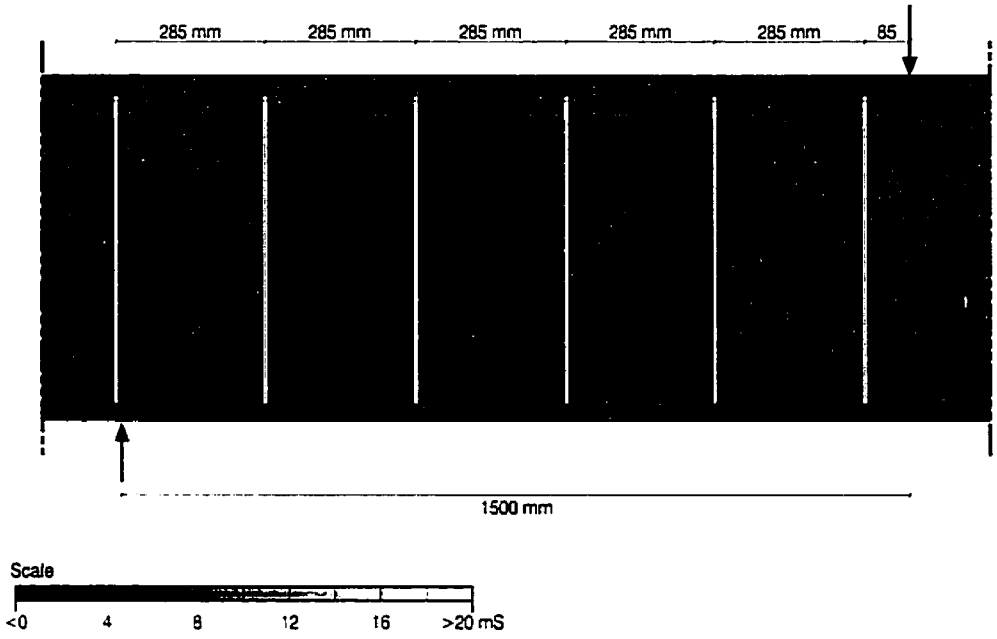

Figure A.1c Vertical strain in web of beam A-G at applied shear force of 300 kN

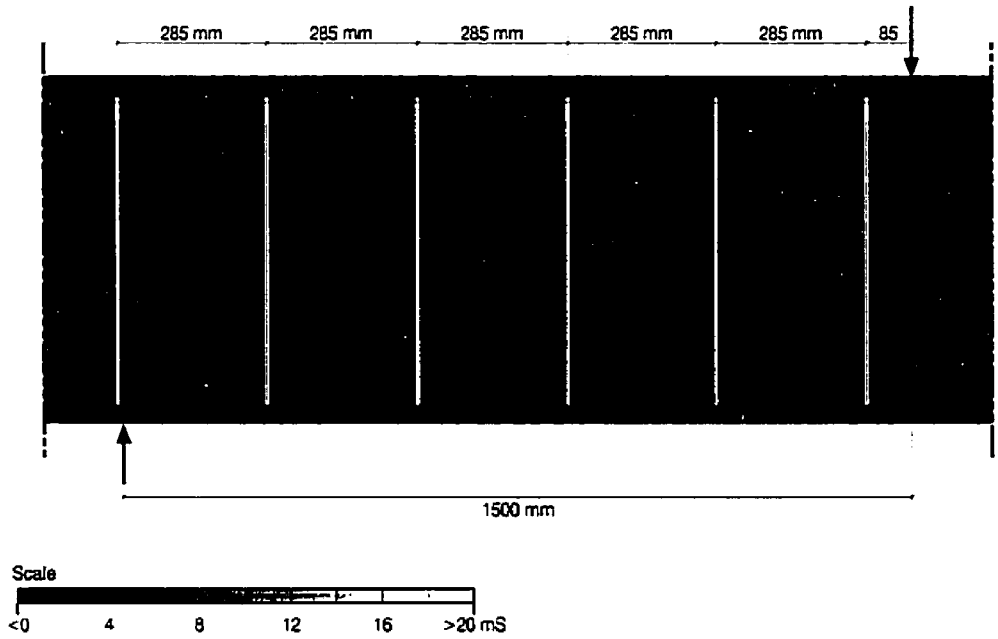

Figure A.1d Vertical strain in web of beam A-G at applied shear force of 325 kN

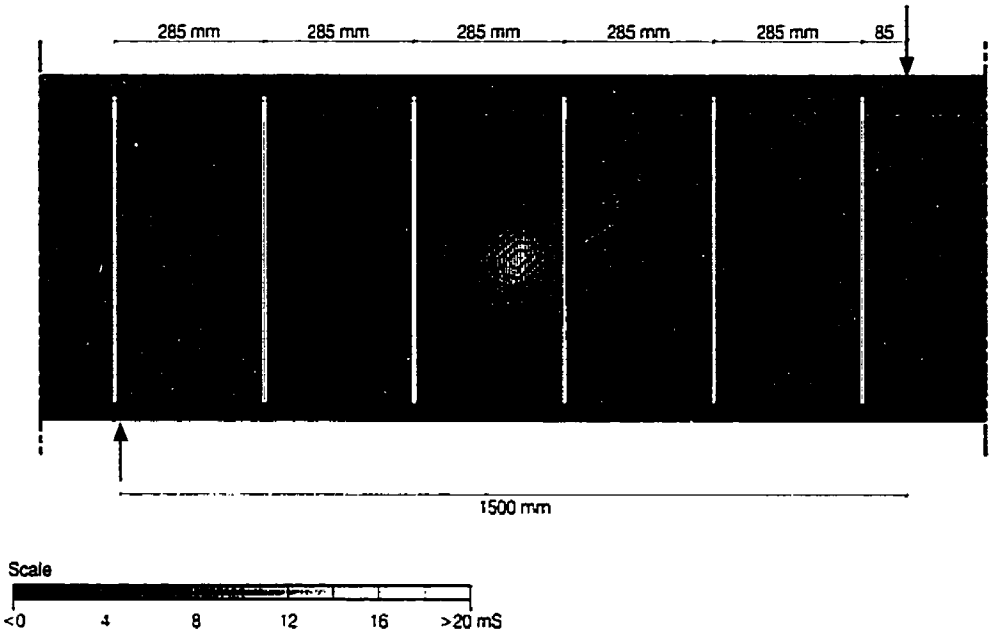

Figure A.1e Vertical strain in web of beam A-G at applied shear force of 350 kN

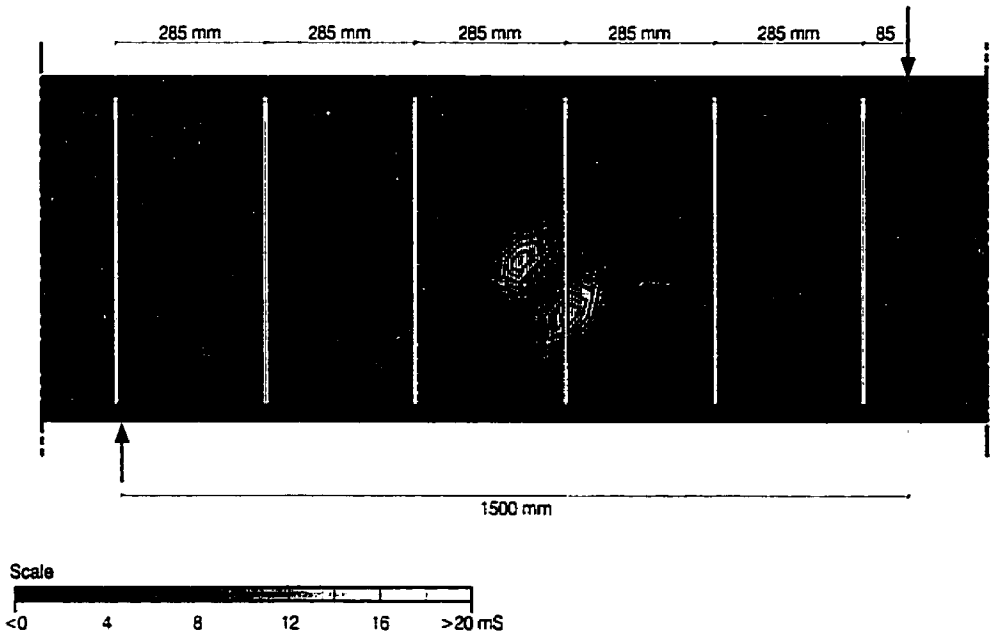

Figure A.1f Vertical strain in web of beam A-G at applied shear force of 367 kN

A.2 Beam B-C

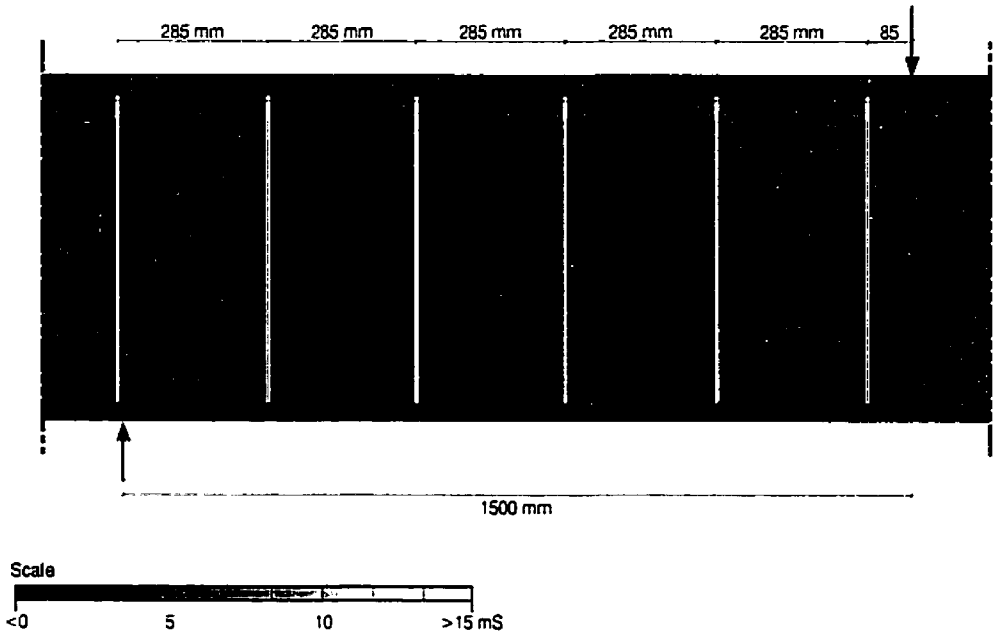

Figure A.2a Vertical strain in web of beam B-C at applied shear force of 100 kN

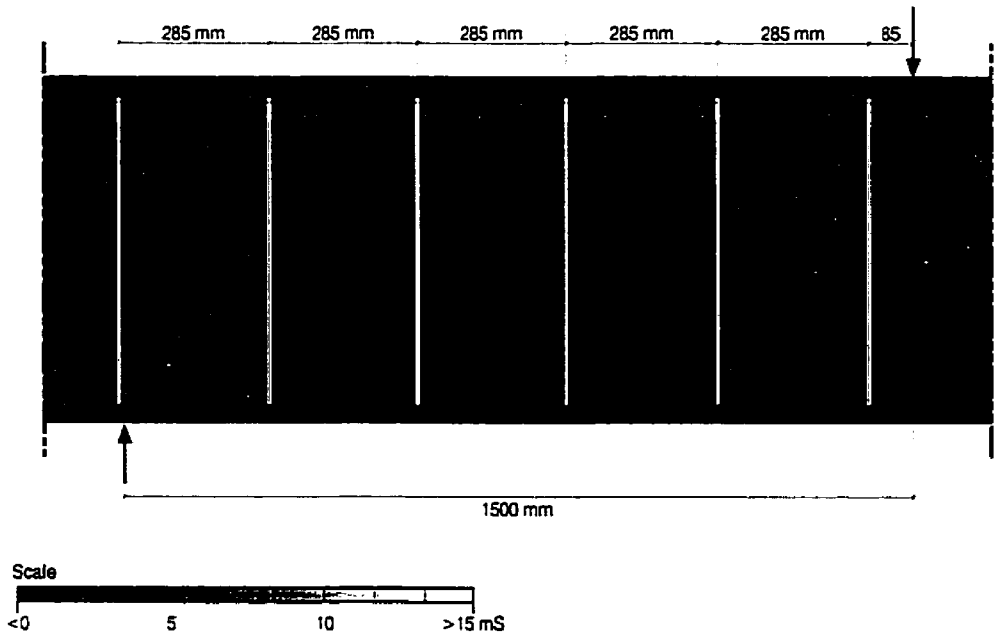

Figure A.2b Vertical strain in web of beam B-C at applied shear force of 200 kN

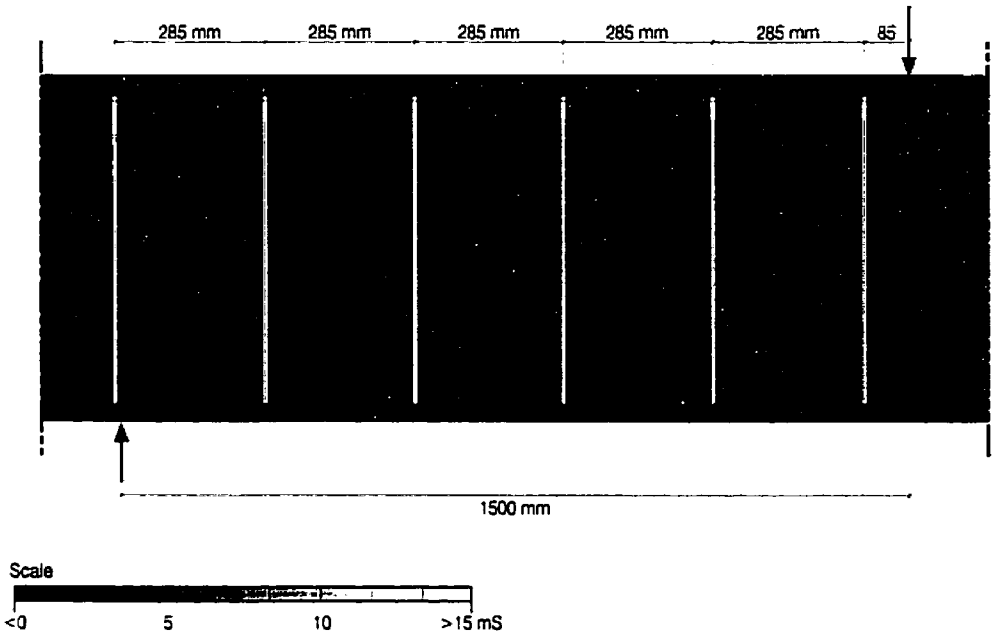

Figure A.2c Vertical strain in web of beam B-C at applied shear force of 300 kN

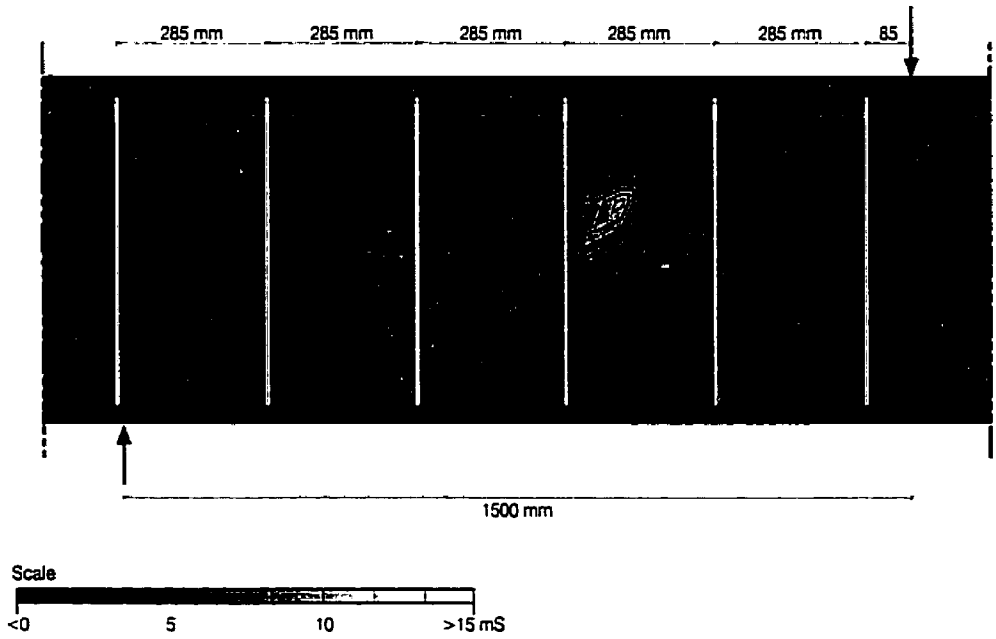

Figure A.2d Vertical strain in web of beam B-C at applied shear force of 400 kN

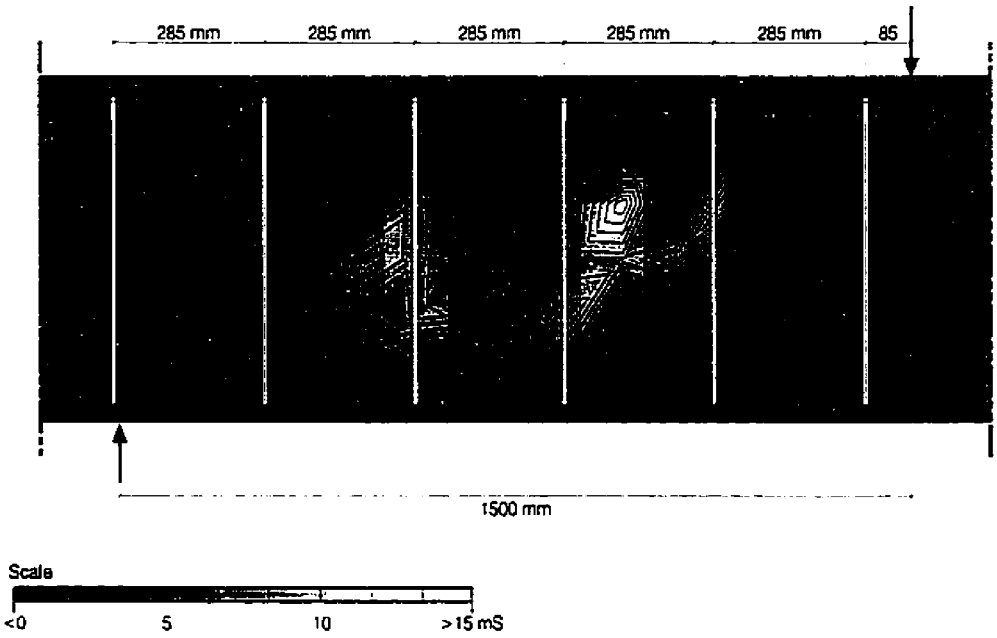

Figure A.2e Vertical strain in web of beam B-C at applied shear force of 417 kN

A.3 Beam C-C

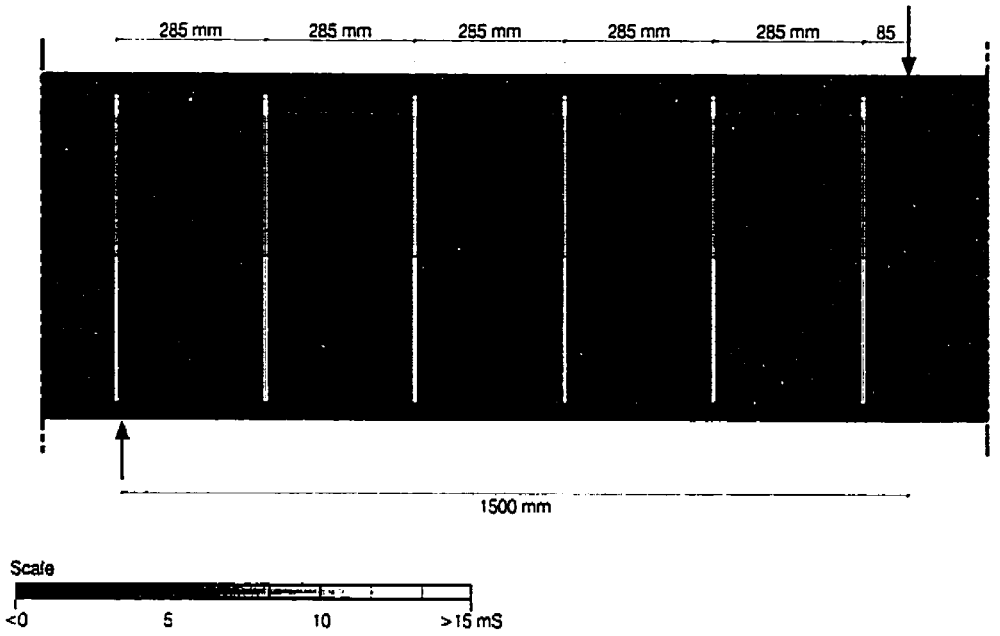

Figure A.3a Vertical strain in web of beam C-C at applied shear force of 125 kN

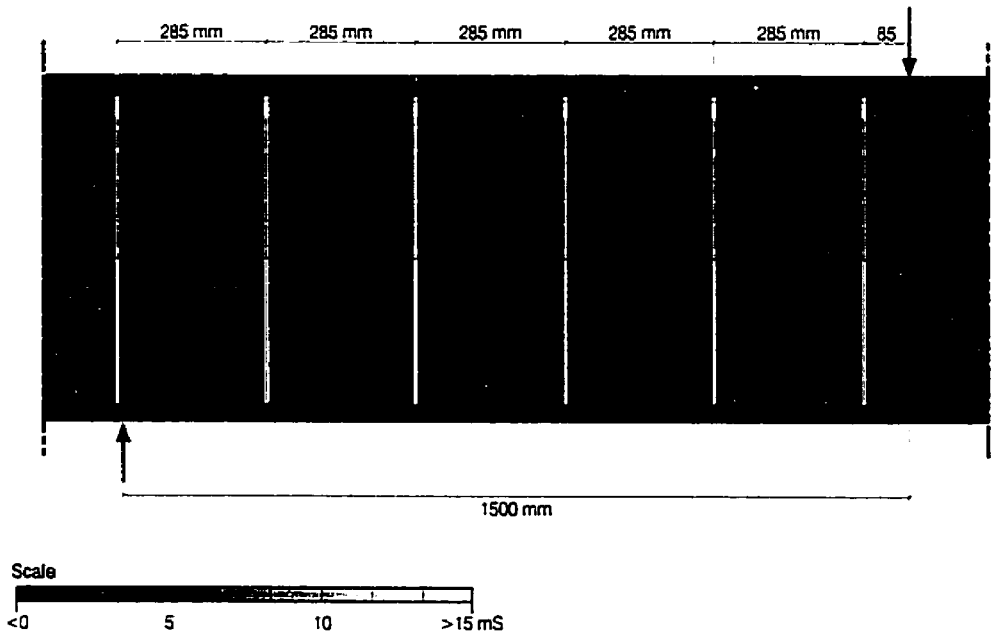

Figure A.3b Vertical strain in web of beam C-C at applied shear force of 200 kN

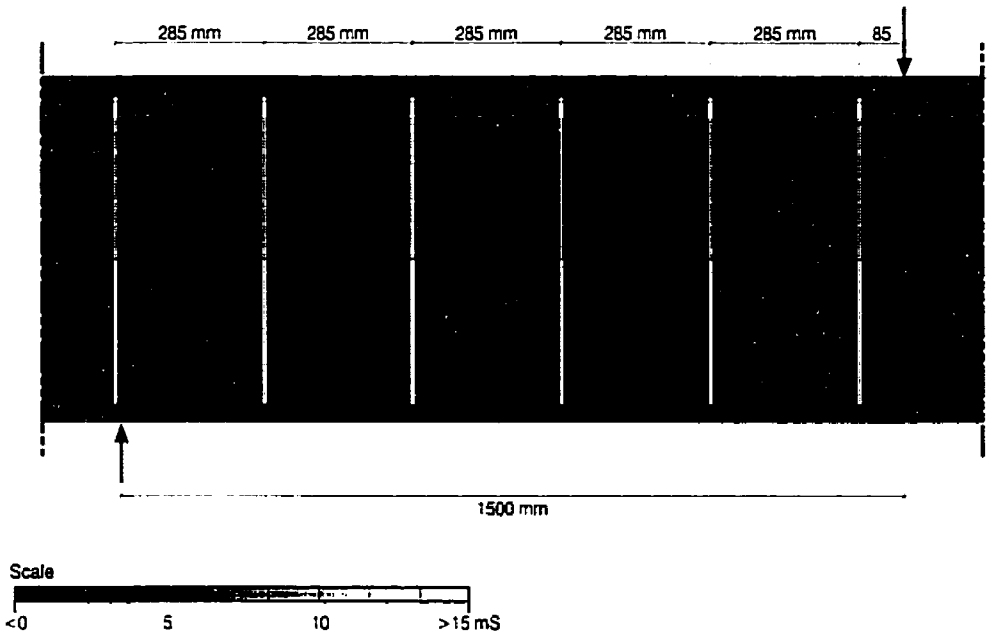

Figure A.3c Vertical strain in web of beam C-C at applied shear force of 300 kN

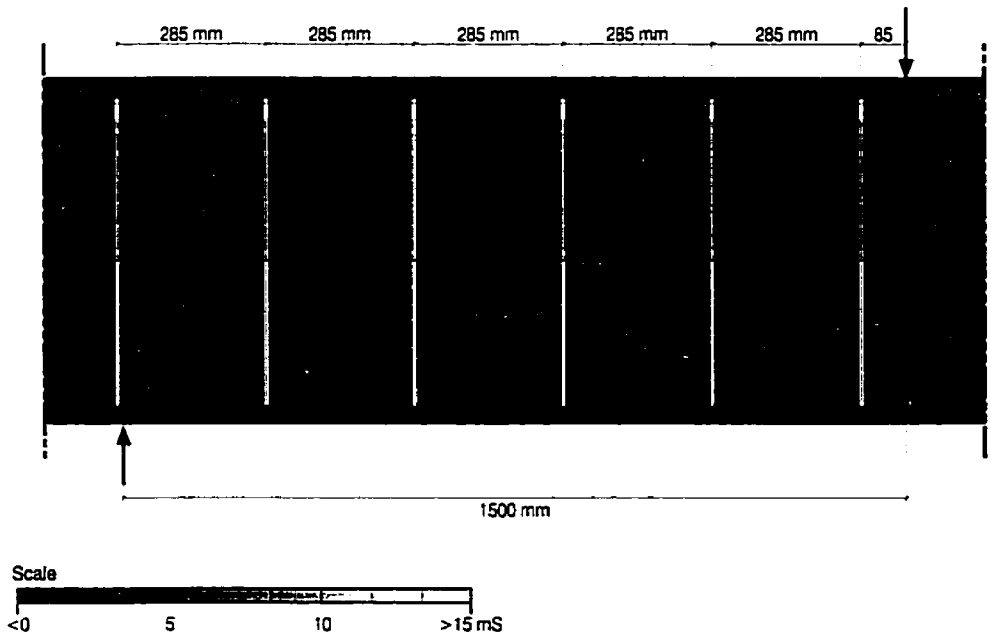

Figure A.3d Vertical strain in web of beam C-C at applied shear force of 350 kN

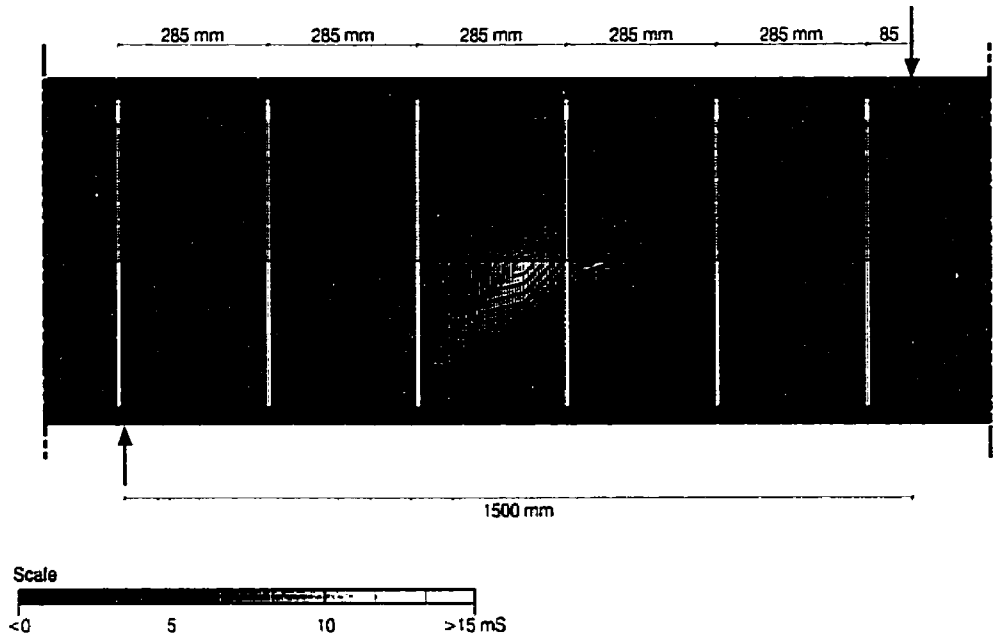

Figure A.3e Vertical strain in web of beam C-C at applied shear force of 375 kN

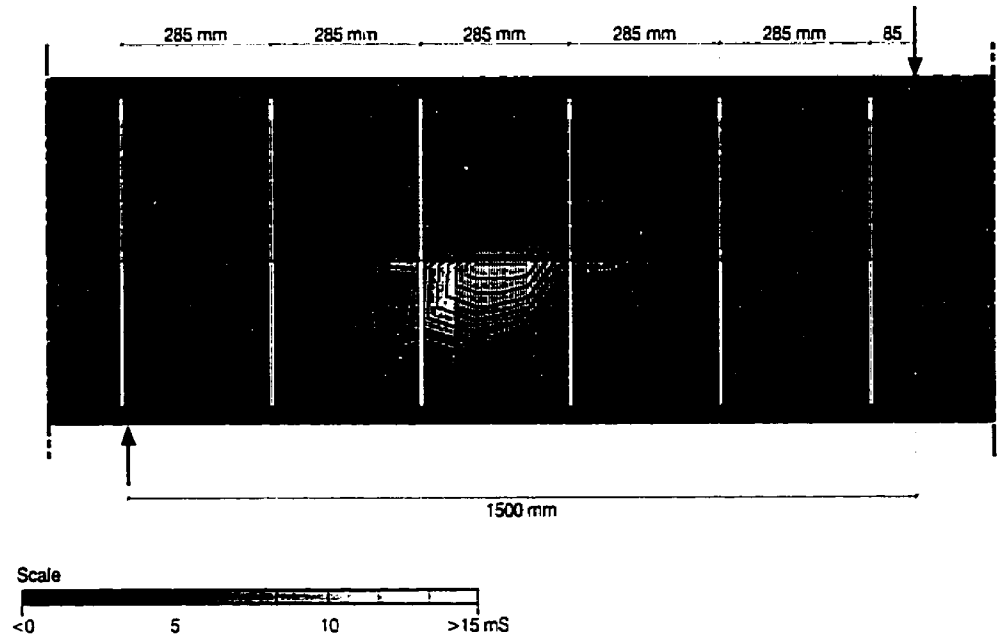

Figure A.3f Vertical strain in web of beam C-C at applied shear force of 390 kN

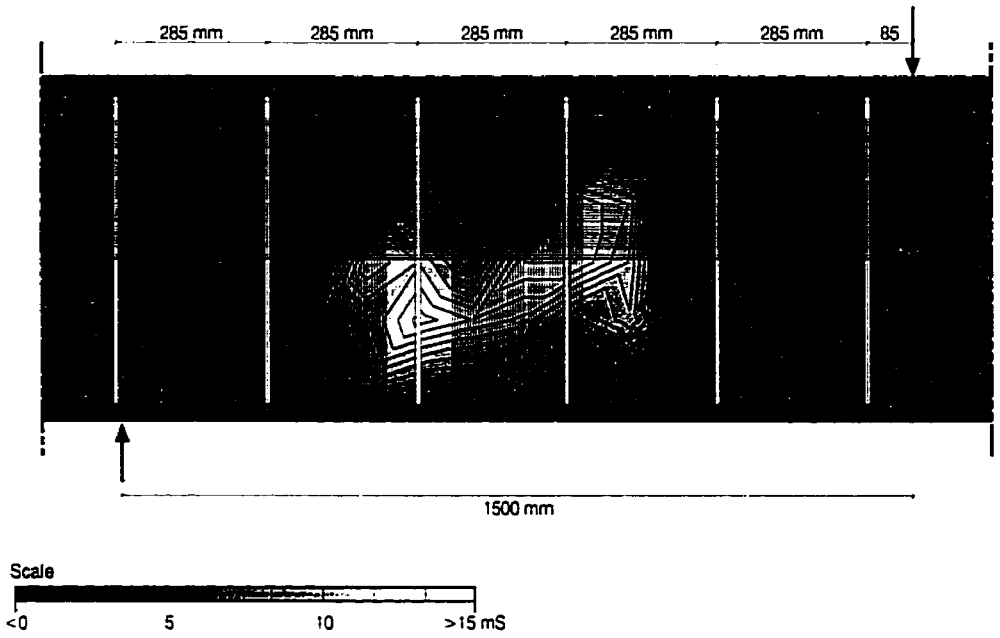

Figure A.3g Vertical strain in web of beam C-C at applied shear force of 404 kN